NASA TECHNICAL MEMORANDUM

NASA TM X-1214

NASA TM X-1214

TRANSONIC AERODYNAMIC CHARACTERISTICS OF A TAILLESS FIXED-WING SUPERSONIC TRANSPORT MODEL

by Edward J. Ray and Robert T. Taylor

Langley Research Center
Langley Station, Hampton, Va.

NATIONAL AERONAUTICS AND SPACE ADMINISTRATION • WASHINGTON, D. C. • MARCH 1966

NASA TM X-1214

TRANSONIC AERODYNAMIC CHARACTERISTICS OF A TAILLESS FIXED-WING SUPERSONIC TRANSPORT MODEL

By Edward J. Ray and Robert T. Taylor

Langley Research Center
Langley Station, Hampton, Va.

NATIONAL AERONAUTICS AND SPACE ADMINISTRATION

For sale by the Clearinghouse for Federal Scientific and Technical Information
Springfield, Virginia 22151 – Price $1.10

TRANSONIC AERODYNAMIC CHARACTERISTICS OF A TAILLESS FIXED-WING SUPERSONIC TRANSPORT MODEL

By Edward J. Ray and Robert T. Taylor
Langley Research Center

SUMMARY

21692

An investigation has been made in the Langley high-speed 7- by 10-foot tunnel to determine the effects of wing planform and twist and camber on the aerodynamic characteristics of a tailless fixed-wing supersonic transport model throughout a Mach number range of 0.40 to 1.14. To determine these effects, three wing planforms with the same aspect ratios were investigated with and without twist and camber. The three wing planforms were a modified delta having an ogee-shaped leading edge, a delta, and a trapezoid. All three plane wings were equipped with trailing-edge elevons to determine the control effectiveness of these devices.

The results of the present study indicated that the wing planform differences had little effect on the aerodynamic center variations with Mach number and on the trimmed lift coefficients at reasonable landing attitudes. The wing twist and camber effects, however, were significant and the results indicated that the trapezoid configuration, which had the highest values of pitching-moment coefficient at zero lift, would exhibit the highest trimmed lift coefficients of the twisted and cambered wing configurations near reasonable landing attitudes.

The static lateral data indicated that the twisted and cambered wing configurations had positive directional stability and positive effective dihedral for all Mach numbers of the investigation. The directional stability, however, of the twisted and cambered delta and trapezoid configurations was considerably greater than the directional stability of the twisted and cambered ogee configurations.

Quelch

INTRODUCTION

The National Aeronautics and Space Administration has investigated a number of configurations which may be suitable for a commercial supersonic transport aircraft. These investigations have covered a variety of design concepts, including both fixed-wing and variable-sweep wing arrangements. Results from investigations to determine the aerodynamic characteristics of fixed-wing supersonic transport models may be found in

references 1 to 17. References 18 to 30 contain results obtained from investigations to determine the aerodynamic characteristics of supersonic transport models having variable-sweep wings or variable-sweep auxiliary wing panels.

The purpose of the present investigation was to determine the subsonic and transonic aerodynamic characteristics of a fixed-wing, tailless, supersonic transport model designed for cruise at a Mach number of 2.2. Three wing shapes, an ogee wing, a delta wing, and a trapezoid wing, of the same aspect ratio and thickness ratio distribution were tested with and without twist and camber to determine the effects of wing planform and wing twist and camber on the aerodynamic characteristics of the model. In addition, the plane wing configurations were provided with flap-type trailing-edge elevons to evaluate the control effectiveness of the three configurations. This paper presents the longitudinal and lateral results which were obtained for these configurations throughout the Mach number range of 0.40 to 1.14.

The study of this model has been extended to supersonic Mach numbers and the data resulting from these investigations are presented in references 31 and 32. The investigation described in reference 31 was conducted at a Mach number of 2.20 to determine the aerodynamic characteristics of the model at cruise speed. Reference 32 presents longitudinal and lateral data for the Mach number range of 1.80 to 2.86 and includes the effects of two forebody modifications.

SYMBOLS

The longitudinal data are referred to the wind-axis system and the lateral data are referred to the body-axis system. The moment center for all configurations is located on the model reference line at a point 61.77 percent of the body length behind the nose. (See figs. 1(a), (b), and (c).)

The units used for the physical quantities defined in this paper are given both in the U.S. Customary Units and in the International System of Units (SI). Factors relating the two systems are given in reference 33.

A	aspect ratio
b	span of wing, 19.25 inches (48.90 centimeters)
c	local wing chord, inches (centimeters)
$\bar{c}$	mean aerodynamic chord, inches (centimeters)

c_{ref}	reference chord of wing, 12.00 inches (30.48 centimeters)
$C_{A,i}$	nacelle internal-axial-force coefficient, $\frac{\text{Internal axial force}}{qS}$
C_D	drag coefficient, $\frac{\text{Drag}}{qS}$
$C_{D,i}$	induced drag coefficient
C_L	lift coefficient, $\frac{\text{Lift}}{qS}$
C_{L_α}	lift-curve slope near $C_L = 0$, $\partial C_L/\partial\alpha$, per degree
C_{L_δ}	effective change in lift coefficient caused by unit angular change in elevon deflection, $\partial C_L/\partial\delta$, per degree
C_l	rolling-moment coefficient, $\frac{\text{Rolling moment}}{qSb}$
C_{l_β}	effective dihedral parameter, $\partial C_l/\partial\beta$, per degree
C_m	pitching-moment coefficient, $\frac{\text{Pitching moment}}{qSc_{ref}}$
$C_{m,o}$	pitching-moment coefficient at $C_L = 0$
$\partial C_m/\partial C_L$	longitudinal stability parameter near $C_L = 0$
C_n	yawing-moment coefficient, $\frac{\text{Yawing moment}}{qSb}$
C_{n_β}	directional stability parameter, $\partial C_n/\partial\beta$, per degree
C_Y	side-force coefficient, $\frac{\text{Side force}}{qS}$
C_{Y_β}	side-force parameter, $\partial C_Y/\partial\beta$, per degree
$(L/D)_{max}$	maximum lift-drag ratio
M	Mach number
q	dynamic pressure, pounds force/foot^2 (newtons/meter^2)

R	Reynolds number
S	wing reference area (includes body intercept), 1.665 foot^2 (0.1547 meter^2)
t/c	thickness-chord ratio
x	distance from wing leading edge parallel to fuselage center line, inches (centimeters)
y	spanwise station, measured perpendicular from model center line, inches (centimeters)
z	vertical distance from wing reference plane to mean camber line, inches (centimeters)
α	angle of attack, degrees
α_δ	control-surface-effectiveness parameter at $C_L = 0$, effective change in wing angle of attack caused by unit angular change in elevon deflection, $C_{L_\delta}/C_{L_\alpha}$
β	sideslip angle, degrees
δ	inboard and outboard elevon deflection, negative trailing edge up (measured from wing chord plane), degrees
$\delta_{e,i}$	inboard elevon deflection, negative trailing edge up (measured from wing chord plane), degrees
$\delta_{e,o}$	outboard elevon deflection, negative trailing edge up (measured from wing chord plane), degrees
ϵ	angle of wing twist, degrees

Wing notations:

Ogee I	plane ogee wing planform
Delta I	plane delta wing planform

Trapezoid I	plane trapezoid wing planform
Ogee II	twisted and cambered ogee wing
Delta II	twisted and cambered delta wing
Trapezoid II	twisted and cambered trapezoid wing
Ogee III	twisted and cambered ogee wing, modified

MODELS

The three wing planforms used in this investigation were a modified delta having an ogee-shaped leading edge, a trapezoid, and a delta. (See figs. 1(a), (b), and (c).) The aspect ratio of the wings was 1.55. The wings without twist and camber will be referred to as Ogee I, Trapezoid I, and Delta I, and the twisted and cambered wings will be denoted as Ogee II, Trapezoid II, and Delta II. The Ogee II wing was modified further to provide additional wing twist and camber outboard of the nacelles, near the leading edge, and this wing will be referred to as the Ogee III wing.

Longitudinal and lateral control was provided by plain, flap-type, trailing-edge elevons located inboard and outboard of the nacelles. Only the plane wings were equipped with elevons. The elevons were attached to the wings with brackets which enabled the elevons to be deflected to angles of 0°, -5°, or -10°. The location and dimensions of the elevons for each planform are shown in figures 1(a), (b), and (c).

The two-dimensional inlet nacelles were fitted to the lower surface of the plane wings and positioned as shown in figures 1(a), (b), and (c). The nacelles were located on the twisted and cambered wings so that the center lines of the nacelles were 3.65 inches (9.27 cm) from the fuselage center line. Details of the nacelle are shown in figure 1(d).

A comparison of the various wing planforms is shown in figure 1(e). As shown in this figure, there was no difference in the projected planform area between the twisted and cambered and the plane delta wings or between the twisted and cambered and the plane trapezoid wings; however, the planform areas of the plane and the twisted and cambered ogee wings differed slightly. The wetted wing area, excluding the area covered by the nacelles, is listed for each planform in table I. An approximate quartic equation for the curved portion of the leading edge of the twisted and cambered ogee wing is shown in figure 1(f).

Ratios of wing thickness to wing chord, as shown in figure 2, varied from 3 percent at the root to 2 percent at the tip. Circular-arc airfoil sections were utilized for all the

wings. The twisted and cambered wings were designed for a lift coefficient of 0.1 at a Mach number of 2.20. (See ref. 34.) Airfoil sections of the twisted and cambered wings were sheared so that the trailing edge of each wing was straight. The twist and camber distributions of the Ogee II, Delta II, and Trapezoid II wings are shown in figure 3. The leading edge of the Ogee II wing was modified to form the Ogee III wing by rolling down the leading edge of the outer 45 percent of the wing semispan an additional 0.10 inch (0.25 cm). A typical section and the twist distribution illustrating this modification are presented in figure 4.

The cross-sectional area distribution of the model, excluding the cavities of the engine nacelles, with the twisted and cambered ogee wings is shown in figure 5 and photographs of this model are presented as figure 6.

TESTS AND CORRECTIONS

The investigation was made in the Langley high-speed 7- by 10-foot tunnel at Mach numbers of 0.40, 0.60, 0.80, 0.90, 0.98, 1.02, and 1.14. The Reynolds number based on the reference chord of the wing c_{ref} and on the average temperature at each Mach number is shown in the following table:

M	R
0.40	2.25×10^6
.60	3.10
.80	3.70
.90	3.90
.94	3.95
.98	4.00
1.02	4.05
1.14	4.10

The model was sting supported and the forces and moments were measured with an internally mounted, six-component, strain-gage balance. The angle-of-attack range varied throughout the Mach number range because of the load limits of the balance. At the low Mach numbers, the angle-of-attack range was generally about from -2° to 20° and at the higher Mach numbers the range extended about from 0° to 14°. Lateral stability data were obtained at all Mach numbers throughout a sideslip-angle range of -12° to 17° at an angle of attack of 0° for the plane ogee configuration and at sideslip angles of 0° and $\pm 5^\circ$ for all the twisted and cambered wing configurations. To insure a turbulent boundary layer, 1/16-inch-wide transition strips of no. 60 carborundum grains were

applied near the leading edge of the wings, 1 inch (2.54 cm) behind the body nose, on the vertical tail, and outside and inside the engine nacelles.

The angles of attack and sideslip have been corrected for sting and balance deflection under load. Jet-boundary and blockage corrections are negligible for the open-slot tunnel configuration and therefore were not applied to the data. The internal skin friction of the two nacelles was calculated and the measured axial force was corrected at each Mach number by the internal axial-force coefficient $C_{A,i}$ in the amount shown in the following table:

M	$C_{A,i}$
0.40	0.00141
.60	.00132
.80	.00125
.90	.00122
.94	.00122
.98	.00121
1.02	.00119
1.14	.00116

Nacelle base pressure measurements were made by using a manifold placed around the solid cross section of the engine nacelle base. The data were corrected to correspond to a condition of free-stream static pressure at the solid portion of the nacelle base and at the base of the fuselage.

Some problems were encountered with regard to the absolute level of the drag measurements on the plane delta and plane trapezoid wings. Although the exact magnitude of the resultant errors in minimum drag cannot, of course, be established, comparisons with subsonic theory based on flat-plate skin friction (ref. 35) and thickness-chord ratio (ref. 36) indicated that the measured minimum drag coefficients for the plane delta and trapezoid configurations were slightly high. In view of this, the drag coefficients for the plane trapezoid wing and plane delta wing configurations were reduced by 0.0010 and 0.0007, respectively, in an attempt to reduce the errors associated with the drag measurement problems encountered on these wings. Because of this somewhat arbitrary correction no comparisons of the subsonic or transonic lift-drag ratios have been made. No problems were encountered and no drag adjustments have been made, however, for the plane ogee wing, all the cambered and twisted wings, and all the supersonic data reproduced from references 31 and 32.

PRESENTATION OF RESULTS

The basic longitudinal results of this investigation are presented in figures 7 to 15 and some of these results are summarized in figures 16 to 23. Lateral data are presented in figures 24 to 25. An outline of the figure content is as follows:

DISCUSSION

Longitudinal Characteristics

Effect of wing planform on longitudinal characteristics.- The effect of plane wing planform on the variation with Mach number of the lift-curve slope C_{L_α} and the longitudinal stability parameter $\partial C_m/\partial C_L$ is shown in figure 16. Figure 16 shows that the plane ogee wing configuration exhibited the largest degree of static longitudinal stability for the plane wing configurations at a given Mach number as a result of its more rearward location of centroid of exposed area. It should be noted here that the longitudinal stability parameters for the three wings were based on a constant reference chord. The maximum variations of longitudinal stability parameters for the ogee and trapezoid wings when based on the mean aerodynamic chords (table I) were slightly larger than the variation indicated for the delta planform. The results of reference 32 indicated that at supersonic Mach numbers ranging from 1.80 to 2.86 the ogee wing configurations would exhibit the largest aerodynamic center variation of the three wing planforms.

The lift-curve slopes for the plane trapezoid configuration, as shown in figure 16, were considerably greater than the lift-curve slopes for the plane ogee and delta wing configurations at Mach numbers higher than 0.40. This effect may be attributed to the lower sweep (fig. 1(e)), and greater exposed area of the plane trapezoid wing configuration. (It should be noted that all data were nondimensionalized by using the same wing reference area.)

The effect of plane wing planform on induced drag at Mach numbers of 0.40, 0.90, and 1.14 are shown in figure 17. The induced drag of the plane trapezoid wing configuration was slightly less than the induced drag for the plane delta and ogee wing configurations throughout the Mach number range of the investigation. This result is as would be

expected since the induced drag of highly swept wing configurations with sharp wing leading edges is inversely proportional to the lift-curve slope.

Figure 18 presents the variation with Mach number of the elevon effectiveness parameter α_δ at a lift coefficient of zero for the three plane wing configurations. As shown in this figure, deflection of the elevons produces the greatest effective change in wing angle of attack for the plane ogee wing configuration, particularly in the subsonic Mach number range. Reference 37 reveals that this effect might be expected since the ogee configuration has a generally higher flap-chord to wing-chord ratio than the trapezoid or delta wing configurations. (See figs. 1(a), (b), and (c).) Figures 8(b), 11(b), and 14(b) indicate, however, that the change in pitching-moment coefficient at zero lift per degree of inboard and outboard elevon deflection was very nearly the same for the three plane wing configurations as a result of the comparable elevon locations and areas.

Effect of twist and camber on longitudinal characteristics.- The effects of twist and camber on the variation with Mach number of the longitudinal stability parameter $\partial C_m/\partial C_L$ for the ogee, delta, and trapezoid wing configurations are presented in figure 19. The maximum aerodynamic center shift occurring for the three wing planform configurations throughout the Mach number range was very nearly the same for the plane wing configurations as for the twisted and cambered wing configurations. However, it will be noted from figure 19 that the longitudinal stability parameters for the twisted and cambered and the plane trapezoid, and the twisted and cambered and the plane delta, wing configurations differed considerably near zero lift. The greater stability levels of the twisted and cambered trapezoid and delta wing configurations, relative to the plane wing configurations, are presumed due to maintaining unseparated flow conditions to higher lift coefficients. The plane trapezoid and delta wing configurations apparently experience leading-edge separation at very low angles of attack in the wing apex region; this separation would tend to reduce the level of longitudinal stability. For the ogee wing configurations, the difference in stability levels between the twisted and cambered and the plane wings is much less and is opposite in direction from that for the delta and trapezoid configurations. The similarity of stability levels exhibited for the ogee wing configurations suggests that the flow conditions at the leading edges of the plane and the twisted and warped wings were similar or that the stability levels of the ogee wing configuration were much less sensitive to differences in flow conditions.

The zero-lift pitching-moment results shown in figure 20 indicate substantially higher values of pitching-moment coefficient at zero lift $C_{m,o}$ throughout the Mach number range of the investigation for the twisted and cambered trapezoid configuration than for the twisted and cambered ogee or delta configurations.

Figure 21 shows that the effect of twist and camber on the variation with Mach number of the lift-curve slope C_{L_α} was not significant for the ogee, delta, or trapezoid planforms.

The effect of twist and camber on the induced drag of the ogee, delta, and trapezoid wing configurations at a Mach number of 0.90 is illustrated in figure 22. In addition to the experimental results, computed drag polars for zero and full leading-edge suction are shown for each planform. The close agreement between the experimental values obtained for the plane wing configurations and the values of drag for zero leading-edge suction might be expected due to the sharpness of the leading edges of the wings. These results indicate that the wing twist and camber of the ogee and delta configurations resulted in some reduction in induced drag at a Mach number of 0.90 but that only slight differences existed between the induced drag of the plane and the twisted and cambered trapezoid wing configurations. The results of the investigation of reference 31, however, indicated that the wing twist and camber of the trapezoid configuration resulted in substantial improvements in the drag characteristics at the design Mach number of 2.20.

Low-speed trimmed lift coefficients and supersonic performance.- The variations of angle of attack with trimmed lift coefficient at a Mach number of 0.40 and of maximum lift-drag ratio with Mach numbers ranging from 1.80 to 2.86 are presented in figure 23. The trimmed lift coefficients shown in figure 23 were determined for the three wing planform configurations at an adjusted longitudinal stability level of 5 percent of the reference chord and the trimmed lift data shown for the twisted and cambered wing configurations were obtained by utilizing the elevon control effectiveness of the plane wing configurations. These results indicate that the effect of wing planform on trimmed lift coefficient at landing attitudes of about 12° was insignificant. Wing twist and camber, however, are shown to have a large effect on the trimmed lift coefficients of the three wing planform configurations. On the basis of the data shown in figure 23, it would be expected that substantially higher trimmed lift coefficients would be expected for the twisted and cambered trapezoid configuration near reasonable landing attitudes than for the twisted and cambered ogee or delta configurations. This effect is attributed to the higher lift-curve slope and higher values of zero-lift pitching-moment coefficient indicated for the twisted and cambered trapezoid configuration. In addition, the supersonic results contained in references 31 and 32 indicated that the trapezoid configurations exhibited larger maximum lift-drag ratios than the delta or ogee configurations throughout the supersonic Mach number range of 1.80 to 2.86. The supersonic results of the aforementioned investigations also indicated larger pitching-moment coefficients at zero lift for the twisted and cambered trapezoid configuration than for the twisted and cambered ogee and delta configurations; these larger coefficients would naturally result in lower trim-drag penalties for the trapezoid configuration at a given level of longitudinal stability.

Lateral Characteristics

Variations of the lateral aerodynamic coefficients of the plane ogee wing with sideslip angle β are presented in figure 24. Figure 25 compares the lateral aerodynamic characteristics of the twisted and cambered wing configurations throughout the Mach number range of the investigation.

Directional stability is evident for the three twisted and cambered wing configurations up to high angles of attack for Mach numbers of 0.40 to 1.14. (See fig. 25.) The static directional stability exhibited by the twisted and cambered delta and trapezoid wing configurations was very nearly the same and considerably greater than the directional stability of the twisted and cambered ogee wing configuration. The smaller values of directional stability indicated for the ogee configuration are presumed to be due in part to the comparatively forward location of the large twist and camber in the leading edge of the wing near the root section. (See figs. 3 and 6.)

The effective dihedral parameters indicate static lateral stability for angles of attack greater than zero degrees for the three twisted and cambered wing configurations throughout the Mach number range of the investigation.

CONCLUDING REMARKS

A study was made at Mach numbers ranging from 0.40 to 1.14 to determine the aerodynamic characteristics of three different wing planforms (ogee, delta, and trapezoid) both with and without wing twist and camber. The experimental results indicated that the wing planform differences had only small effects on the aerodynamic center shifts with Mach number and on the trimmed lift coefficients at landing attitudes. The wing twist and camber effects, however, were significant and the results indicated that the trapezoid configurations, which had the highest values of pitching-moment coefficient at zero lift, would exhibit the highest trimmed lift coefficients of the twisted and cambered wing configurations near reasonable landing attitudes.

The static lateral data indicated that the twisted and cambered wing configurations have positive directional stability and positive effective dihedral throughout the Mach number range of 0.40 to 1.14. The directional stability, however, of the twisted and cambered delta and trapezoid configurations was considerably greater than the directional stability of the twisted and cambered ogee configurations.

Langley Research Center,
National Aeronautics and Space Administration,
Langley Station, Hampton, Va., November 30, 1965.

REFERENCES

1. Sleeman, William C., Jr.; Reed, James D.; and Gainer, Thomas G.: Aerodynamic Characteristics of a Transport Airplane Configuration Having Tail Surfaces Located Outboard of the Wing Tips at Mach Numbers of 2.30, 2.96, 3.95, and 4.63. NASA TM X-556, 1961.

2. Sleeman, William C., Jr.; Ray, Edward J.; and Fournier, Paul G.: Low-Speed Effects of High-Lift Devices on the Aerodynamic Characteristics of a Supersonic Transport Model With Outboard Tails. NASA TM X-895, 1963.

3. Carraway, Ausley, B.; Gregory, Donald T.; and Carmel, Melvin M.: An Exploratory Investigation of a Transport Configuration Designed for Supersonic Cruise Flight Near a Mach Number of 3. NASA TM X-216, 1960.

4. Morris, Owen G.; Carmel, Melvin M.; and Carraway, Ausley B.: An Investigation at Mach Numbers From 0.20 to 4.63 of the Aerodynamic Performance, Static Stability, and Trimming Characteristics of a Canard Configuration Designed for Efficient Supersonic Cruise Flight. NASA TM X-617, 1961.

5. Carraway, Ausley B.; Morris, Owen G.; and Carmel, Melvin M.: Aerodynamic Characteristics at Mach Numbers From 0.20 to 4.63 of a Canard-Type Supersonic Commercial Air Transport Configuration. NASA TM X-628, 1962.

6. Spencer, Bernard, Jr.: Low-Speed Wind-Tunnel Investigation of the Effects of Canard Planform and Wing High-Lift Devices on the Longitudinal Aerodynamic Characteristics of a Supersonic Transport Configuration. NASA TM X-753, 1963.

7. Whitcomb, Richard T.: An Approach to Obtaining Increased Supersonic Lift-Drag Ratios and Reduced Sonic Boom. NASA TM X-799, 1963.

8. Whitcomb, Richard T.; Patterson, James C., Jr.; and Kelly, Thomas C.: An Investigation of Subsonic, Transonic, and Supersonic Aerodynamic Characteristics of a Proposed Arrow-Wing Transport Airplane Configuration. NASA TM X-800, 1963.

9. Whitcomb, Richard T.; and Loving, Donald L.: An Investigation of the Landing and Take-Off Characteristics of a Proposed Arrow-Wing Transport Airplane Configuration. NASA TM X-801, 1963.

10. Patterson, James C., Jr.: Subsonic, Transonic, and Supersonic Aerodynamic Characteristics of a Modified Arrow-Wing Transport Airplane Configuration. NASA TM X-911, 1964.

11. Phillips, W. Pelham; and Spencer, Bernard, Jr.: Low-Speed Aerodynamic Characteristics of a Proposed Supersonic Transport Configuration Having a 53.13^{o} Delta Wing and Forward and Aft Controls in Combination. NASA TM X-823, 1963.

12. Brady, James A.; Page, V. Robert; and Koenig, David G.: Large-Scale Low-Speed Wind-Tunnel Tests of a Delta Winged Supersonic Transport Model With a Delta Canard Control Surface. NASA TM X-643, 1962.

13. Koenig, David G.; Brady, James A.; and Page, V. Robert: Large-Scale Wind-Tunnel Tests at Low Speed of a Delta Winged Supersonic Transport Model in the Presence of the Ground. NASA TM X-644, 1962.

14. Fletcher, LeRoy S.: Static Stability Characteristics of a Delta-Winged Configuration With a Canard Control and Nacelles at Mach Numbers From 0.25 to 3.50. NASA TM X-651, 1962.

15. Fletcher, LeRoy S.: Static Stability Characteristics of a Delta-Winged Airplane Configuration With Nacelles, a Trapezoidal Canard and a Drooped Tail at Mach Numbers From 0.70 to 3.52. NASA TM X-780, 1963.

16. Fletcher, LeRoy S.: Dynamic Rotary Stability Derivatives of a Delta-Winged Configuration With a Canard Control and Nacelles at Mach Numbers From 0.25 to 3.50. NASA TM X-781, 1963.

17. Koenig, David G.; and Corsiglia, Victor R.: Large-Scale Low-Speed Wind-Tunnel Tests of a Delta Wing Supersonic Transport Model With Various Canard, Horizontal-Tail, and Wing Modifications. NASA TM X-857, 1964.

18. Henderson, William P.: Selected Results From a Low-Speed Investigation of the Aerodynamic Characteristics of a Supersonic Transport Configuration Having an Outboard-Pivot Variable-Sweep Wing. NASA TM X-839, 1963.

19. Jernell, Lloyd S.: The Effects of Conical Camber on the Longitudinal Aerodynamic Characteristics of a Variable-Sweep Wing-Fuselage Configuration at Mach Numbers From 0.50 to 3.50. NASA TM X-804, 1963.

20. Ward, Robert J.; and McKee, John W.: Low-Speed Aerodynamic Stability and Control Characteristics of a Cambered Fuselage, Variable-Sweep Supersonic Transport Configuration. NASA TM X-632, 1962.

21. Vogler, Raymond D.; and Turner, Thomas R.: Exploratory Low-Speed Wind-Tunnel Stability Investigation of a Supersonic Transport Configuration With Variable-Sweep Wings. NASA TM X-597, 1961.

22. Vogler, Raymond D.: Low-Speed Wind-Tunnel Stability Investigation of a Supersonic Transport Model With Variable-Sweep Wings Equipped With High-Lift Devices. NASA TM X-728, 1962.

23. Sleeman, William C., Jr.; and Robins, A. Warner: Low-Speed Investigation of the Aerodynamic Characteristics of a Variable-Sweep Supersonic Transport Configuration Having a Blended Wing and Body. NASA TM X-619, 1962.

24. Sleeman, William C., Jr.: Low-Speed Investigation of the Effects of Horizontal Tail Height and Extension of the Wing-Root Leading-Edge Sections on a Variable-Sweep Supersonic Transport Configuration. NASA TM X-681, 1962.

25. Henderson, William P.: Low-Speed Longitudinal Stability Characteristics of a Supersonic Transport Configuration With Variable-Sweep Wings Employing a Double Inboard Pivot. NASA TM X-744, 1962.

26. Shaw, David S.; and Henderson, William P.: Wind-Tunnel Investigation at Mach Numbers From 1.60 to 2.86 of the Static Aerodynamic Characteristics of a Supersonic Transport Configuration With Variable-Sweep Wings Employing a Double Inboard Pivot. NASA TM X-745, 1962.

27. Alford, William J., Jr.; Hammond, Alexander D., and Henderson, William P.: Low-Speed Stability Characteristics of a Supersonic Transport Model With a Blended Wing-Body, Variable-Sweep Auxiliary Wing Panels, Outboard Tail Surfaces, and Simplified High-Lift Devices. NASA TM X-802, 1963.

28. Robins, A. Warner; Spearman, M. Leroy; and Harris, Roy V., Jr.: Aerodynamic Characteristics at Mach Numbers of 2.30, 2.60, and 2.96 of a Supersonic Transport Model With a Blended Wing-Body, Variable-Sweep Auxiliary Wing Panels, Outboard Tail Surfaces, and a Design Mach Number of 2.6. NASA TM X-815, 1963.

29. Driver, Cornelius; Spearman, M. Leroy; and Corlett, William A.: Aerodynamic Characteristics at Mach Numbers From 1.61 to 2.86 of a Supersonic Transport Model With a Blended Wing-Body, Variable-Sweep Auxiliary Wing Panels, Outboard Tail Surfaces and a Design Mach Number of 2.2. NASA TM X-817, 1963.

30. Lockwood, Vernard E.; McKinney, Linwood W.; and Lamar, John E.: Low-Speed Aerodynamic Characteristics of a Supersonic Transport Model With a High-Aspect-Ratio Variable-Sweep Warped Wing. NASA TM X-979, 1964.

31. Foster, Gerald V.; and Corlett, William A.: Aerodynamic Characteristics of a Tailless Fixed-Wing Supersonic Transport Configuration at Mach Number 2.20. NASA TM X-960, 1964.

32. Corlett, William A.; and Foster, Gerald V.: Aerodynamic Characteristics of a Tailless Fixed-Wing Supersonic Transport Model at Mach Numbers From 1.60 to 2.86. NASA TM X-992, 1964.

33. Mechtly, E. A.: The International System of Units – Physical Constants and Conversion Factors. NASA SP-7012, 1964.

34. Carlson, Harry W.; and Middleton, Wilbur D.: A Numerical Method for the Design of Camber Surfaces of Supersonic Wings With Arbitrary Planforms. NASA TN D-2341, 1964.

35. Sommer, Simon C.; and Short, Barbara J.: Free-Flight Measurements of Turbulent-Boundary-Layer Skin Friction in the Presence of Severe Aerodynamic Heating at Mach Numbers From 2.8 to 7.0. NACA TN 3391, 1955.

36. Hoerner, Sighard F.: Fluid-Dynamic Drag. Publ. by the author (148 Busteed Drive, Midland Park, N.J.), 1958.

37. Lowry, John G.; and Polhamus, Edward C.: A Method for Predicting Lift Increments Due to Flap Deflection at Low Angles of Attack in Incompressible Flow. NACA TN 3911, 1957.

TABLE I.- GEOMETRIC CHARACTERISTICS OF MODEL

[Scale 1/40]

Ogee wings:		
Aspect ratio	1.55	
Span	19.25 in^2	48.90 cm^2)
Plane wing wetted area (excludes nacelle area)	325.18 in^2	(2097.93 cm^2)
Twisted and cambered wing wetted area (excludes nacelle area)	329.98 in^2	(2128.90 cm^2)
Reference area	239.76 in^2	(1546.84 cm^2)
Root chord	27.78 in.	(70.56 cm)
Reference chord	12.00 in.	(30.48 cm)
Mean aerodynamic chord	16.81 in.	(42.70 cm)
Delta wings:		
Sweep of leading edge	68°	
Aspect ratio	1.55	
Span	19.25 in.	(48.90 cm)
Wetted wing area (excludes nacelle area)	335.94 in^2	(2167.35 cm^2)
Reference area	239.76 in^2	(1546.84 cm^2)
Root chord	24.87 in.	(63.17 cm)
Reference chord	12.00 in.	(30.48 cm)
Mean aerodynamic chord	16.56 in.	(42.06 cm)
Trapezoid wings:		
Sweep of leading edge	65°	
Aspect ratio	1.55	
Span	19.25 in.	(48.90 cm)
Wetted wing area (excludes nacelle area)	344.90 in^2	(2225.16 cm^2)
Reference area	239.76 in^2	(1546.84 cm^2)
Root chord	23.30 in.	(59.18 cm)
Tip chord	1.84 in.	(4.67 cm)
Reference chord	12.00 in.	(30.48 cm)
Mean aerodynamic chord	15.46 in.	(39.27 cm)
Fuselage:		
Length	42.50 in.	(107.95 cm)
Balance chamber area	2.40 in^2	(15.48 cm^2)
Vertical tail:		
Root chord	7.64 in.	(19.48 cm)
Tip chord	2.40 in.	(6.10 cm)
Area	21.64 in^2	(139.61 cm^2)
Nacelles:		
Length	10.25 in.	(26.04 cm)
Capture area (each)	1.04 in^2	(6.71 cm^2)
Base area (each)	0.96 in^2	(6.19 cm^2)

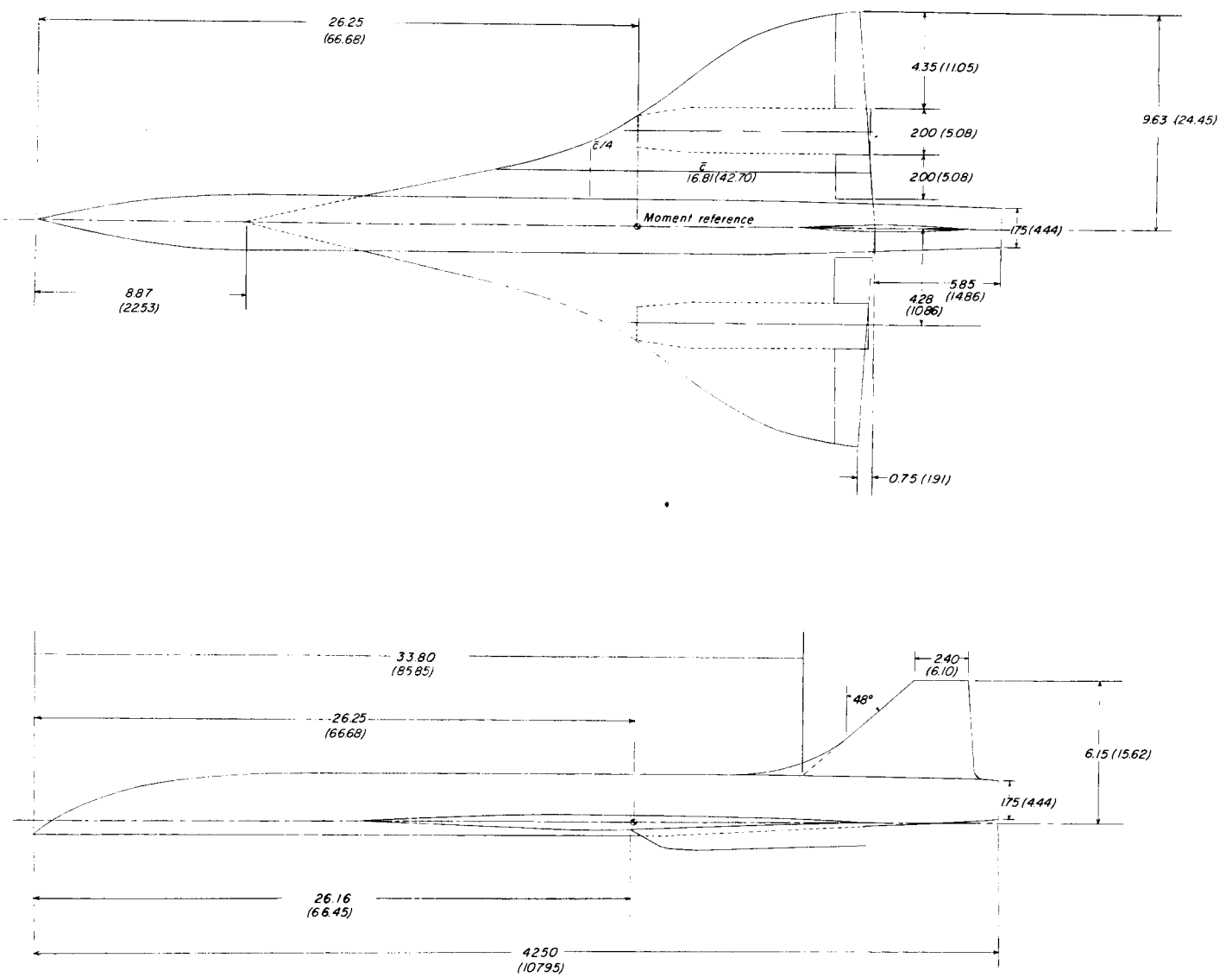

(a) Ogee wing configuration.

Figure 1.- Details of model. All linear dimensions in inches (centimeters).

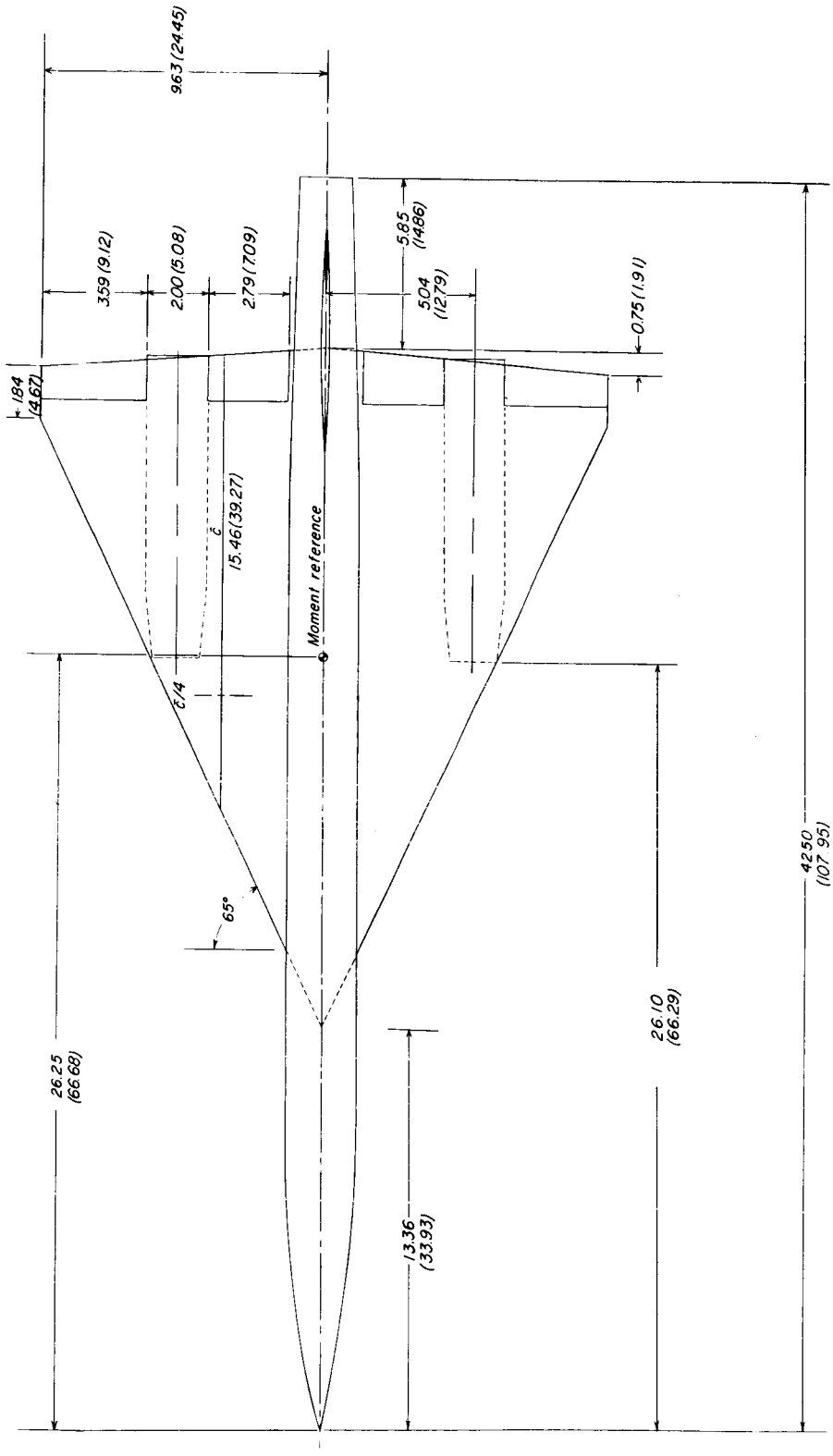

(b) Trapezoid wing configuration.

Figure 1.- Continued.

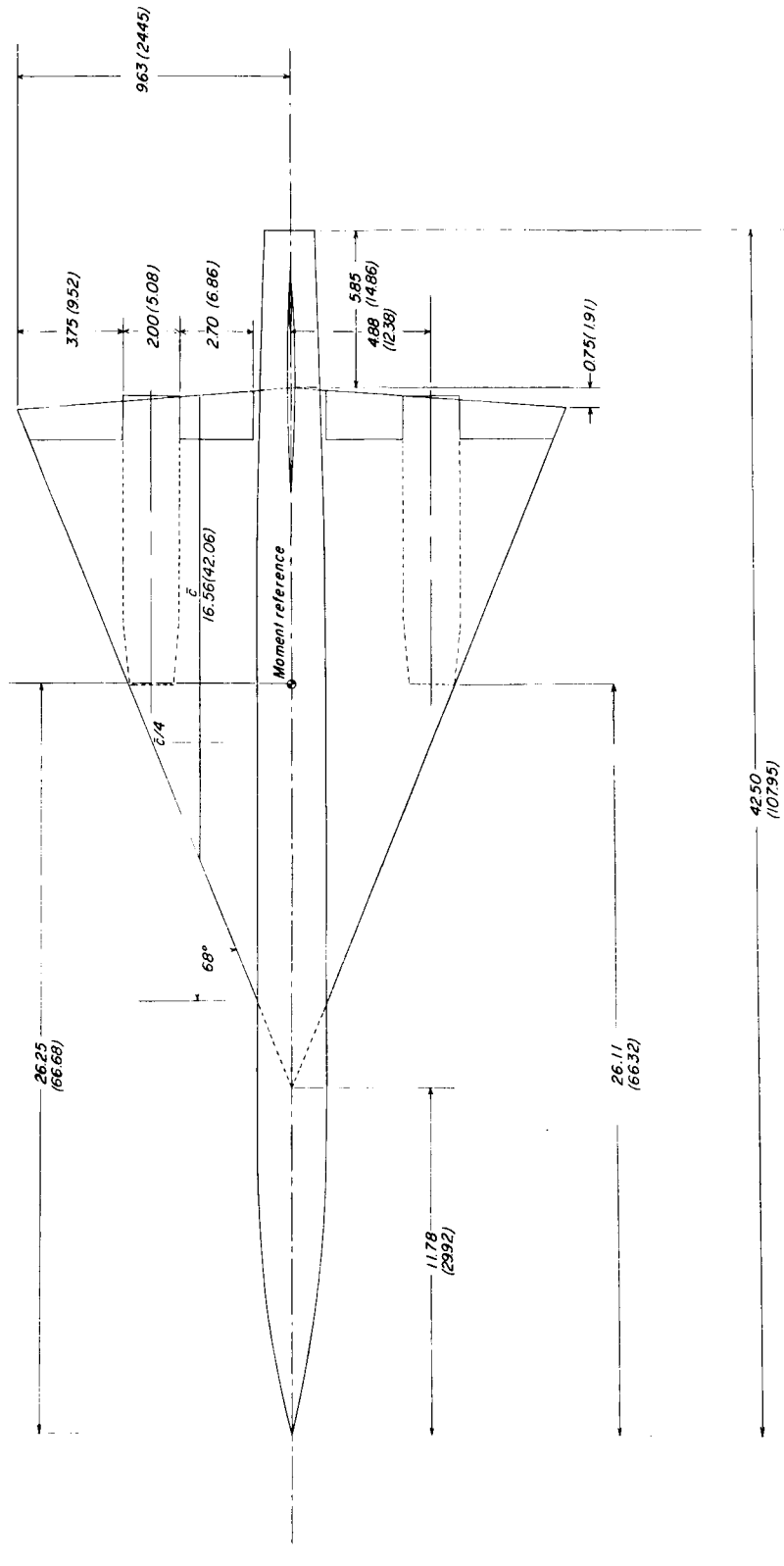

(c) Delta wing configuration.

Figure 1.- Continued.

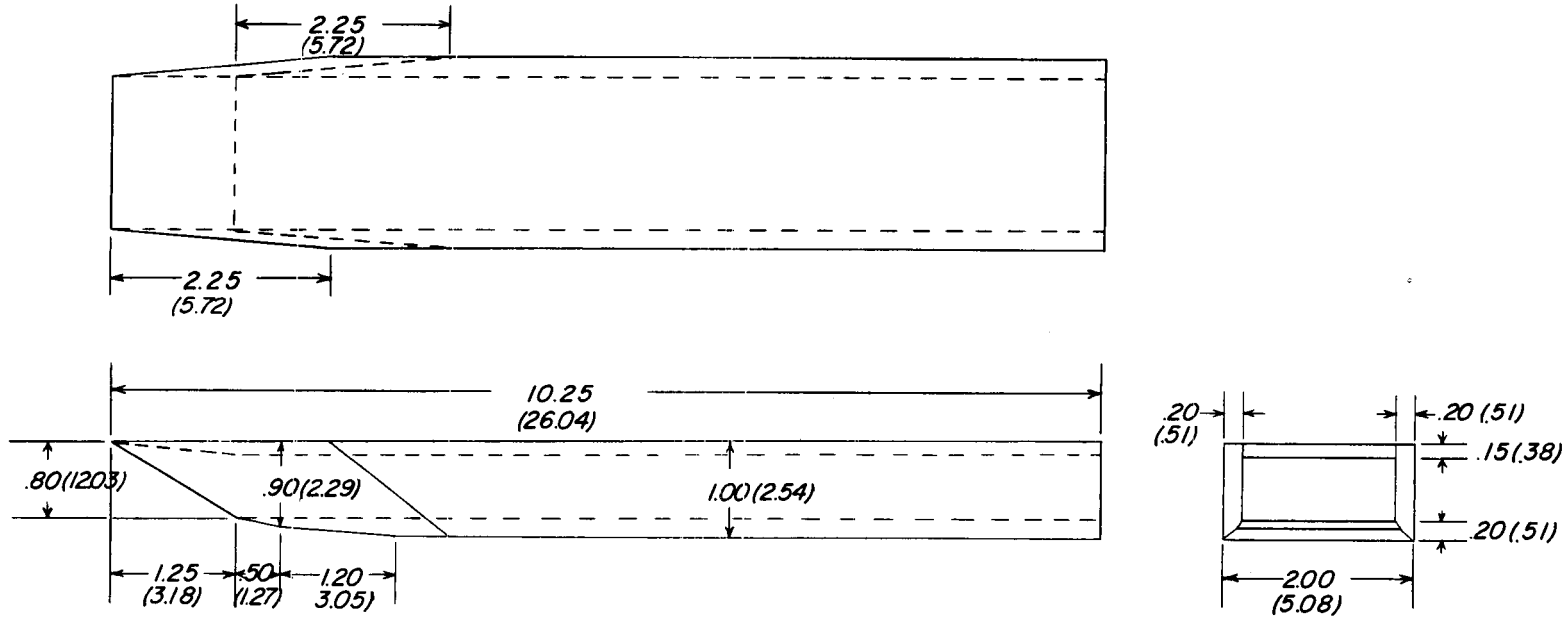

(c) Nacelle details.

Figure 1.- Continued.

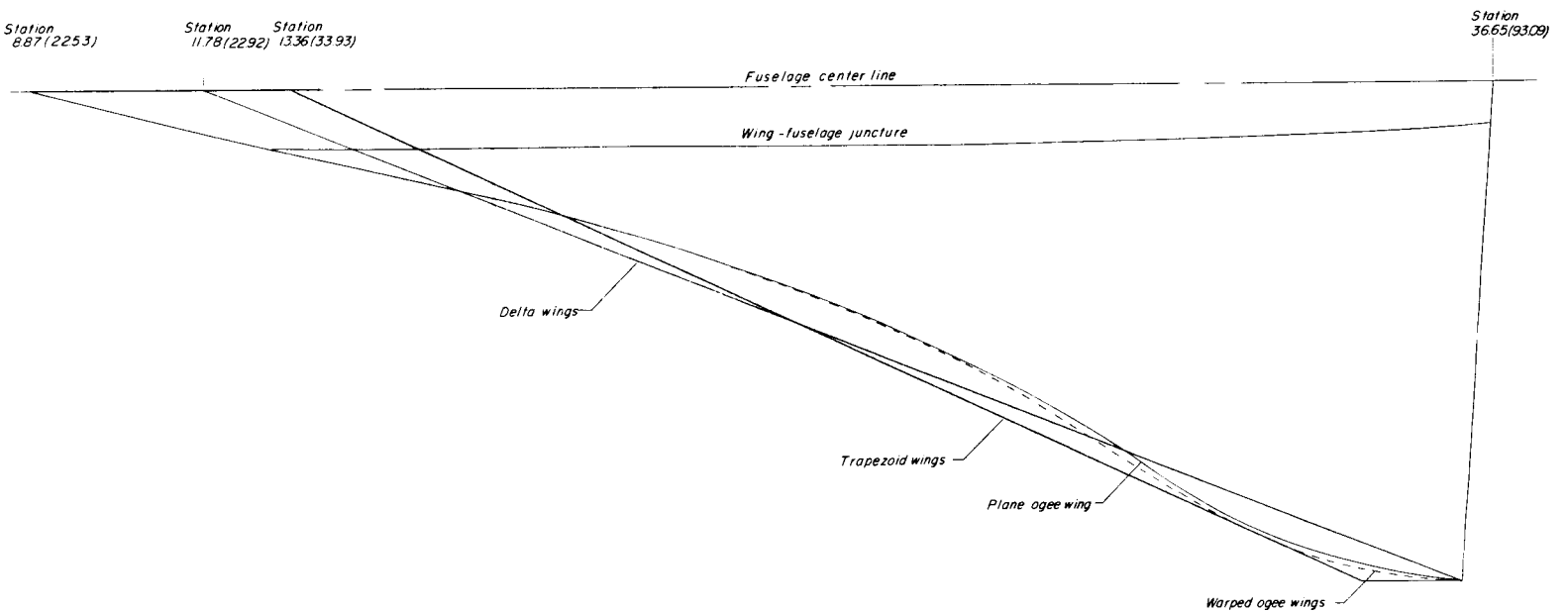

(e) Comparison of wing planforms.

Figure 1.- Continued.

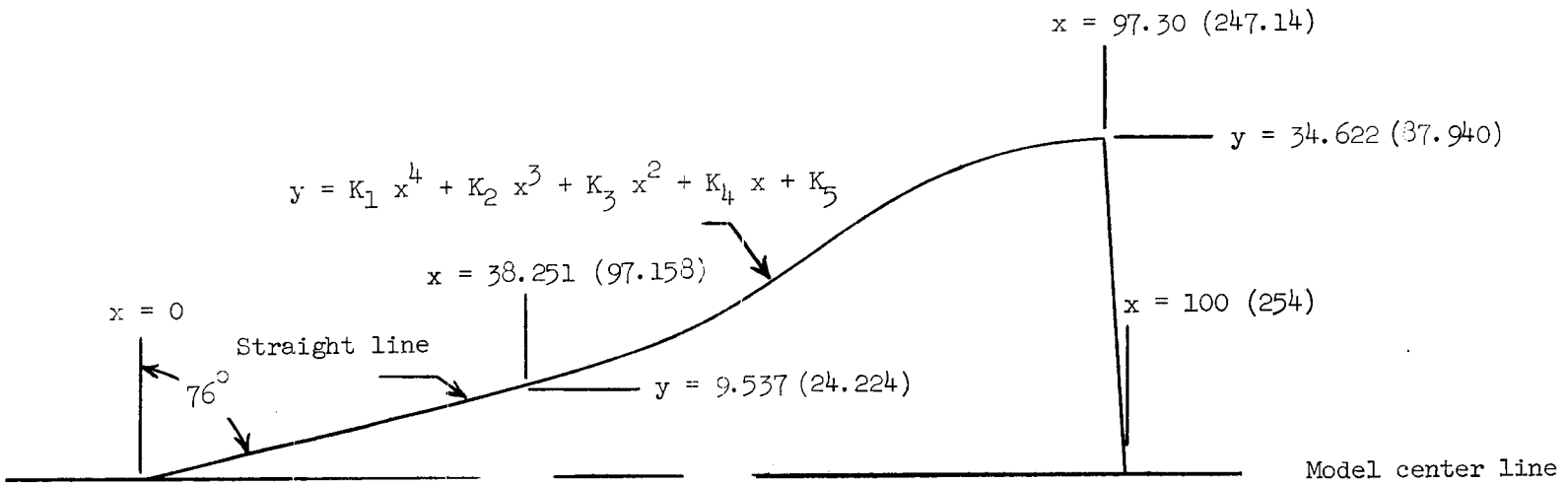

For $y \leq 9.537$ (24.224), $y = 0.24933x$

$y \geq 9.537$ (24.224), $y = K_1 x^4 + K_2 x^3 + K_3 x^2 + K_4 x + K_5$

Where:
$K_1 = -0.0000010$
$K_2 = 0.0001155$
$K_3 = -0.0004708$
$K_4 = 0.29036$
$K_5 = 15.04824$

(f) Equations for leading edge of twisted and cambered ogee wing configuration, Ogee II.

Figure 1.- Concluded.

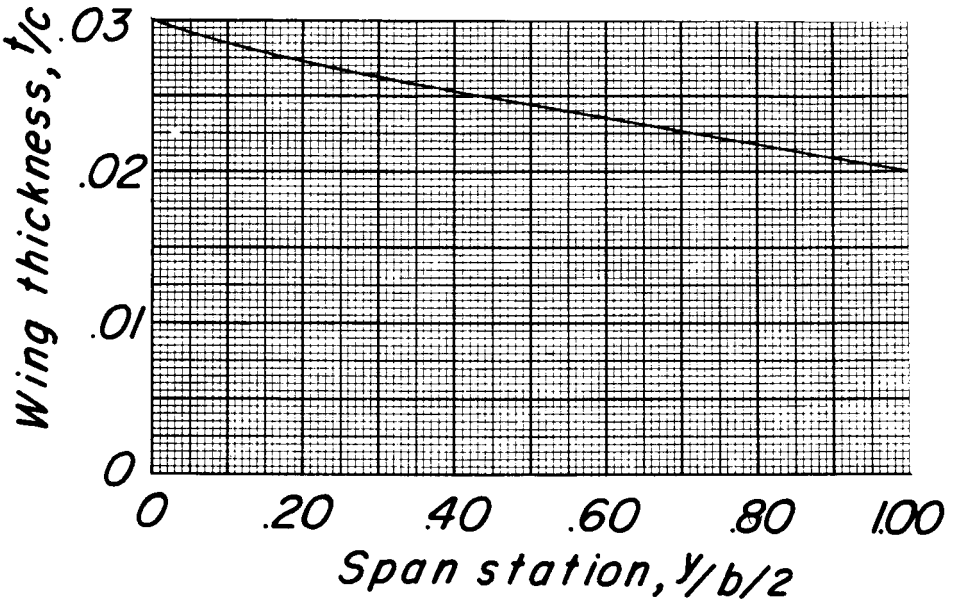

Figure 2.- Spanwise thickness distribution of wing planforms.

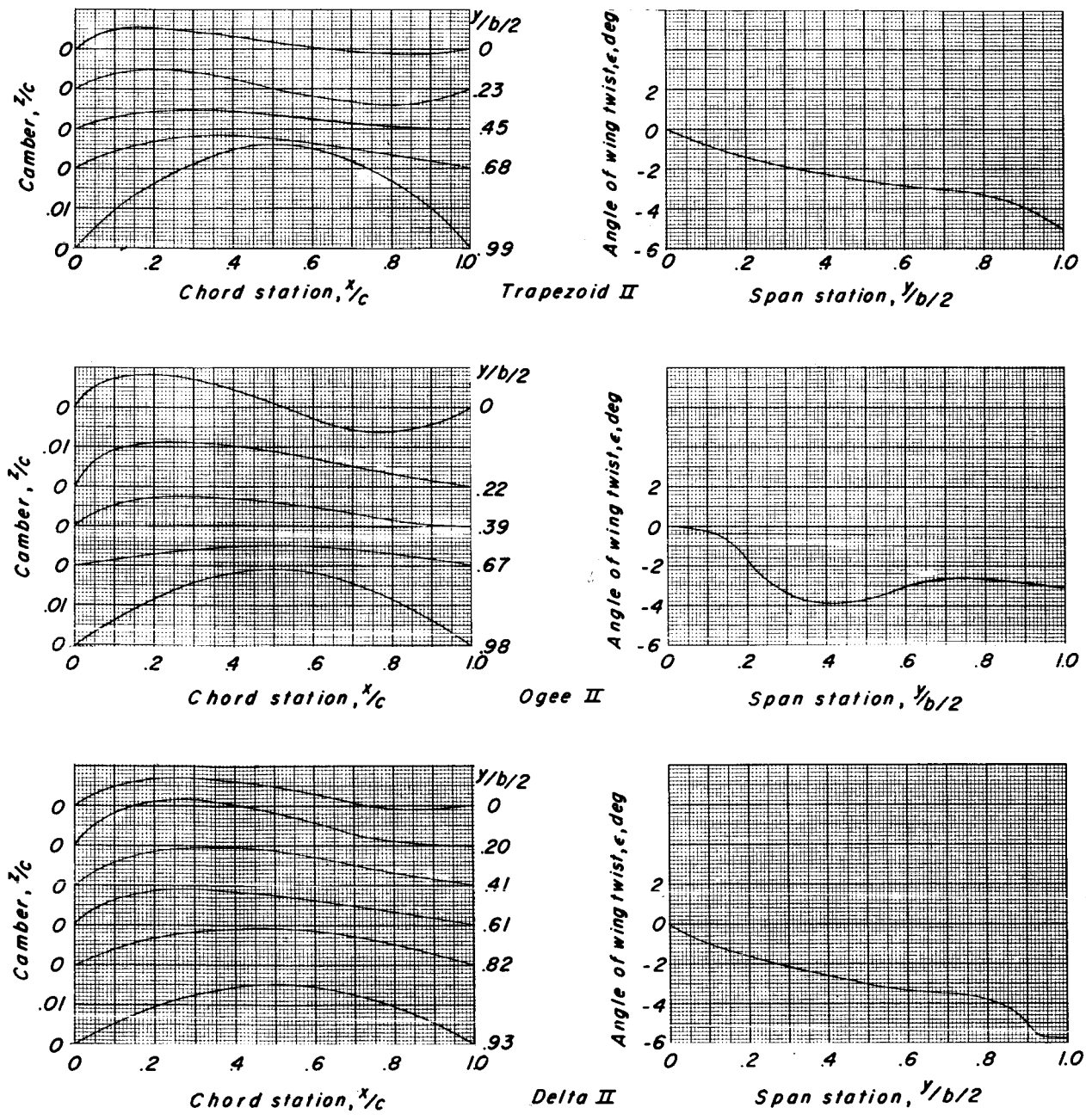

Figure 3.- Camber and twist distributions for ogee, delta, and trapezoid wing configurations (Ogee II, Delta II, and Trapezoid II).

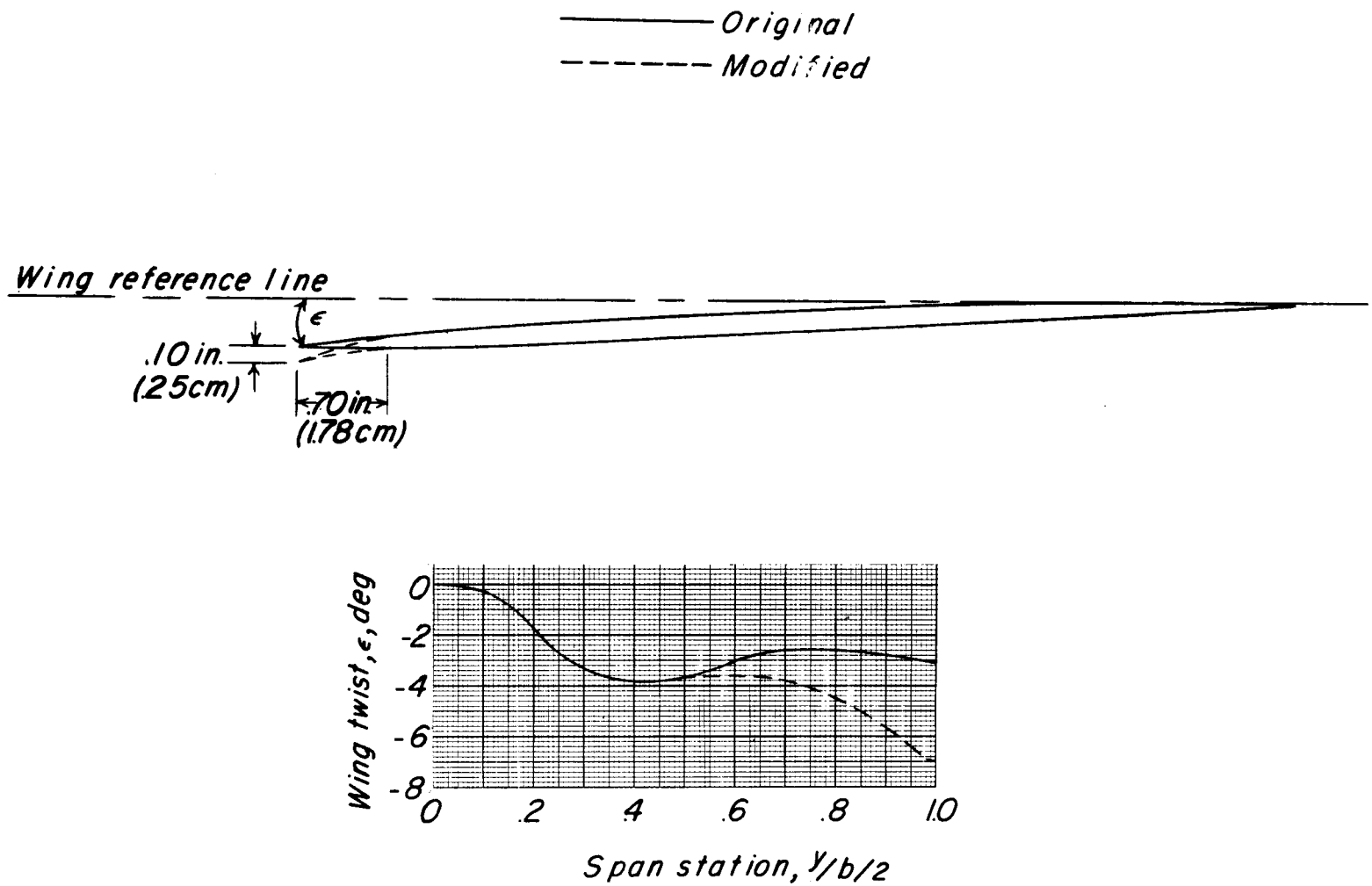

Figure 4.- Twist variation and typical section for modified twisted and cambered ogee wing configuration, Ogee III.

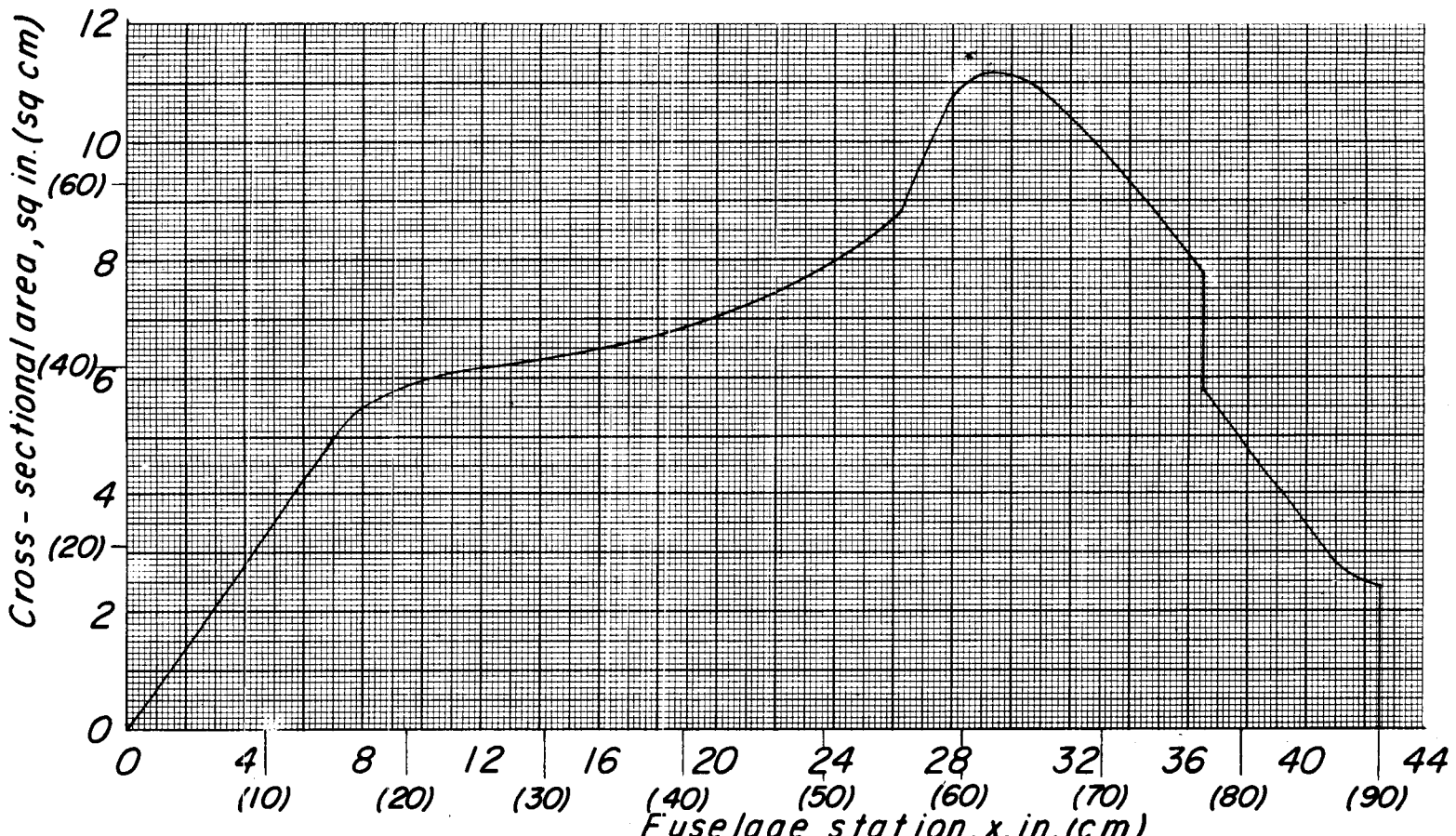

Figure 5.- Cross-sectional area distribution of twisted and cambered ogee wing configuration, Ogee II.

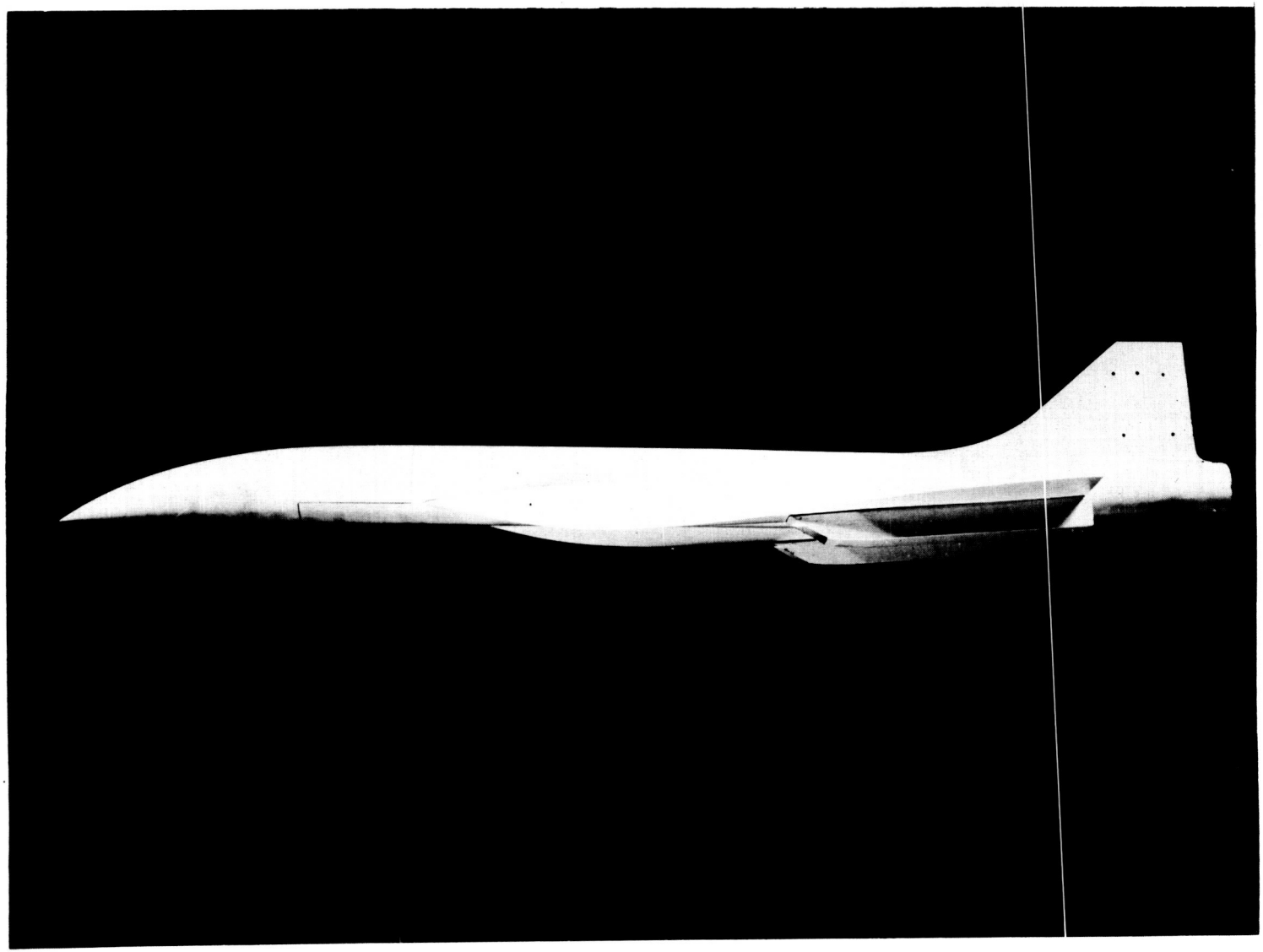

(a) Side view.

L-63-10126

Figure 6.- Photographs of twisted and cambered ogee wing configuration, Ogee II.

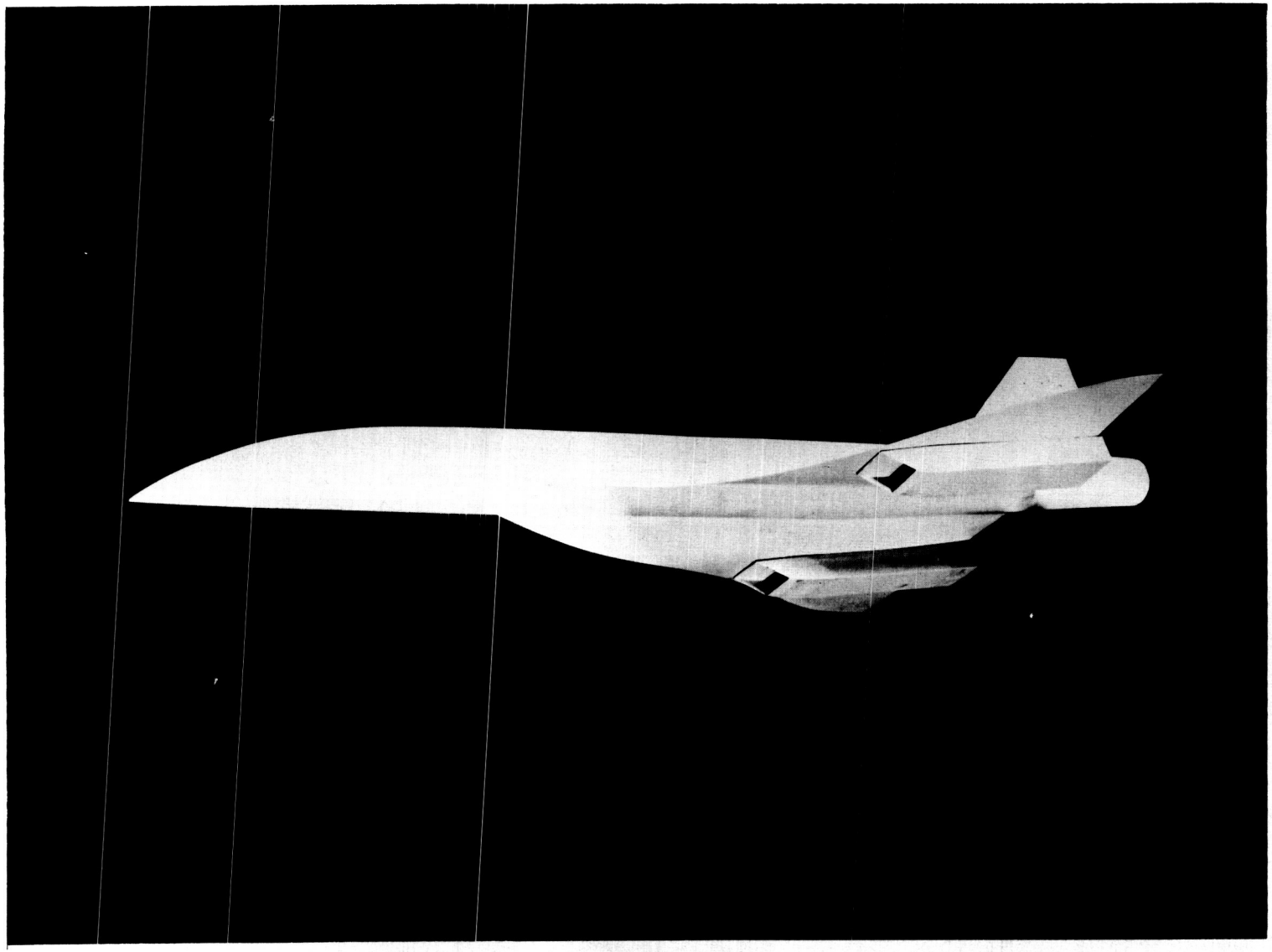

(b) Three-quarter front view. L-63-10127

Figure 6.- Concluded.

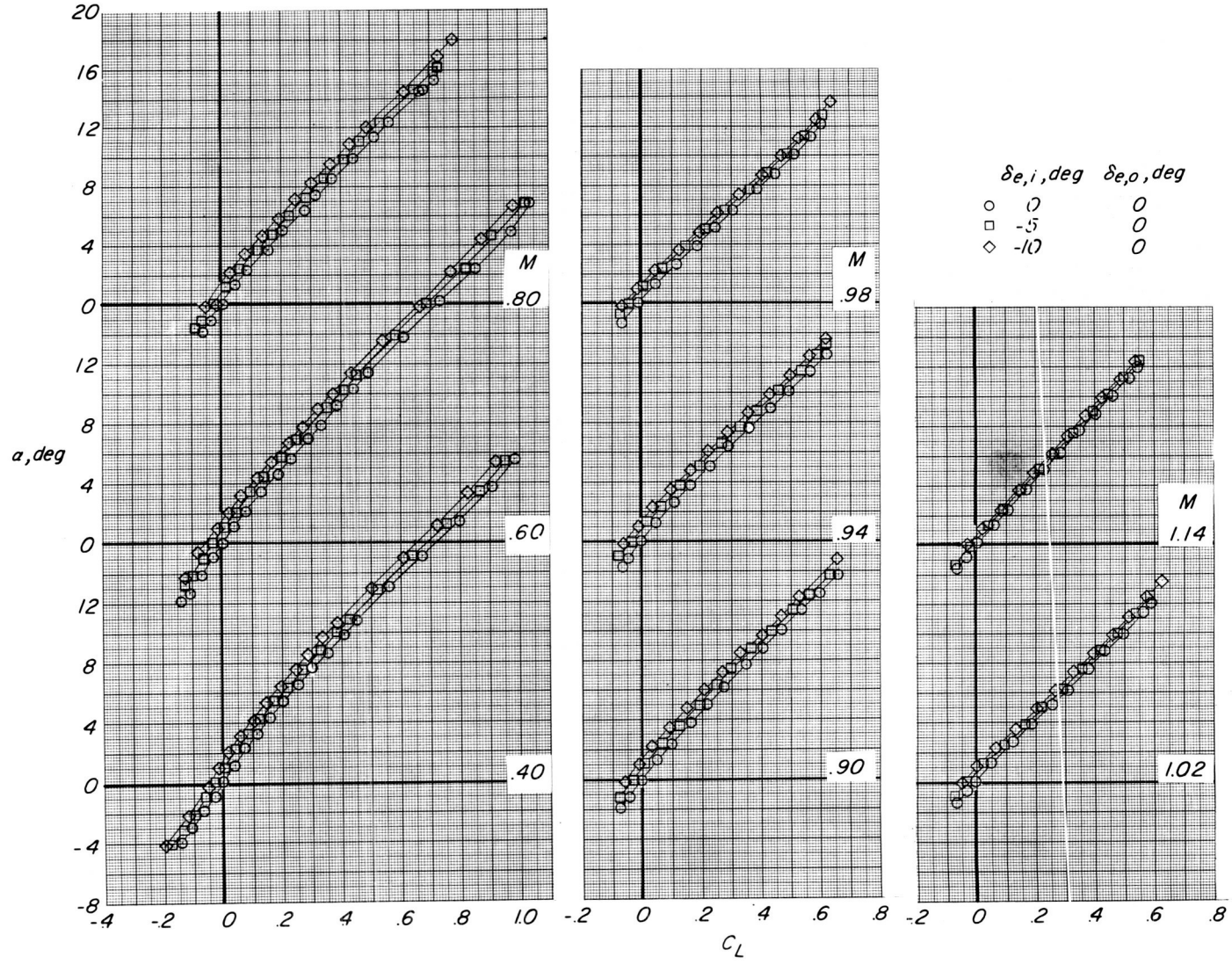

(a) Variation of α with C_L.

Figure 7.- Effect of inboard elevon deflection on longitudinal aerodynamic characteristics of plane ogee wing configuration at Mach numbers from 0.40 to 1.14.

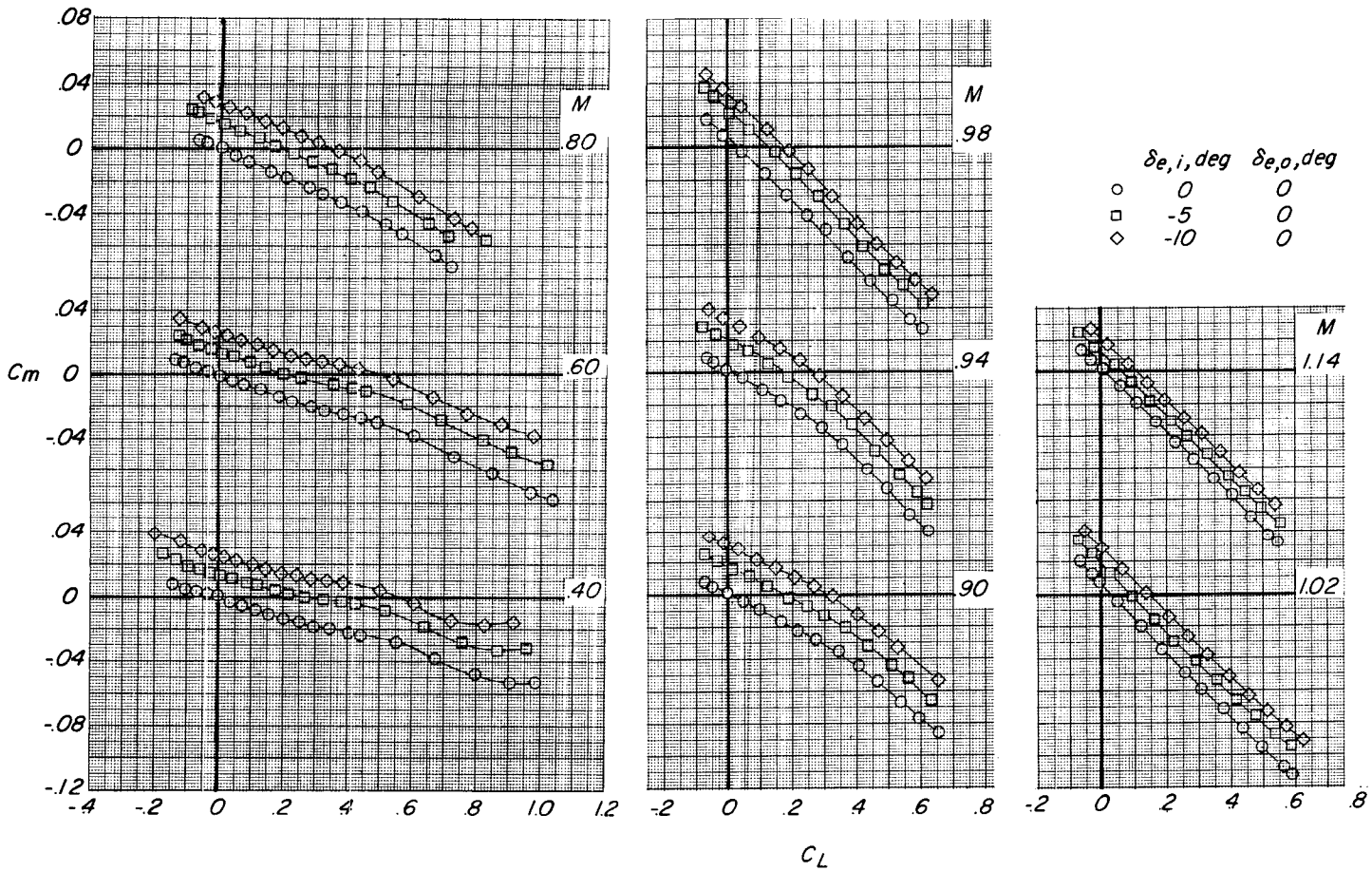

(b) Variation of C_m with C_L.

Figure 7.- Continued.

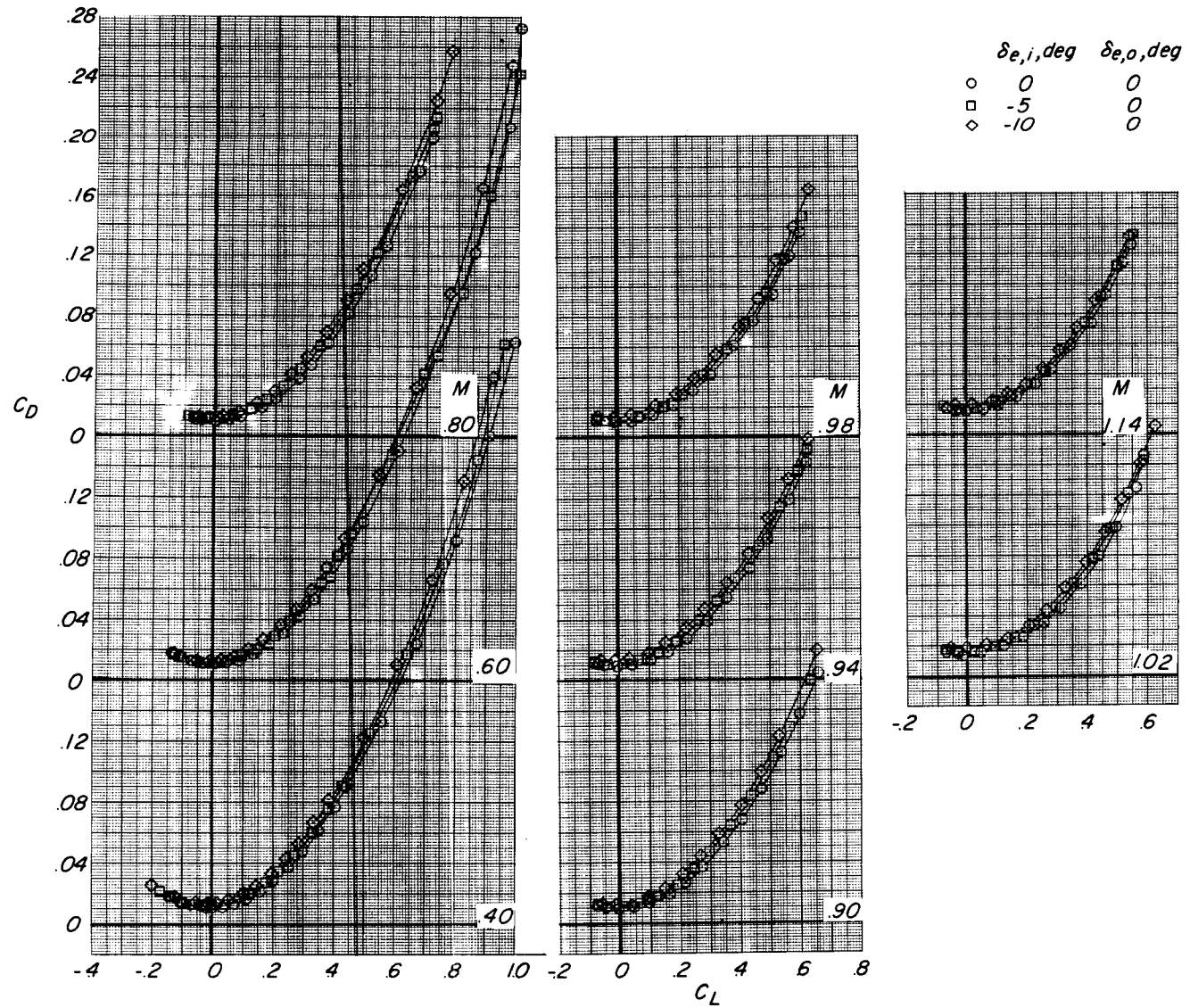

(c) Variation of C_D with C_L.

Figure 7.- Concluded.

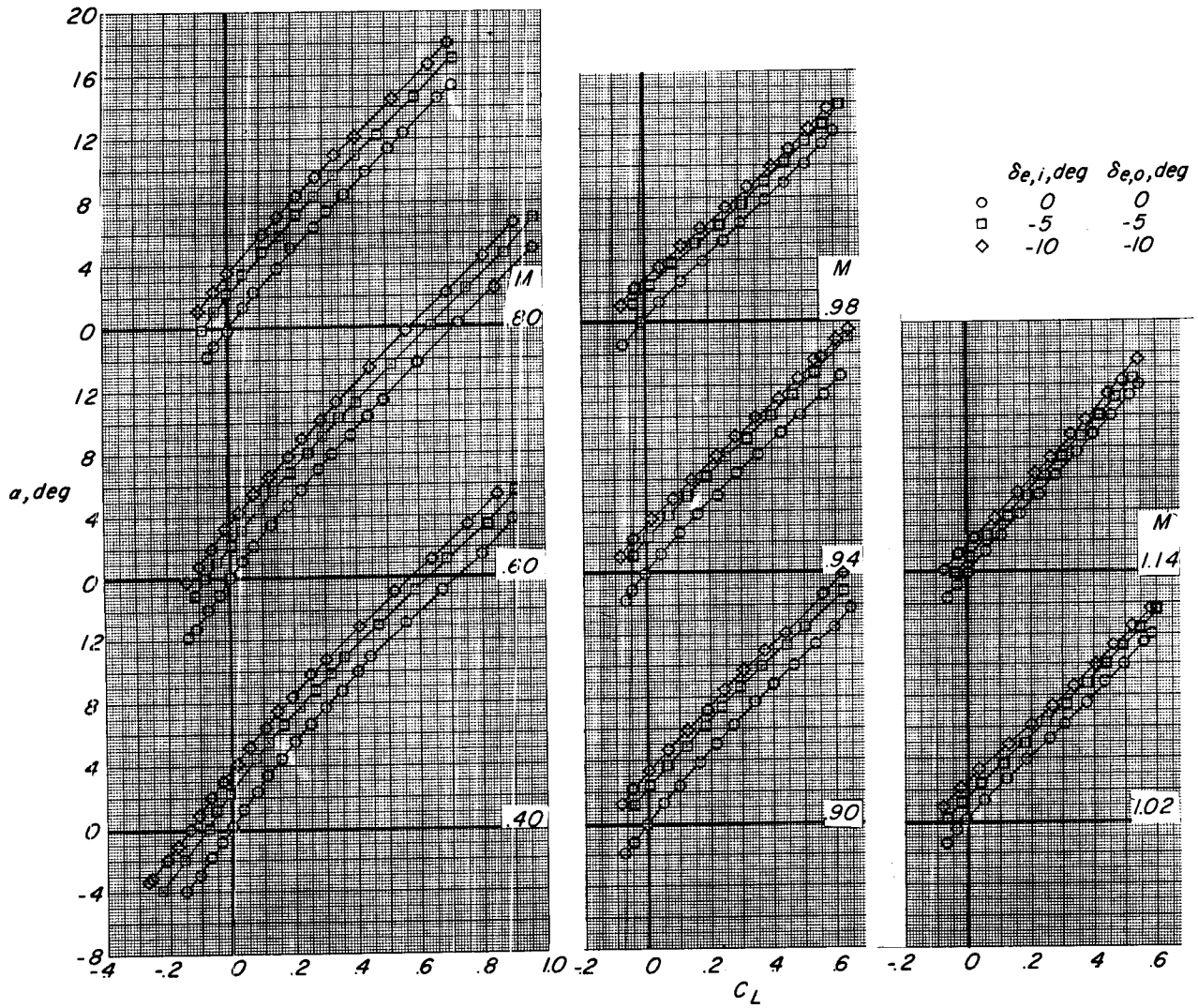

(a) Variation of α with C_L.

Figure 8.- Effect of inboard and outboard elevon deflection on longitudinal aerodynamic characteristics of plane ogee wing configuration at Mach numbers from 0.40 to 1.14.

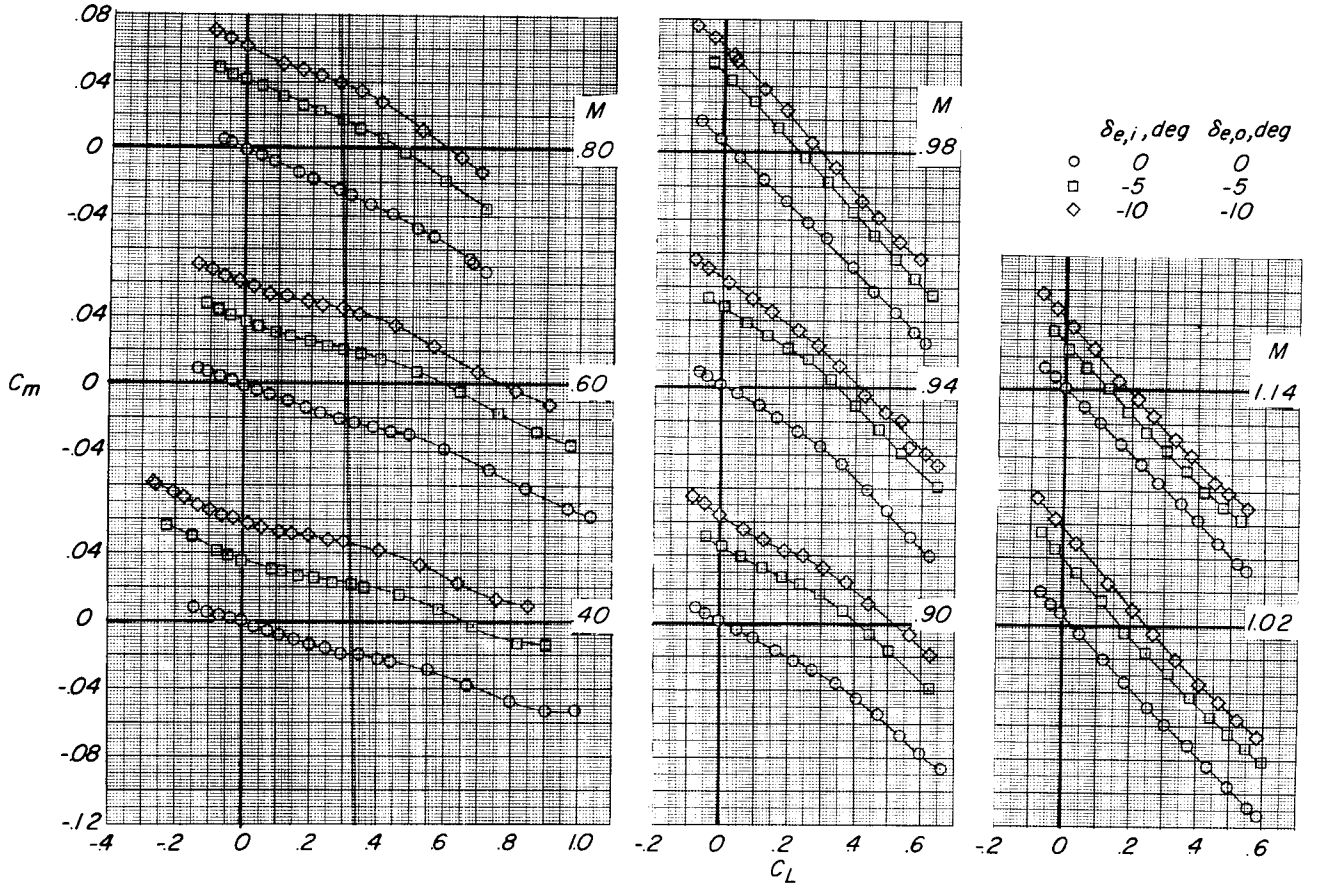

(b) Variation of C_m with C_L.

Figure 8.- Continued.

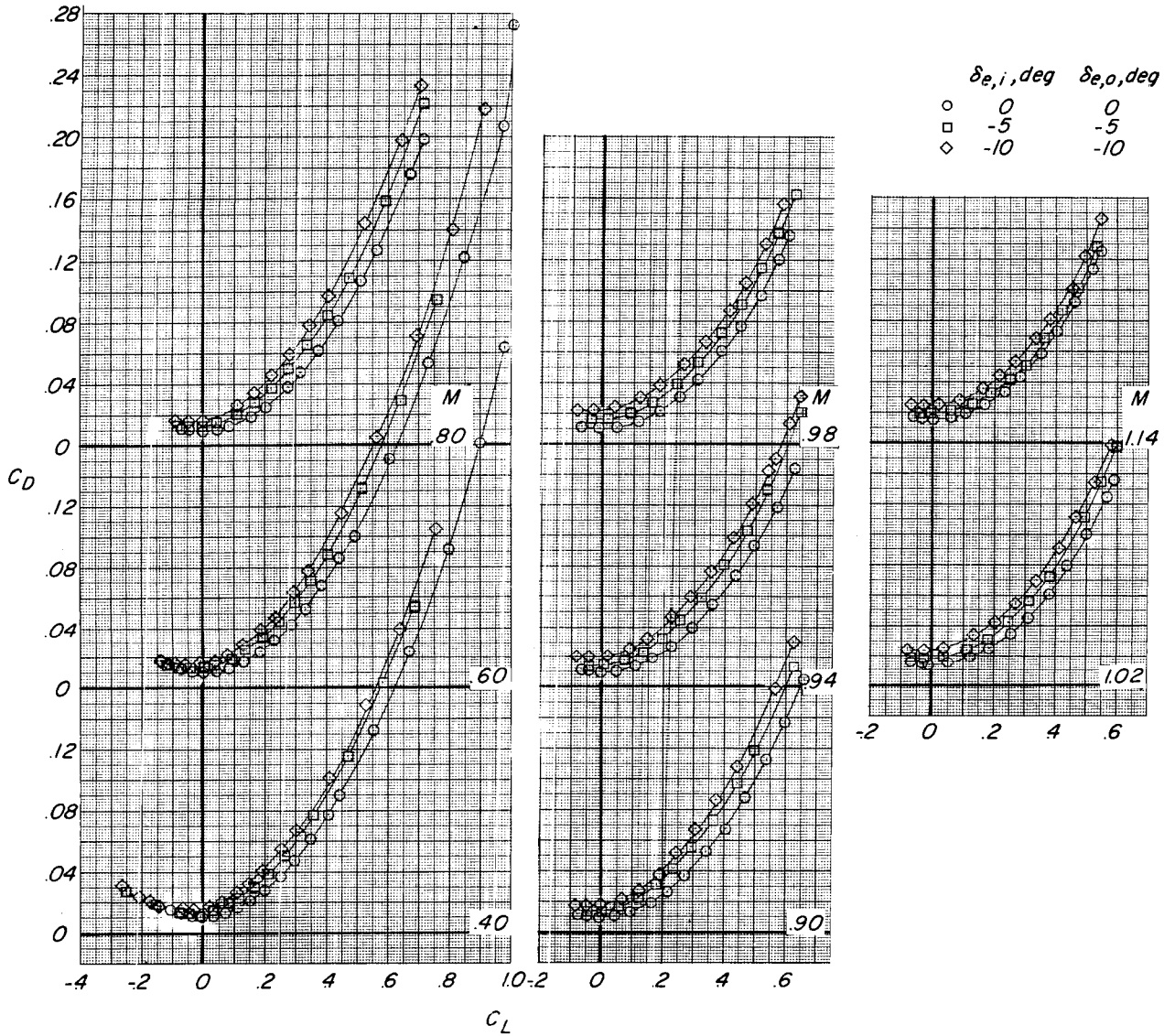

(c) Variation of C_D with C_L.

Figure 8.- Concluded.

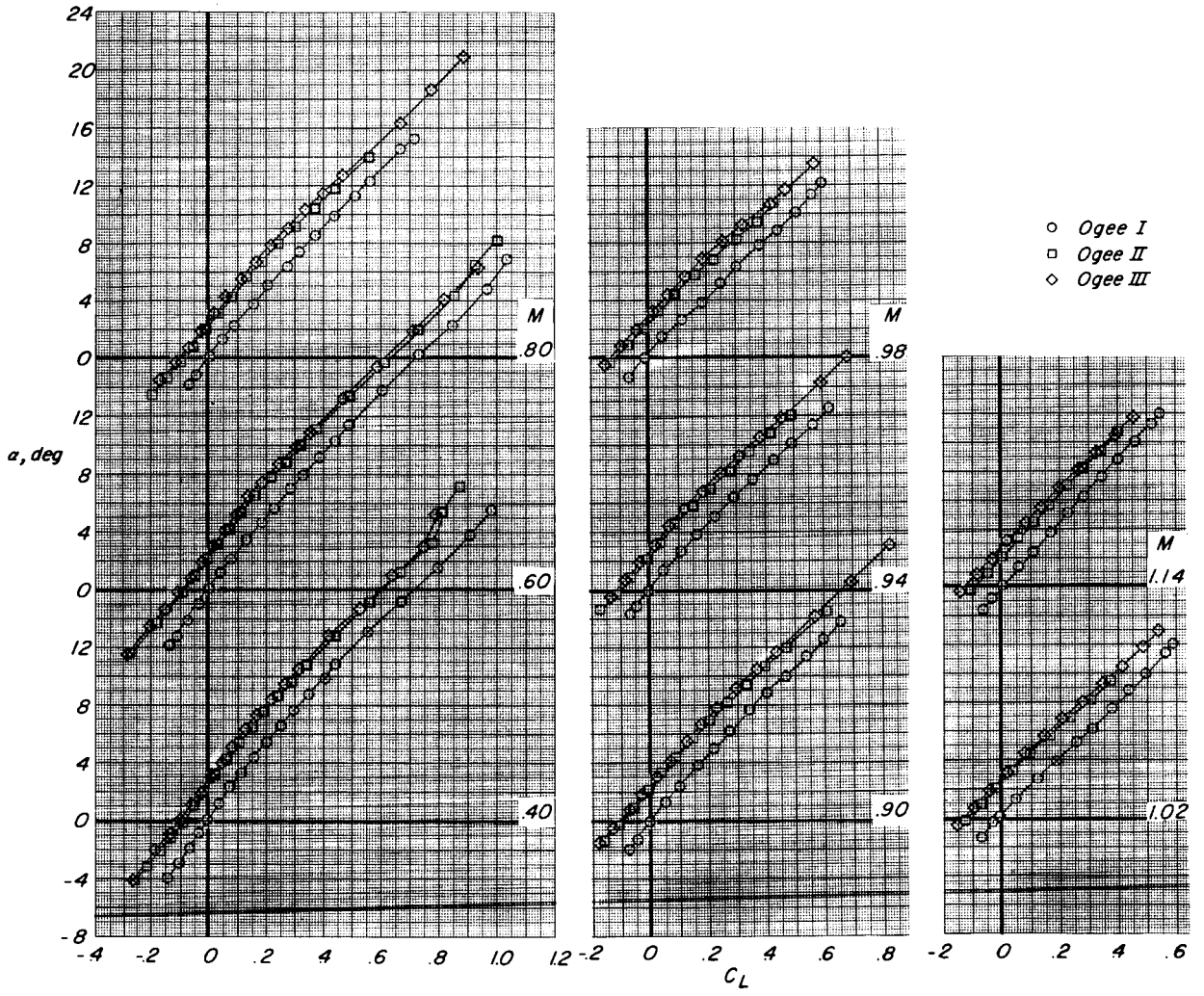

(a) Variation of α with C_L.

Figure 9.- Effect of twist and camber on longitudinal aerodynamic characteristics of ogee wing configurations at Mach numbers from 0.40 to 1.14.

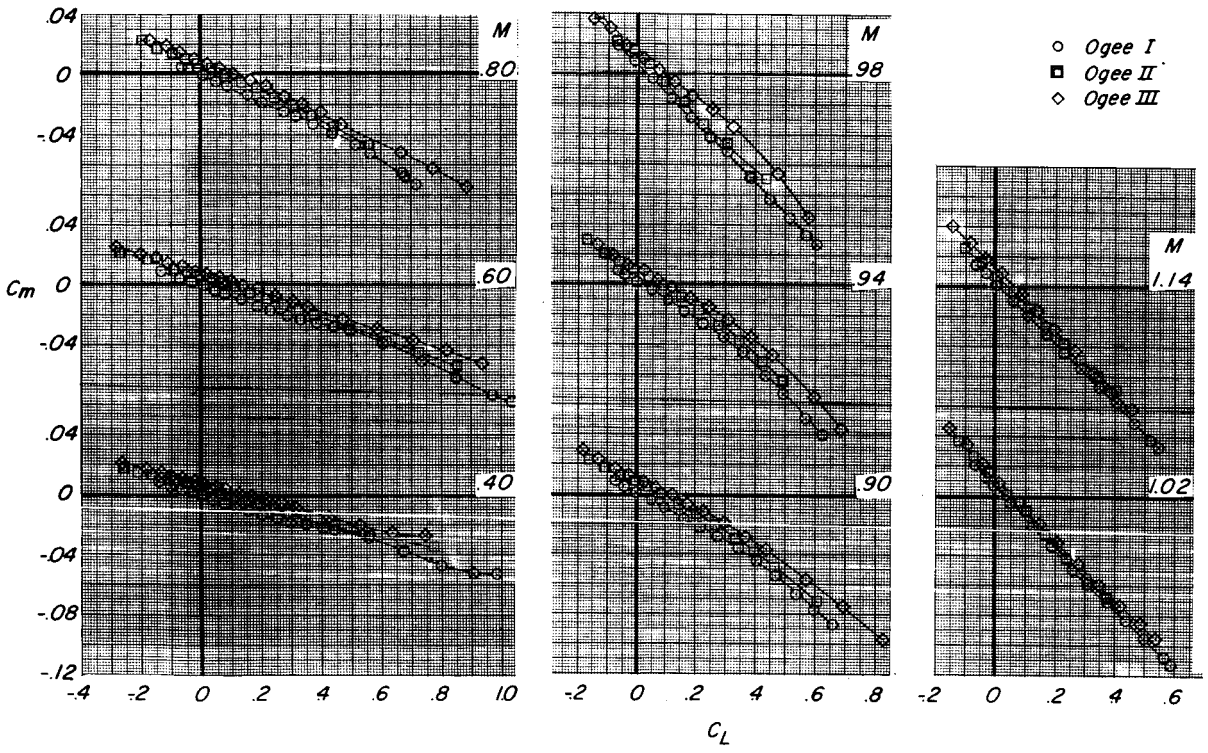

(b) Variation of C_m with C_L.

Figure 9.- Continued.

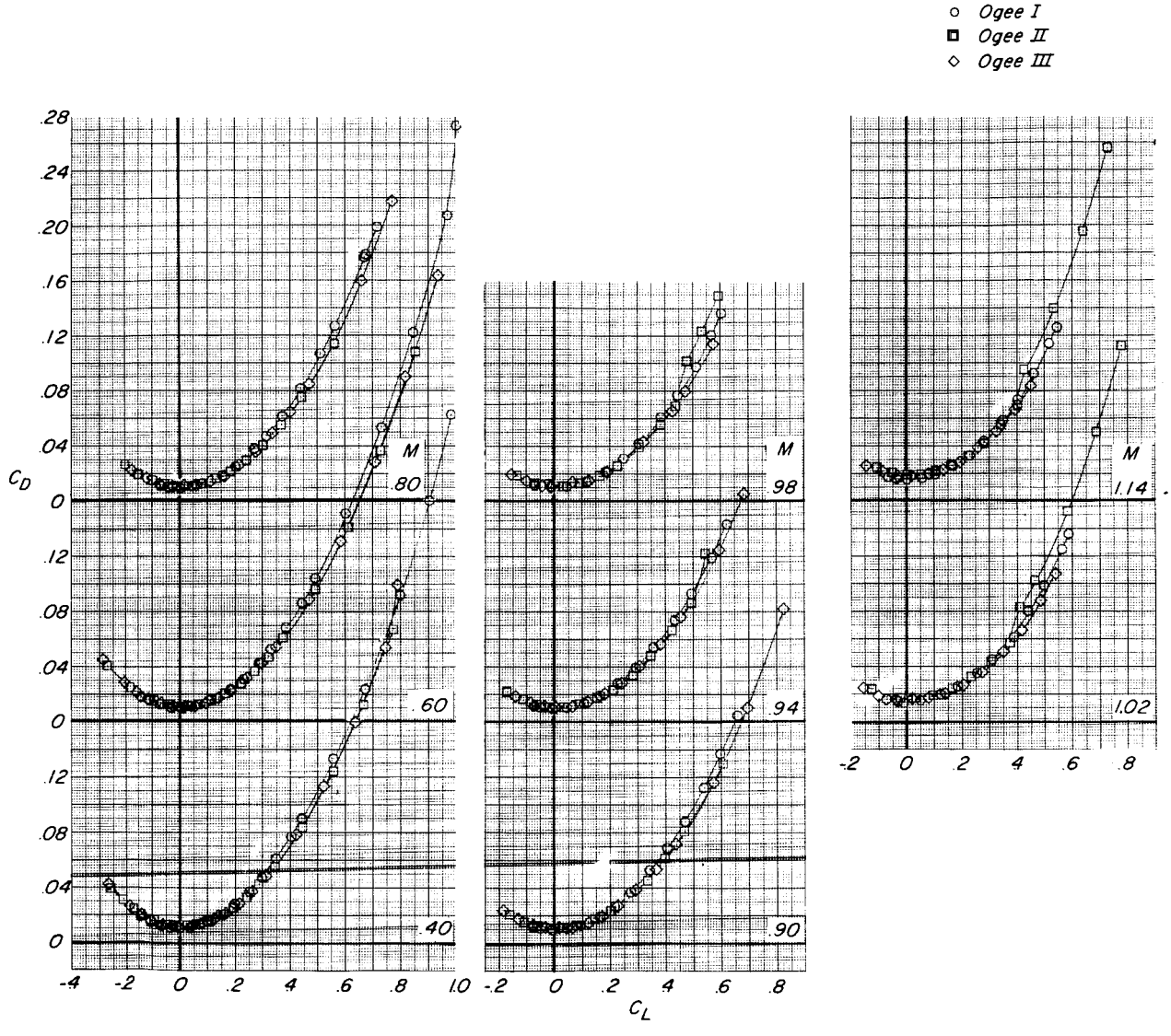

(c) Variation of C_D with C_L.

Figure 9.- Concluded.

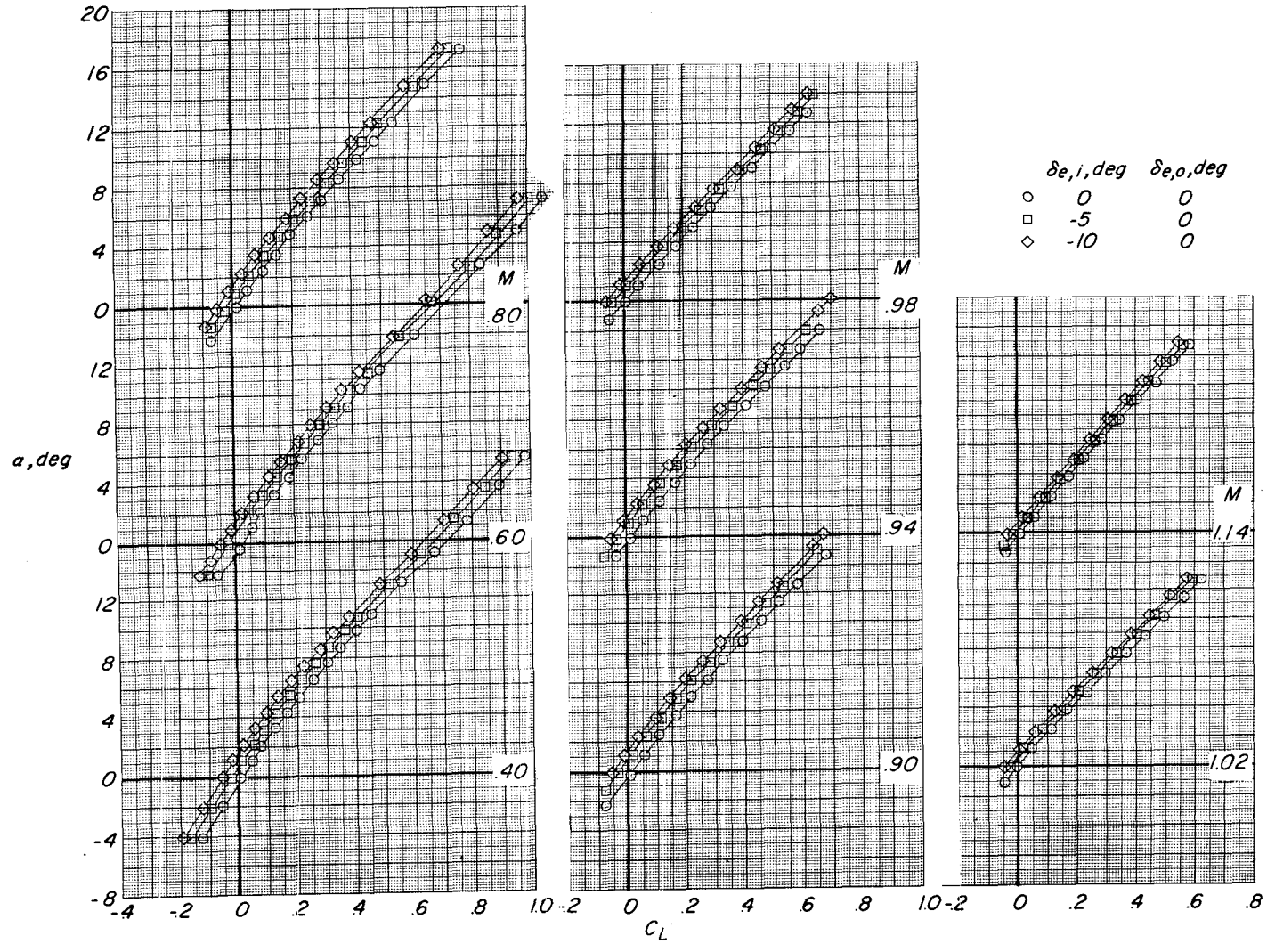

(a) Variation of α with C_L.

Figure 10.- Effect of inboard elevon deflection on longitudinal aerodynamic characteristics of plane delta wing configuration at Mach numbers from 0.40 to 1.14.

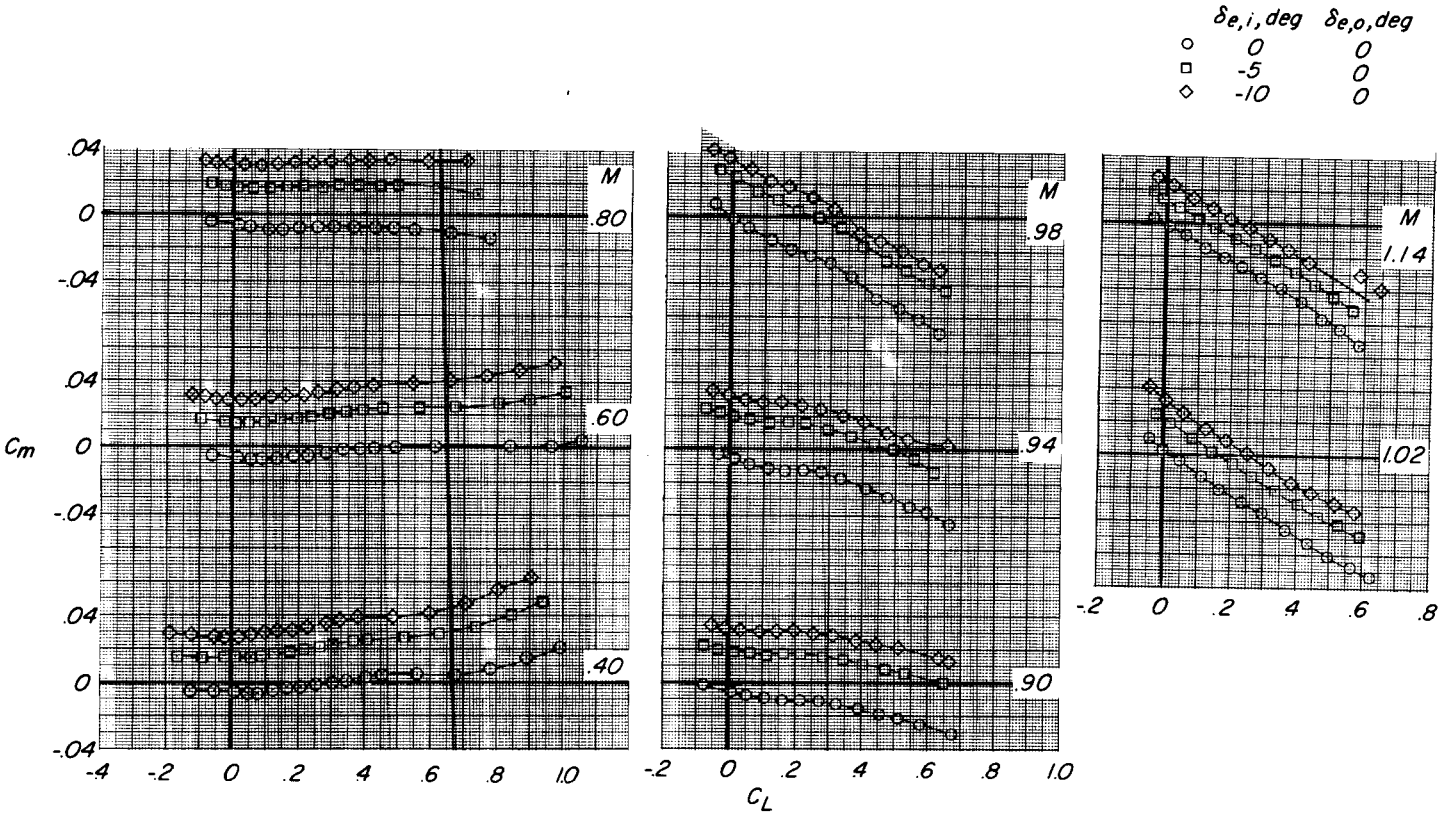

(b) Variation of C_m with C_L.

Figure 10.- Continued.

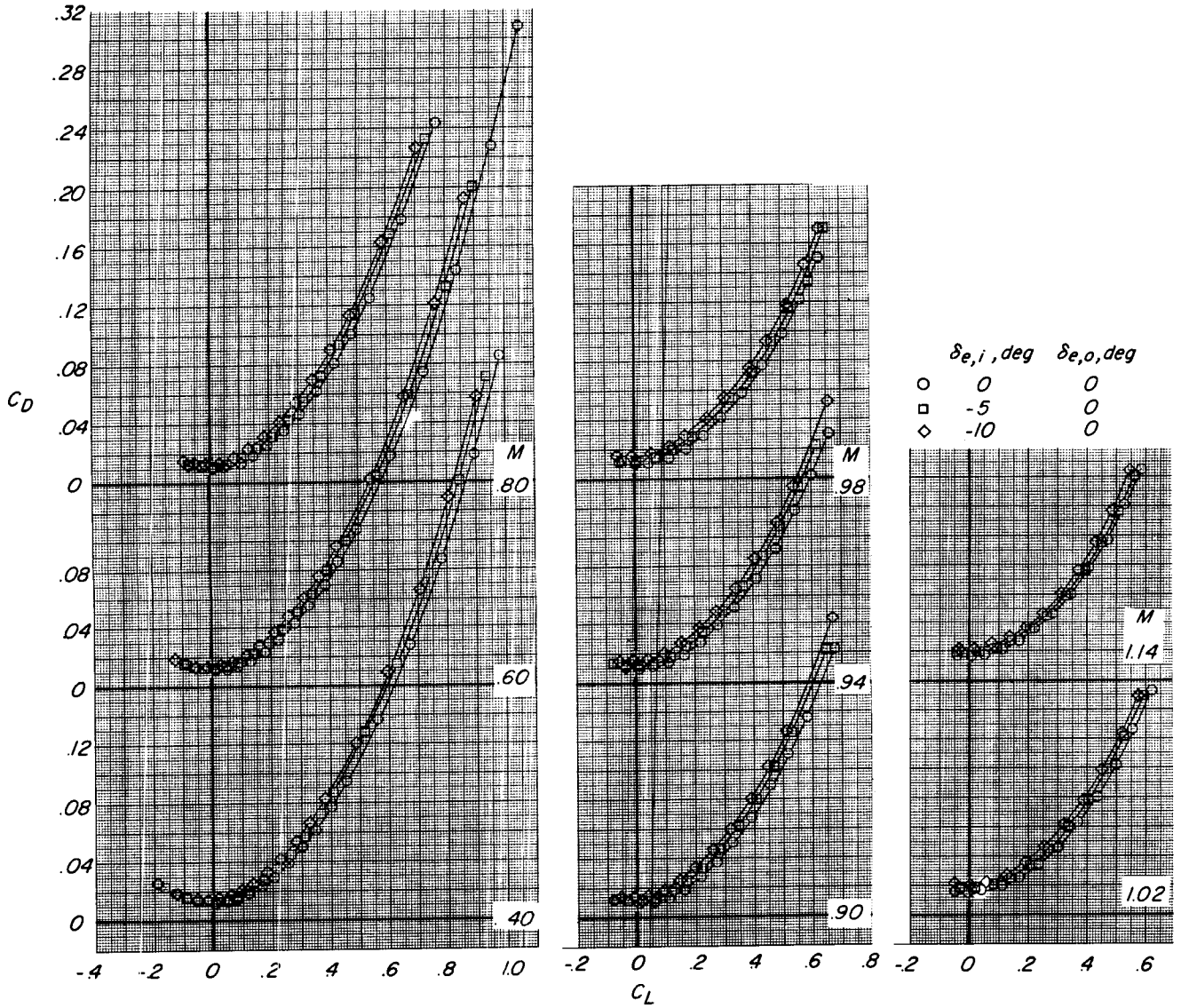

(c) Variation of C_D with C_L.

Figure 10.- Concluded.

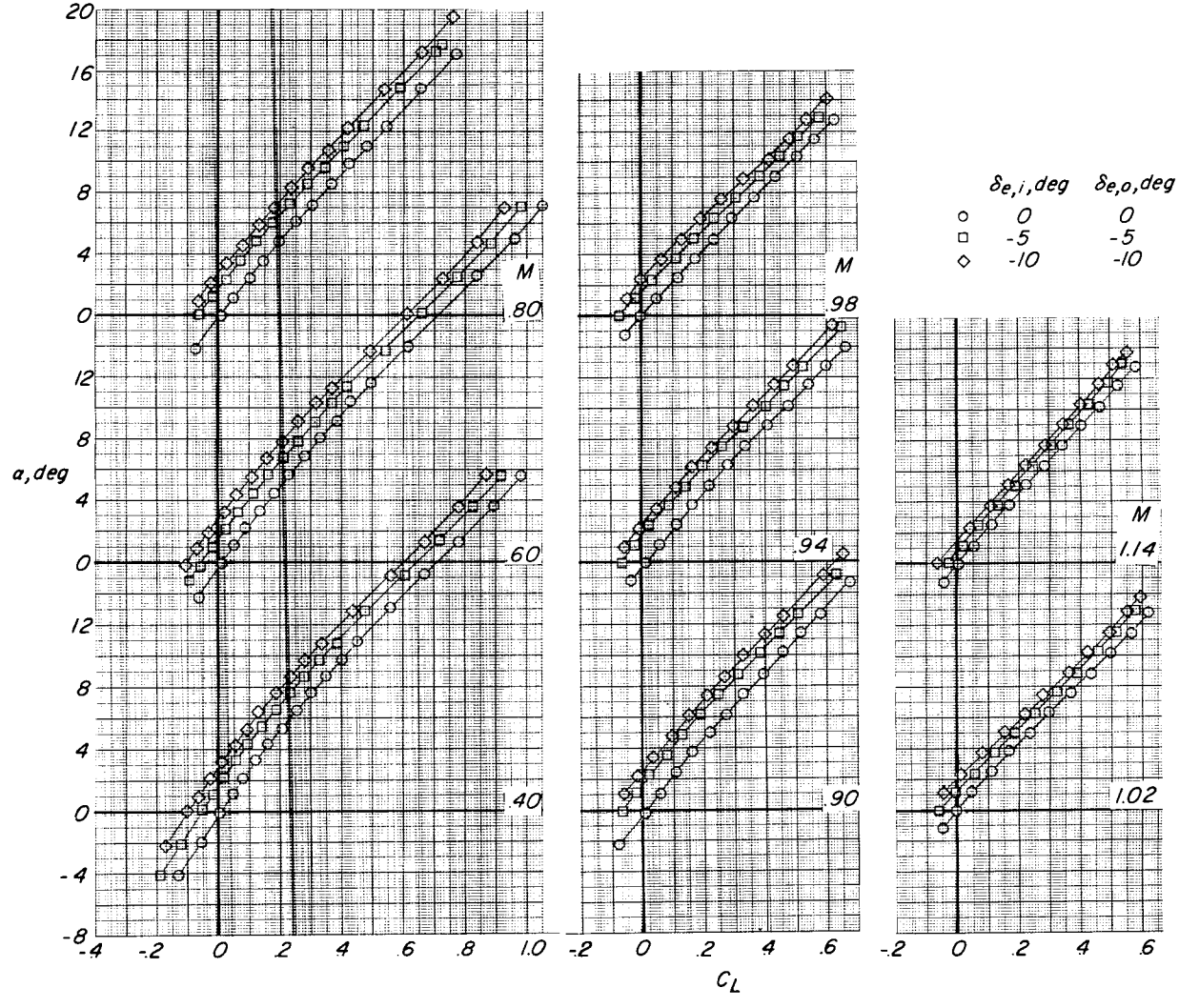

(a) Variation of α with C_L.

Figure 11.- Effect of inboard and outboard elevon deflection on longitudinal aerodynamic characteristics of plane delta wing configuration at Mach numbers from 0.40 to 1.14.

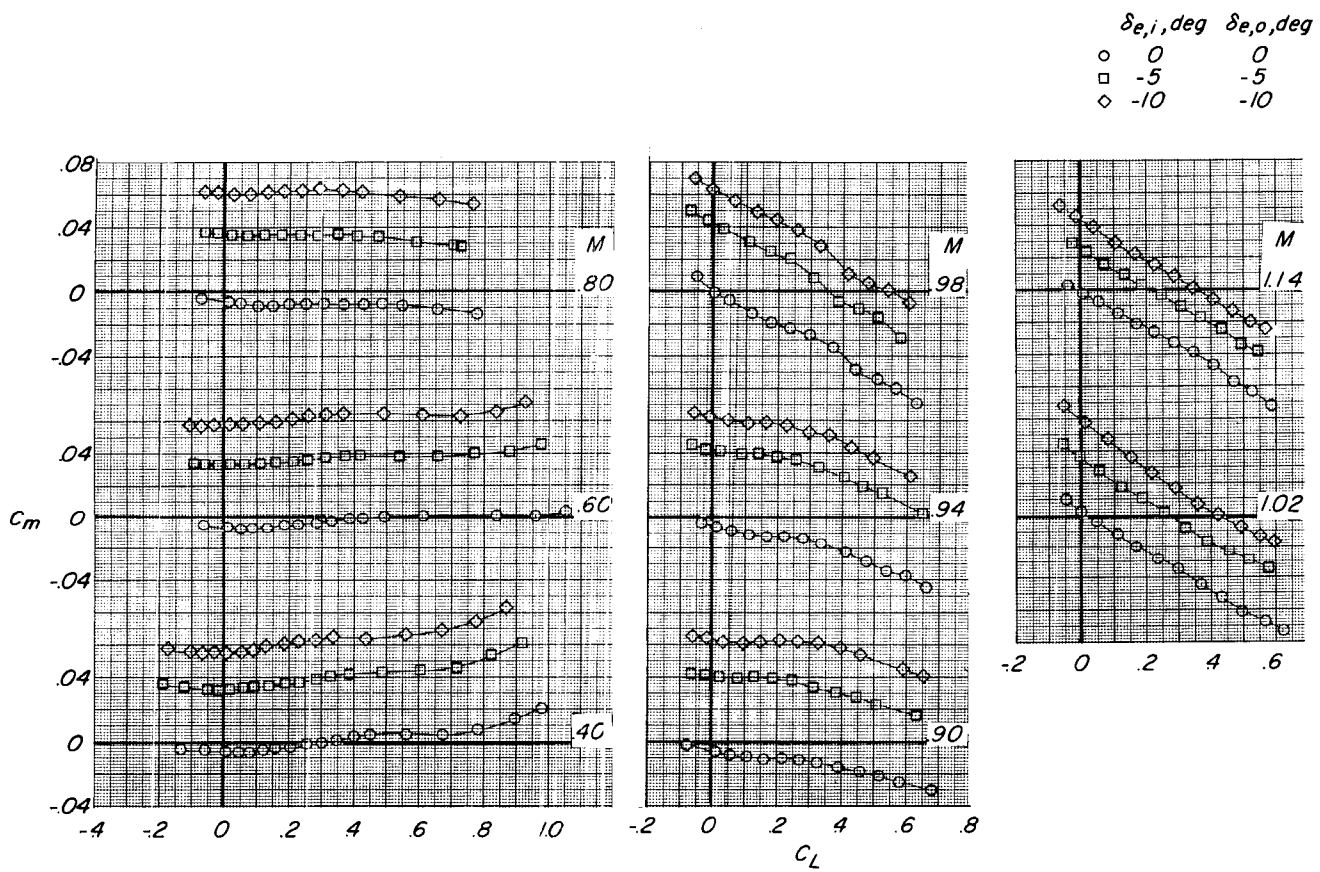

(b) Variation of C_m with C_L.

Figure 11.- Continued.

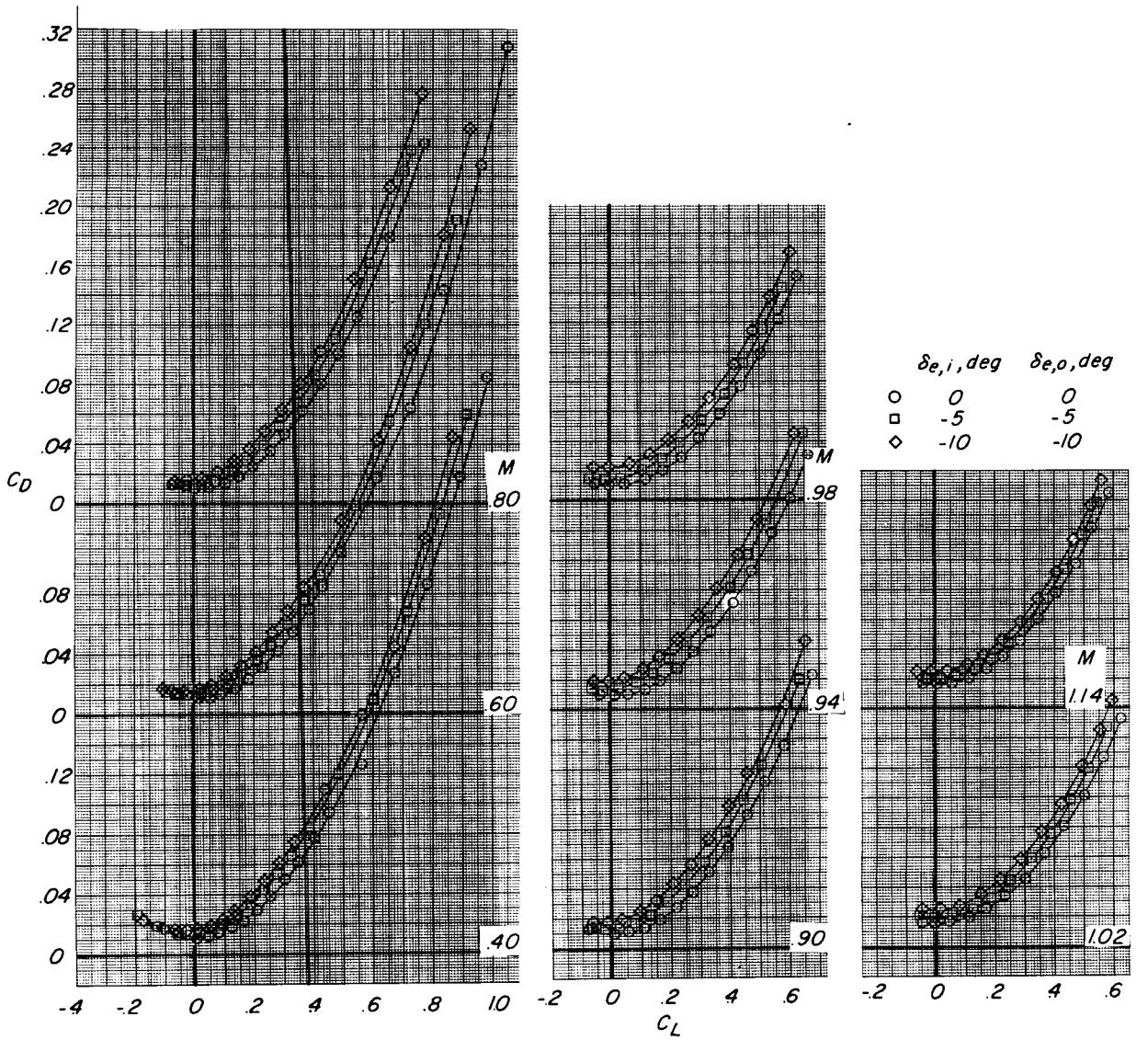

(c) Variation of C_D with C_L.

Figure 11.- Concluded.

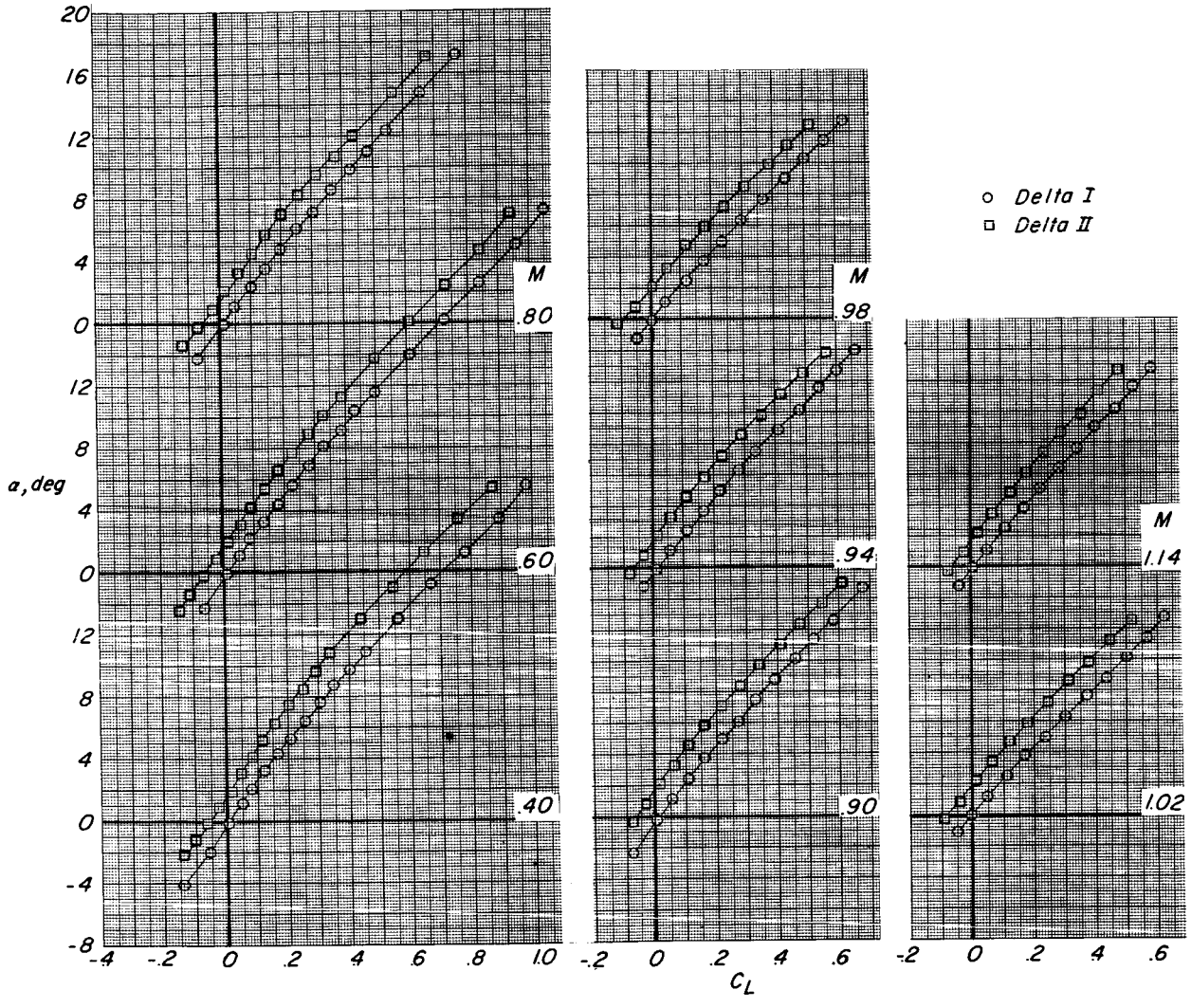

(a) Variation of α with C_L.

Figure 12.- Effect of twist and camber on longitudinal aerodynamic characteristics of delta wing configurations at Mach numbers from 0.40 to 1.14.

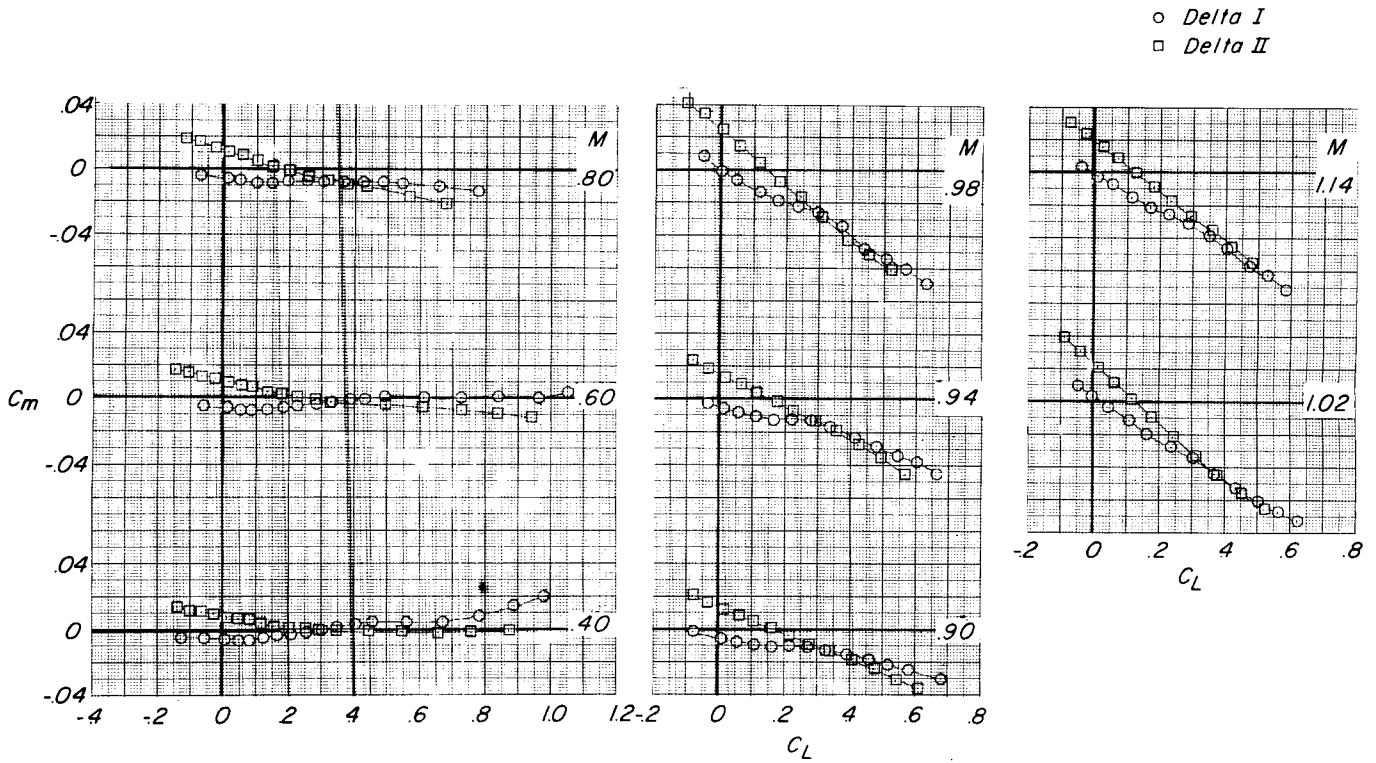

(b) Variation of C_m with C_L.

Figure 12.- Continued.

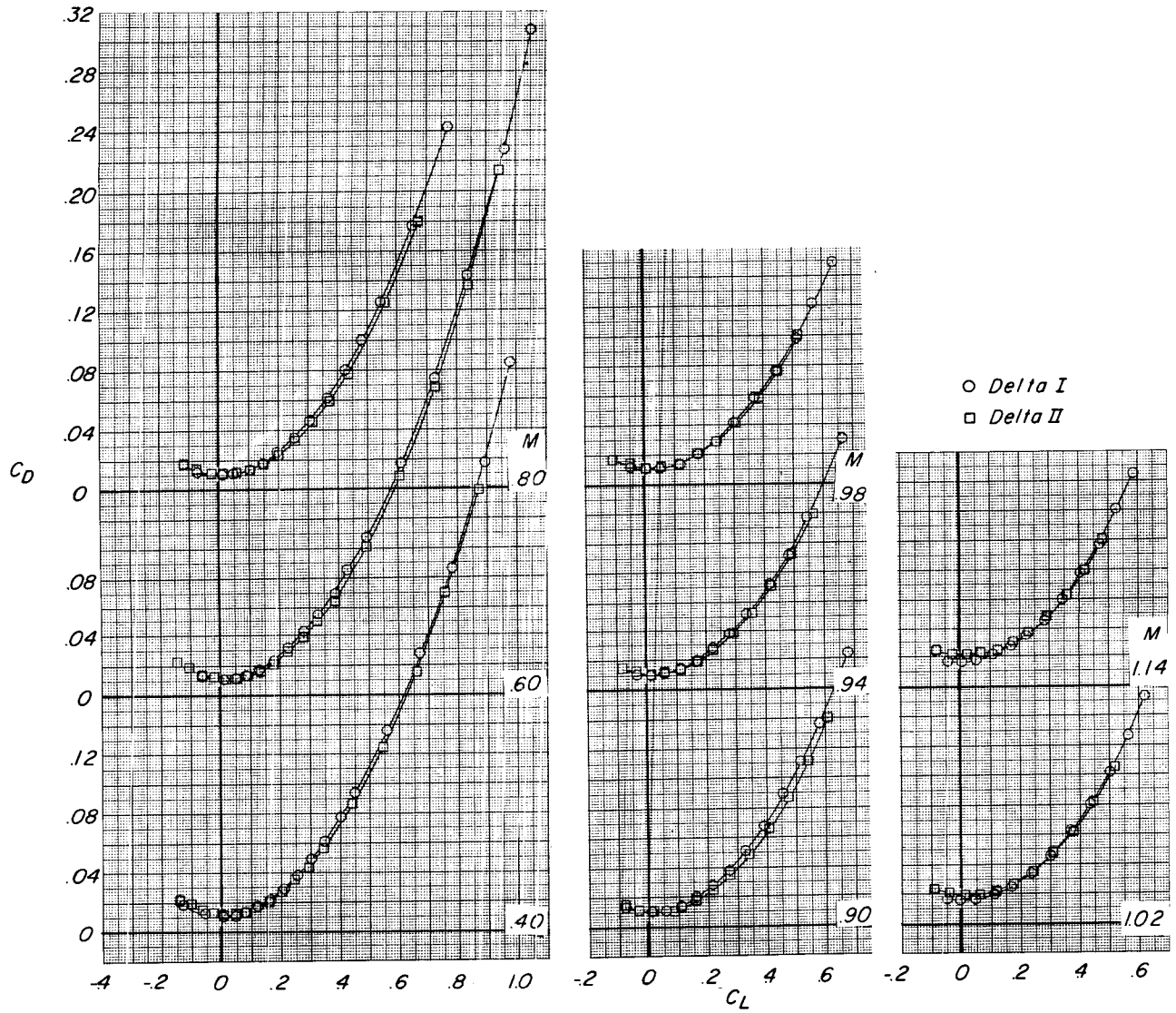

(c) Variation of C_D with C_L.

Figure 12.- Concluded.

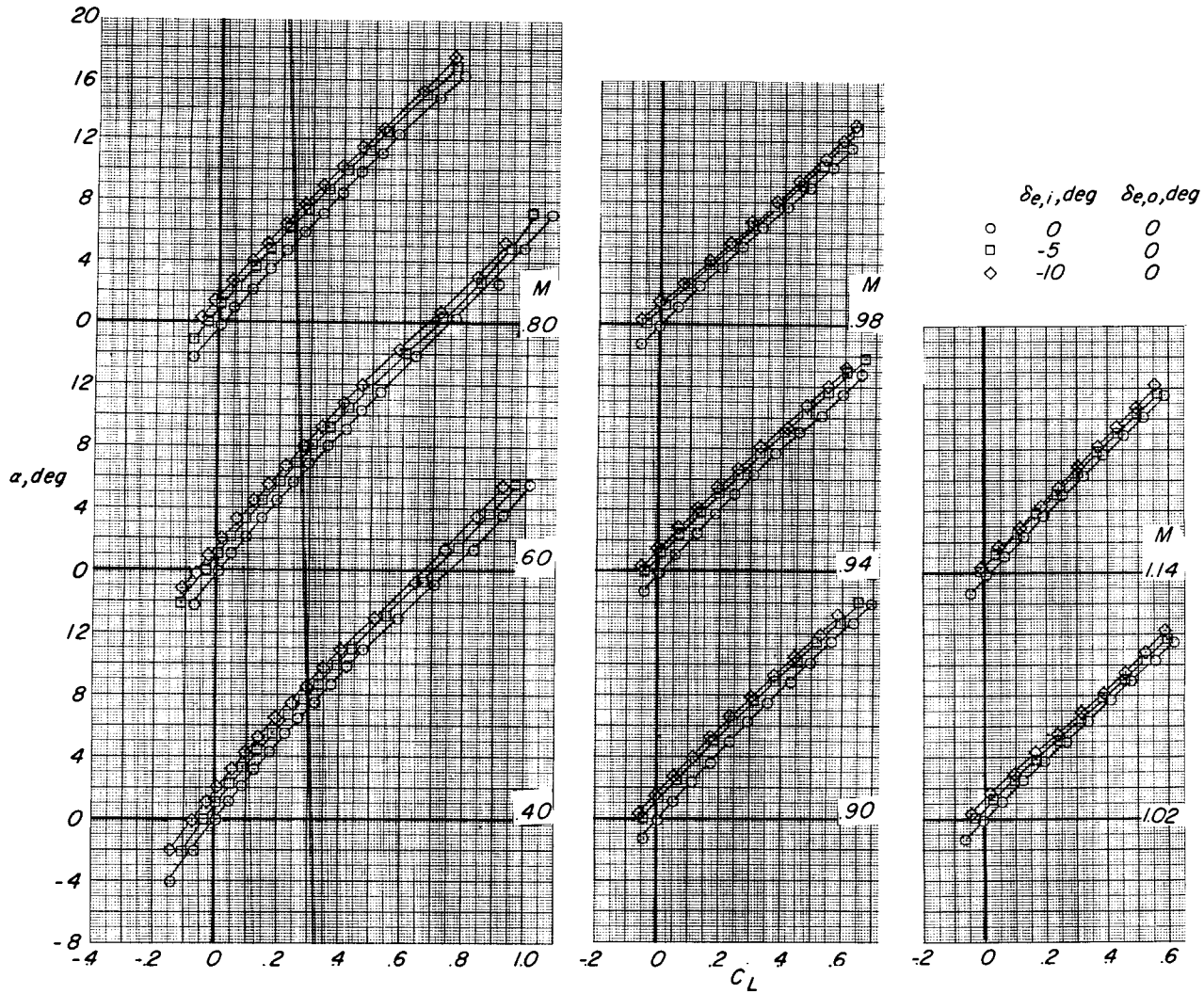

(a) Variation of α with C_L.

Figure 13.- Effect of inboard elevon deflection on longitudinal aerodynamic characteristics of plane trapezoid wing configuration at Mach numbers from 0.40 to 1.14.

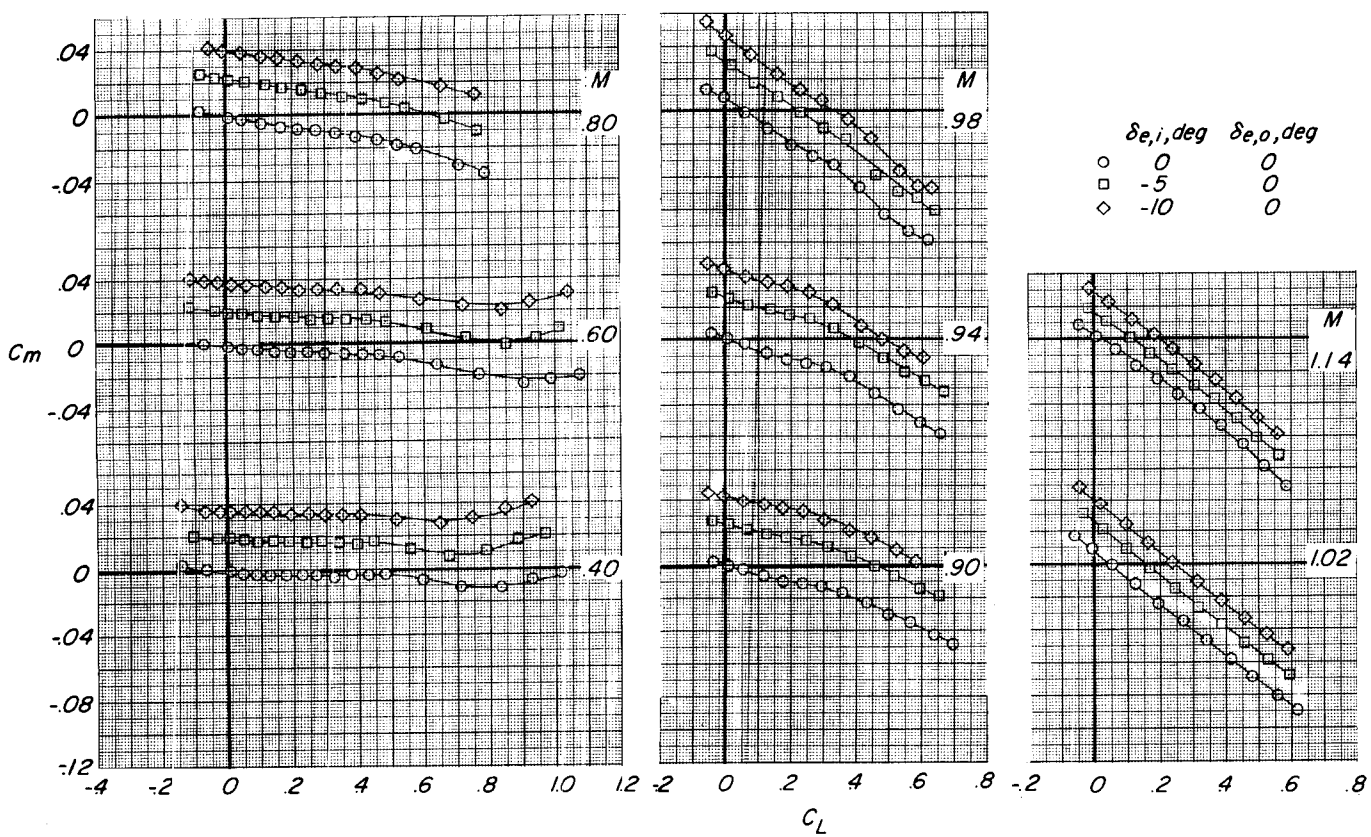

(b) Variation of C_m with C_L.

Figure 13.- Continued.

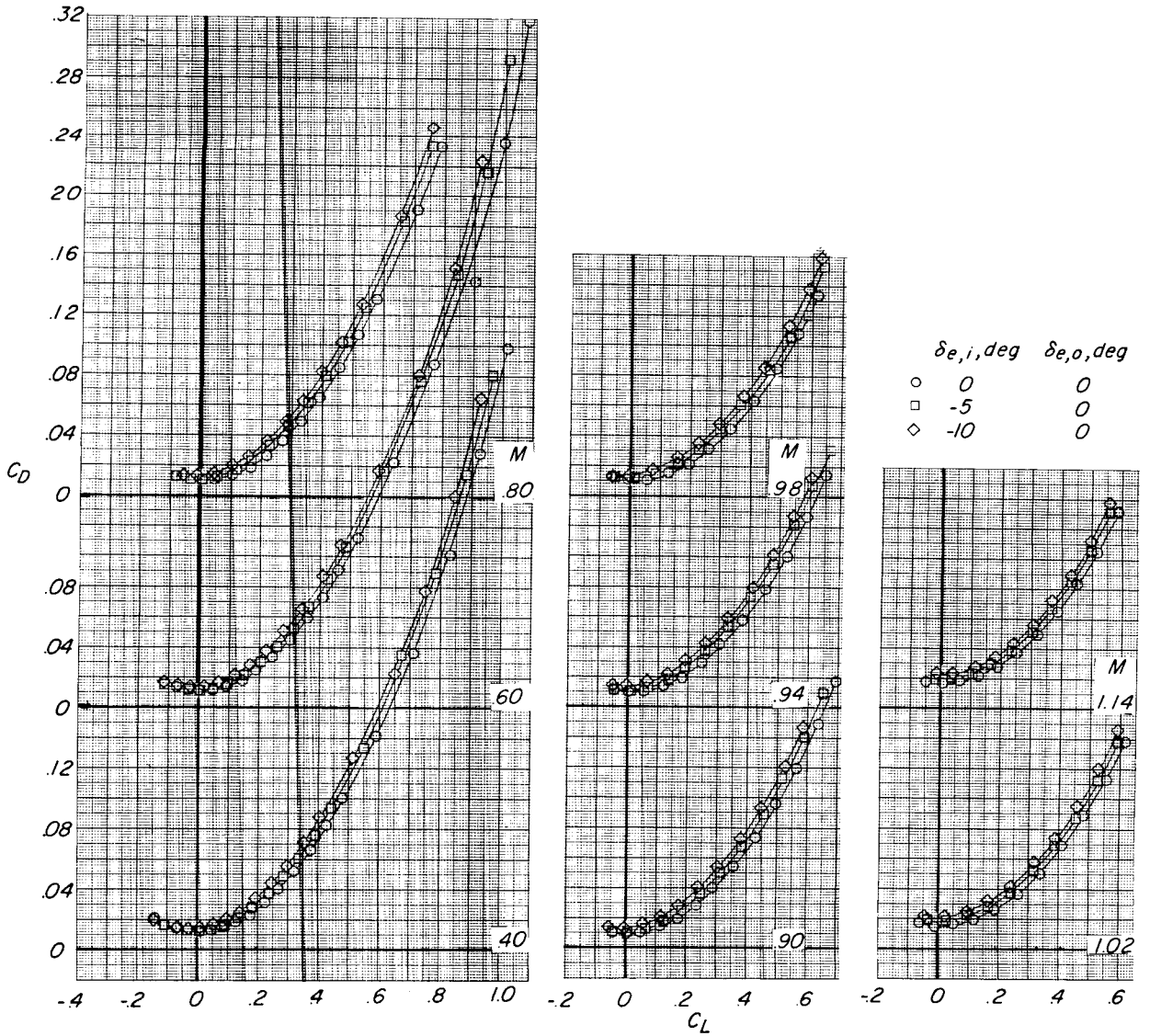

(c) Variation of C_D with C_L.

Figure 13.- Concluded.

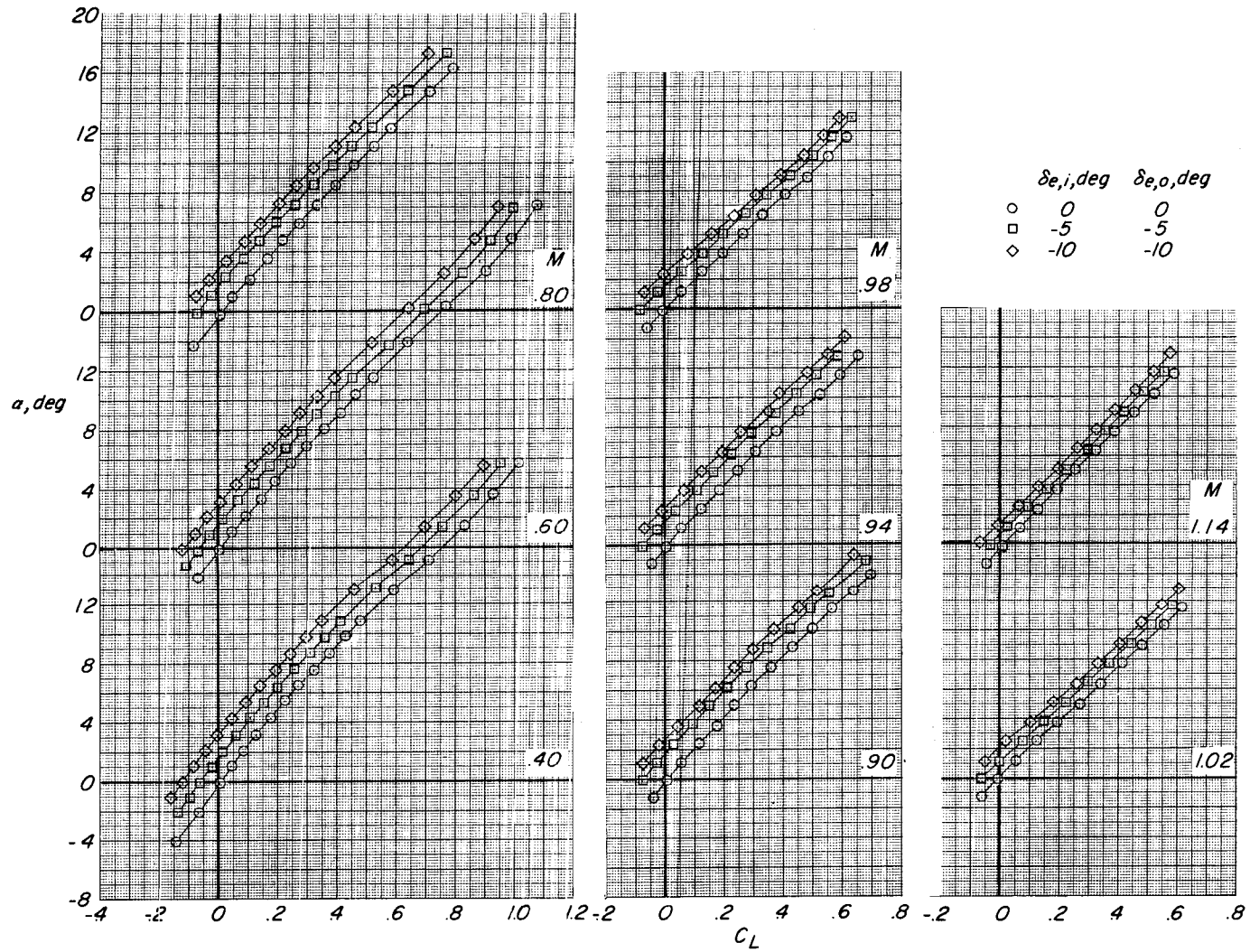

(a) Variation of α with C_L.

Figure 14.- Effect of inboard and outboard elevon deflection on longitudinal aerodynamic characteristics of plane trapezoid wing configuration at Mach numbers from 0.40 to 1.14.

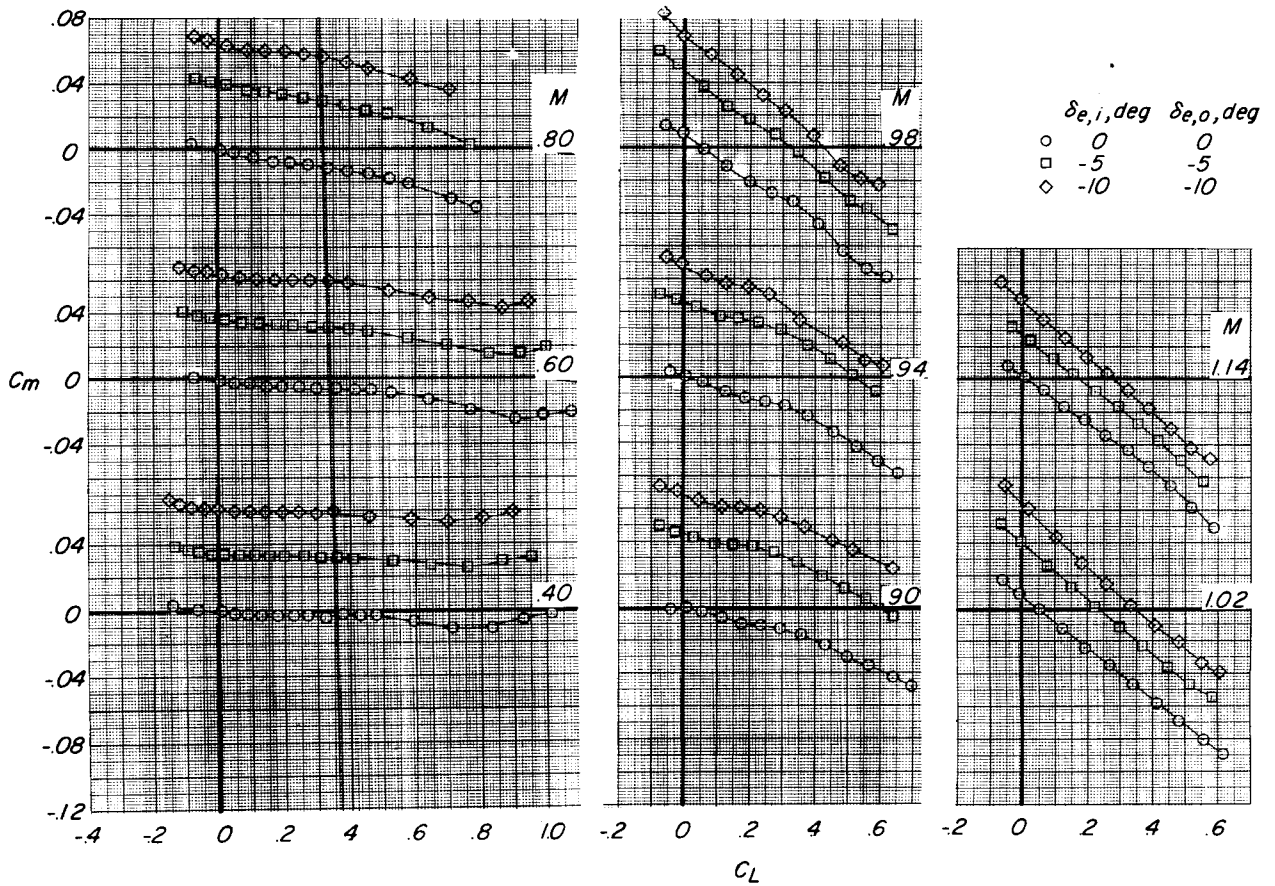

(b) Variation of C_m with C_L.

Figure 14.- Continued.

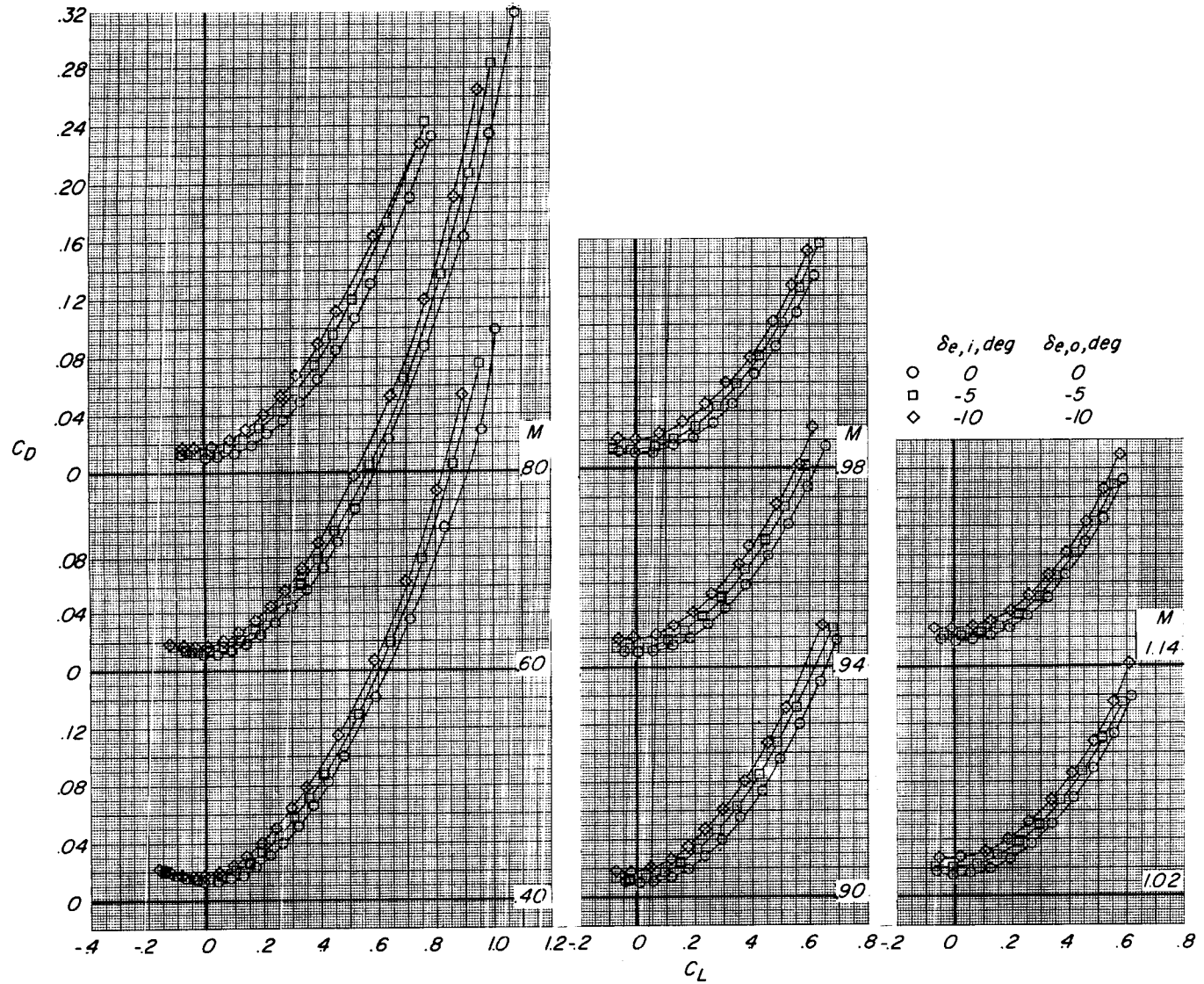

(c) Variation of C_D with C_L.

Figure 14.- Concluded.

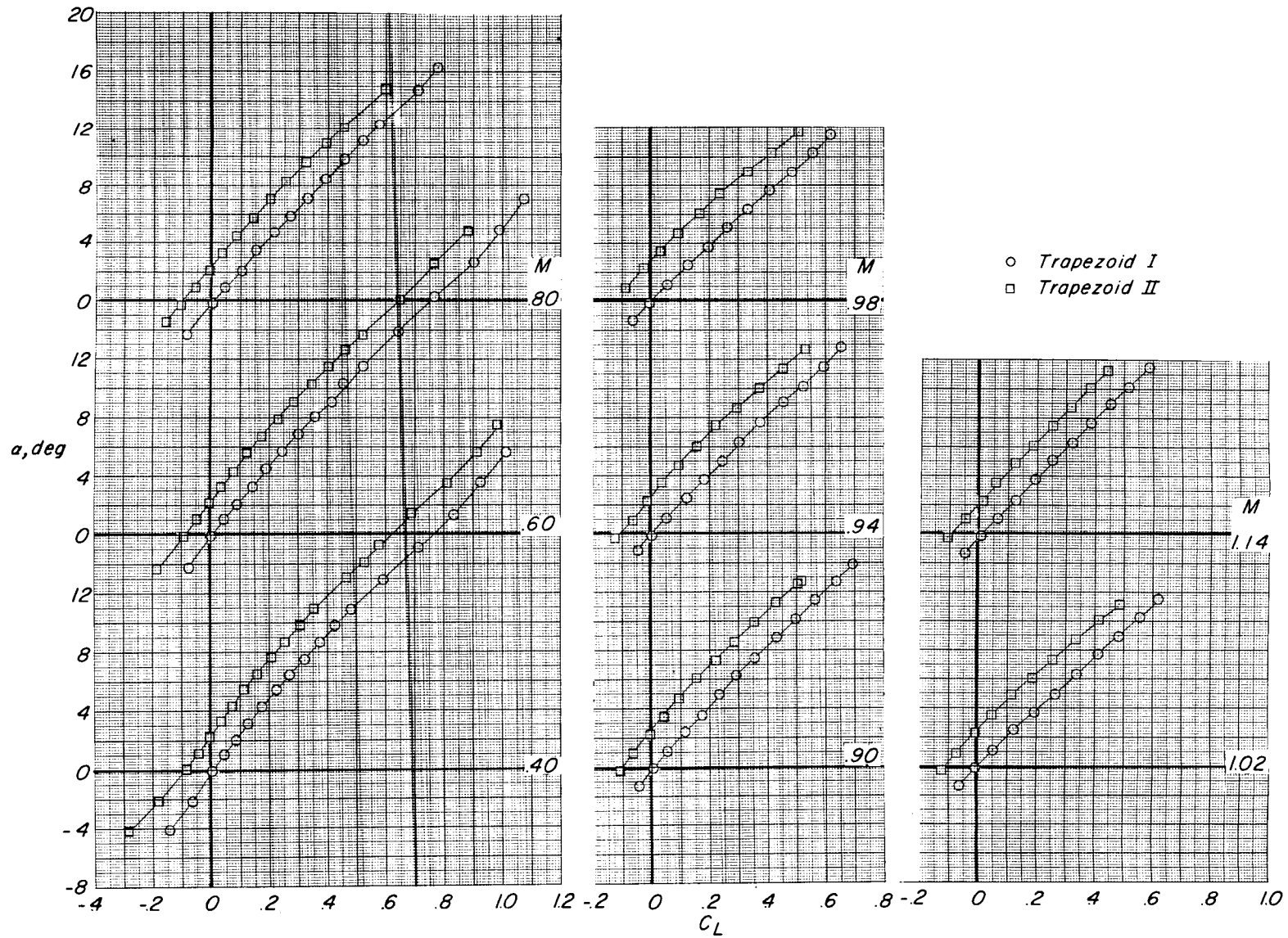

(a) Variation of α with C_L.

Figure 15.- Effect of twist and camber on longitudinal aerodynamic characteristics of trapezoid wing configurations at Mach numbers from 0.40 to 1.14.

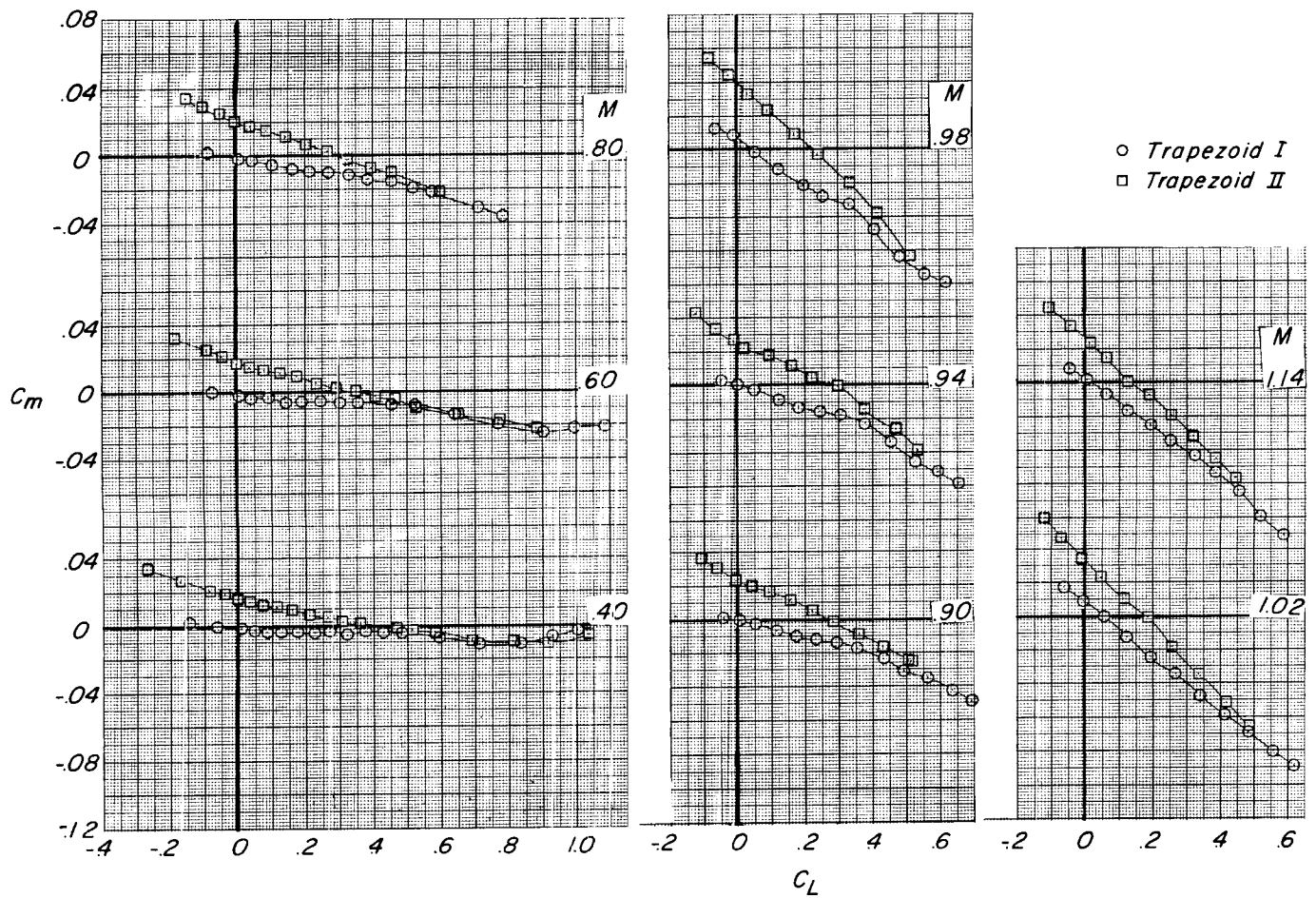

(b) Variation of C_m with C_L.

Figure 15.- Continued.

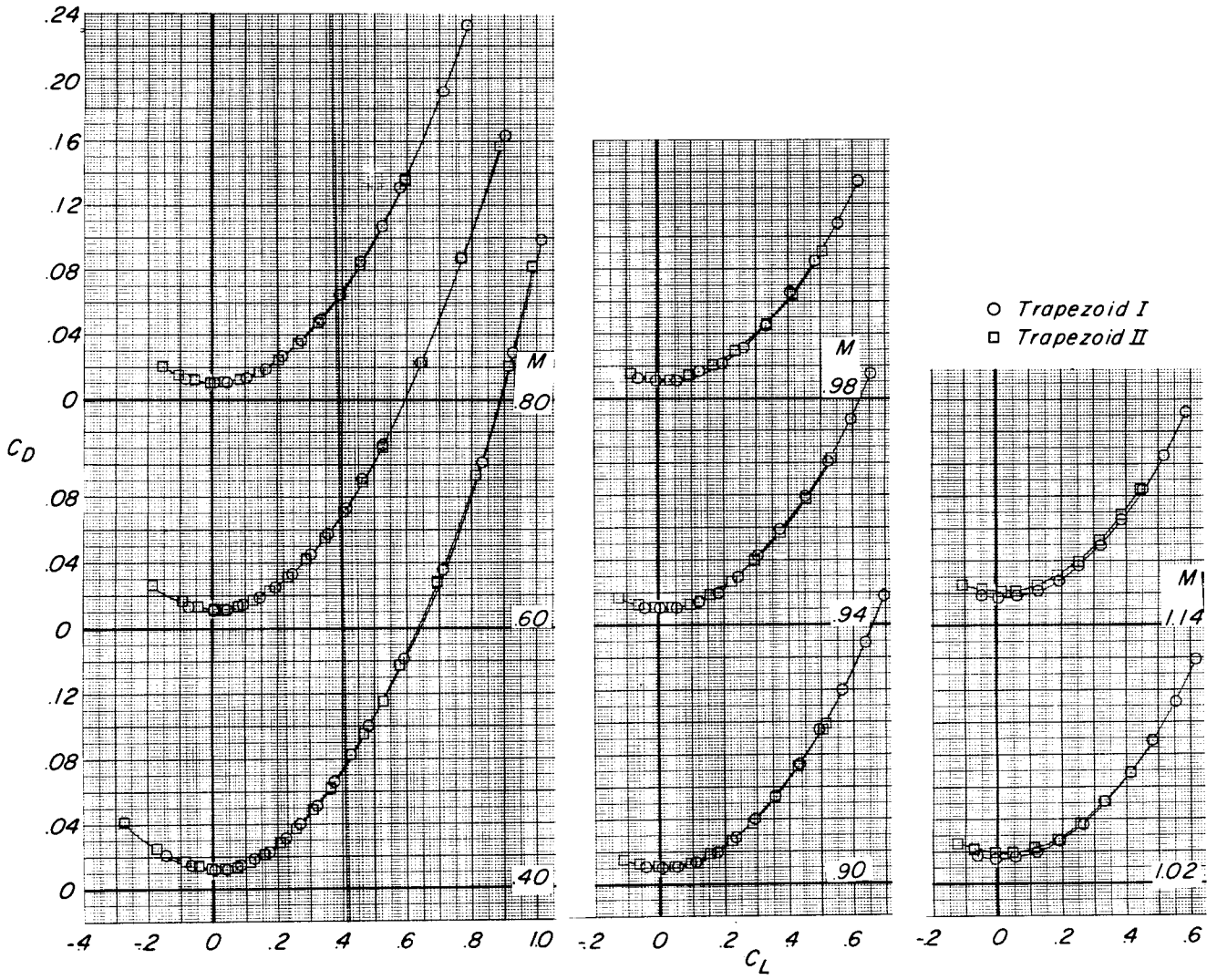

(c) Variation of C_D with C_L.

Figure 15.- Concluded.

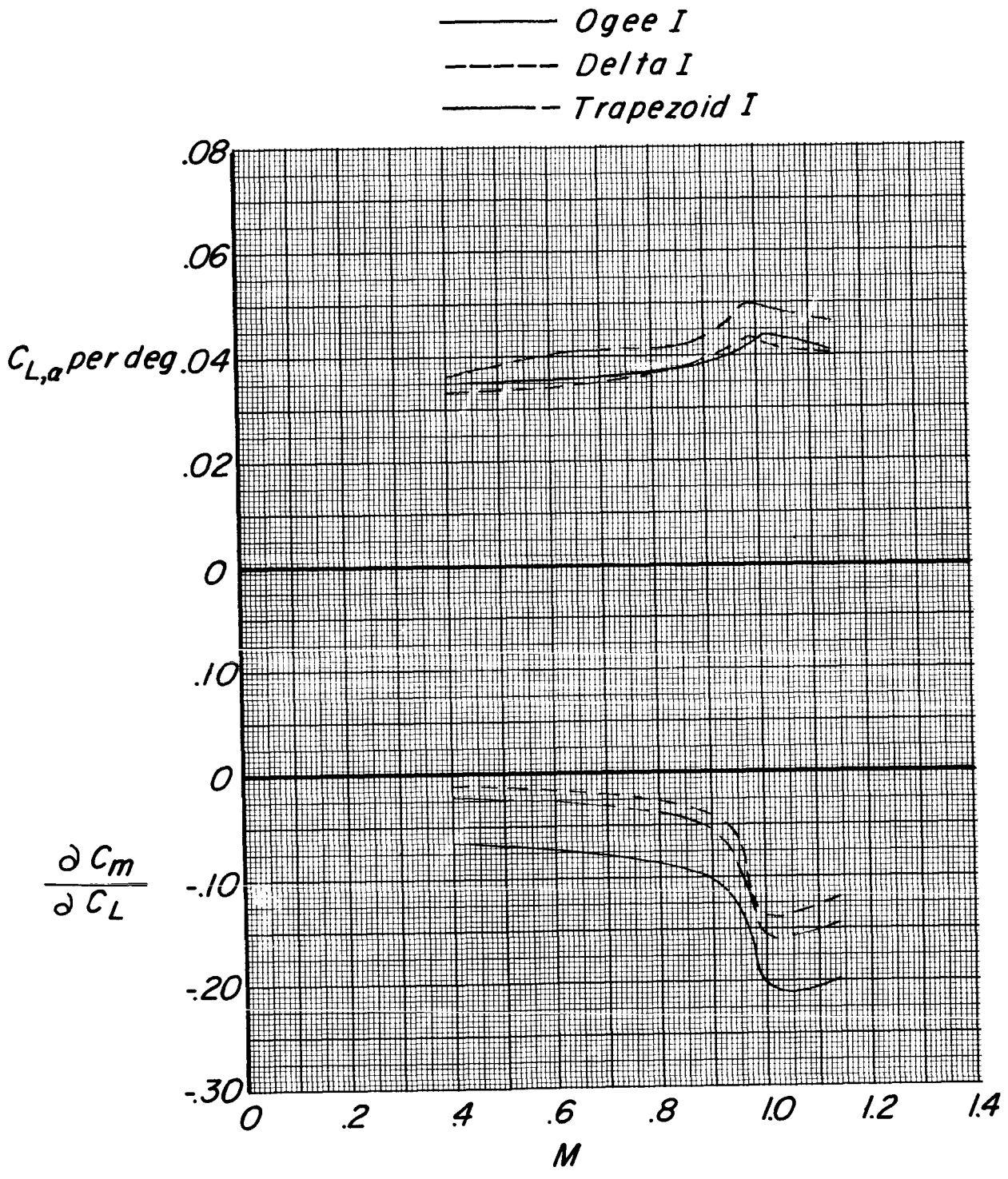

Figure 16.- Effect of plane wing planform on variation with Mach number of lift-curve slope C_{L_α} and longitudinal stability parameter $\partial C_m/\partial C_L$.

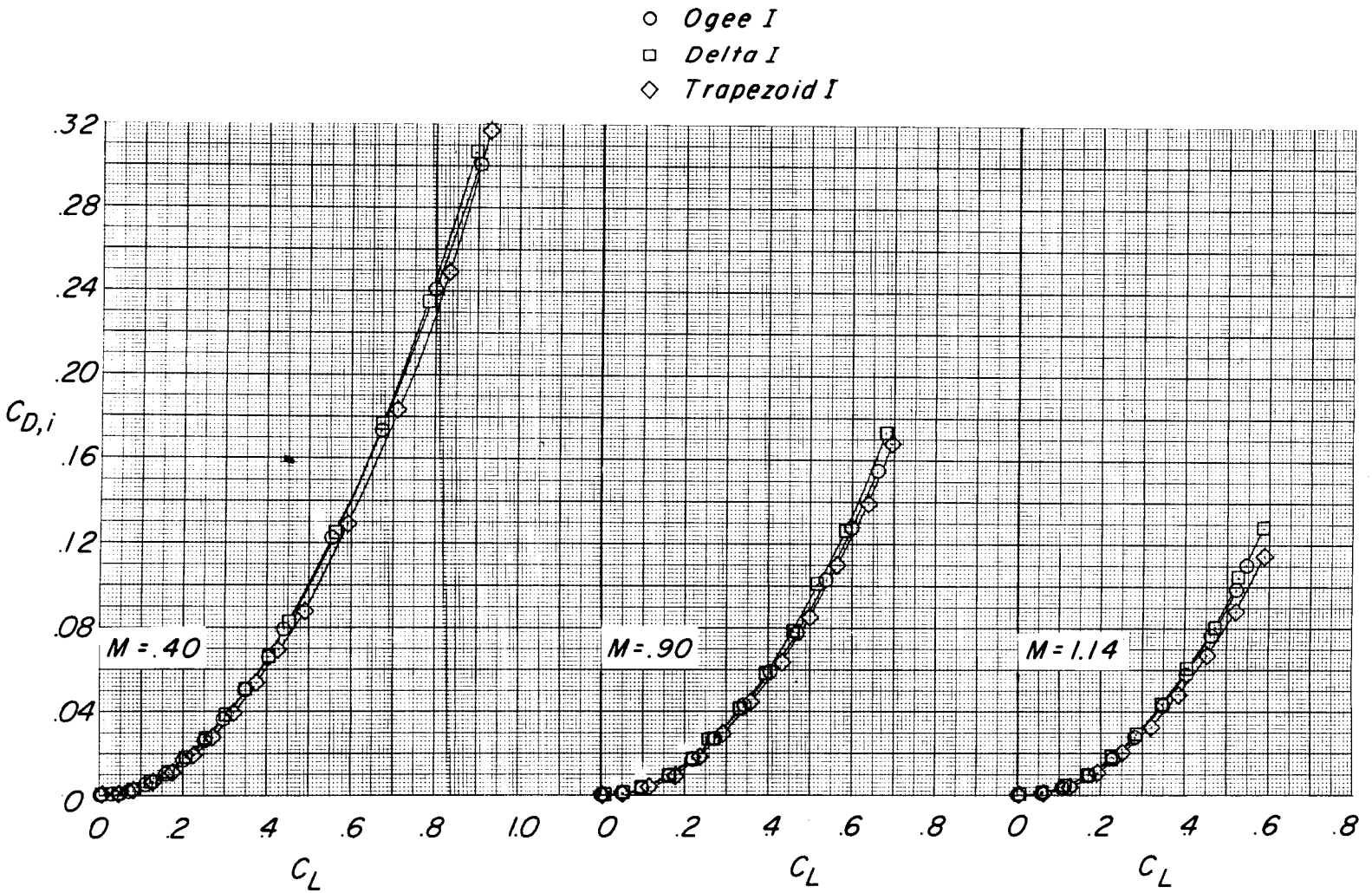

Figure 17.- Effect of plane wing planform on induced drag $C_{D,i}$ at M = 0.40, 0.90, and 1.14.

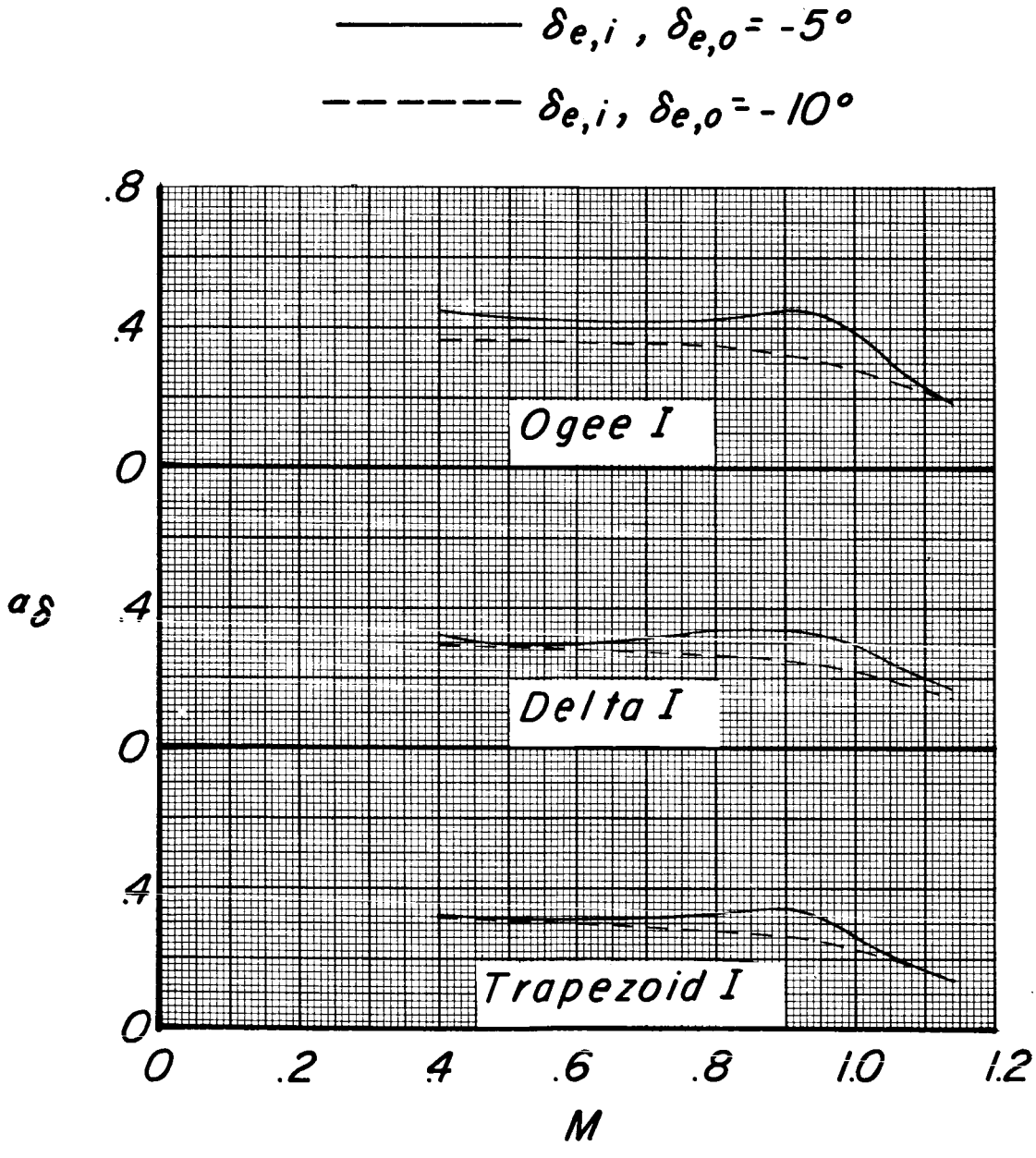

Figure 18.- Variation with Mach number of elevon effectiveness parameter α_δ for plane ogee, delta, and trapezoid wing configurations.

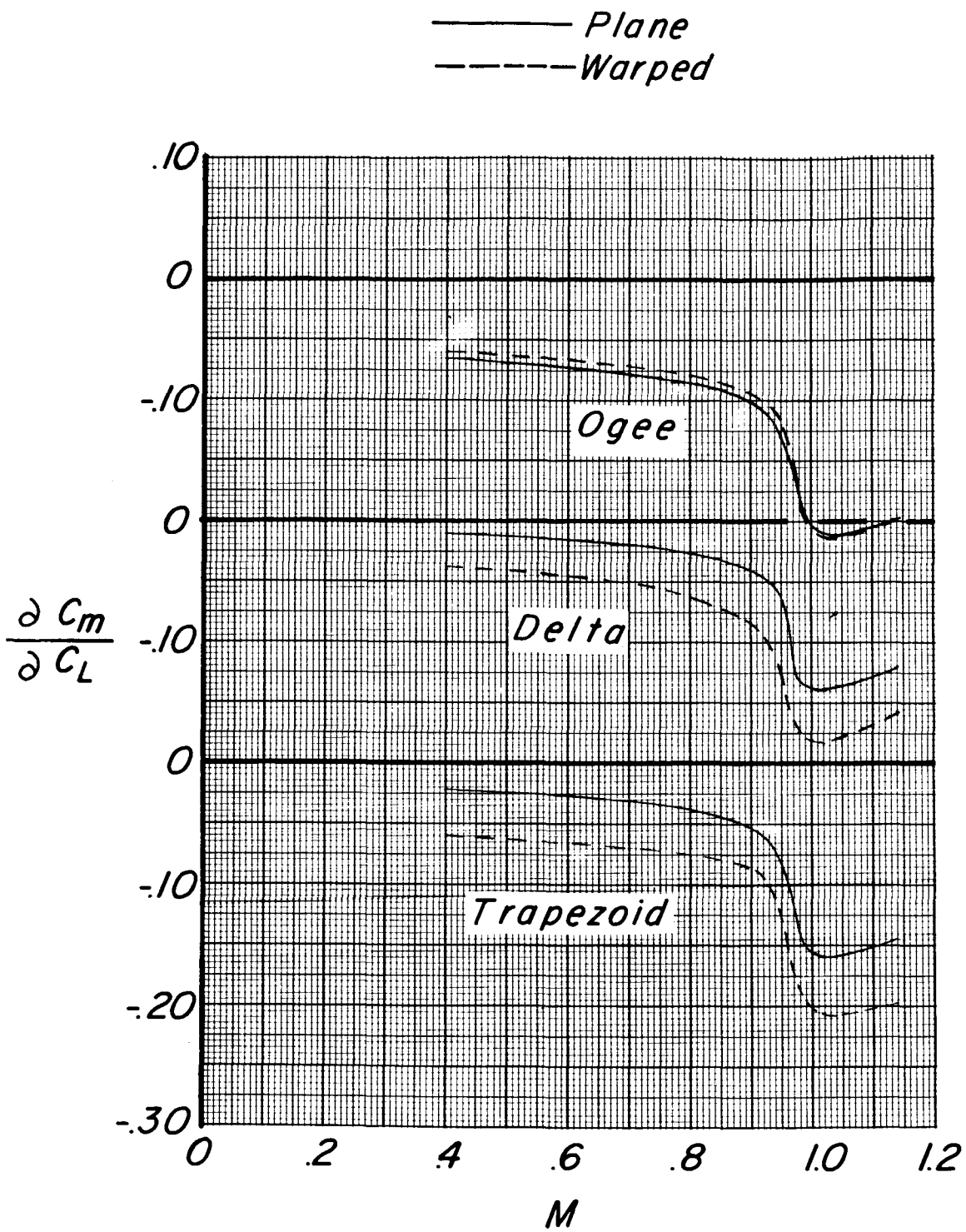

Figure 19.- Effect of twist and camber on variation with Mach number of longitudinal stability parameter $\partial C_m/\partial C_L$ for ogee, delta, and trapezoid wing configurations.

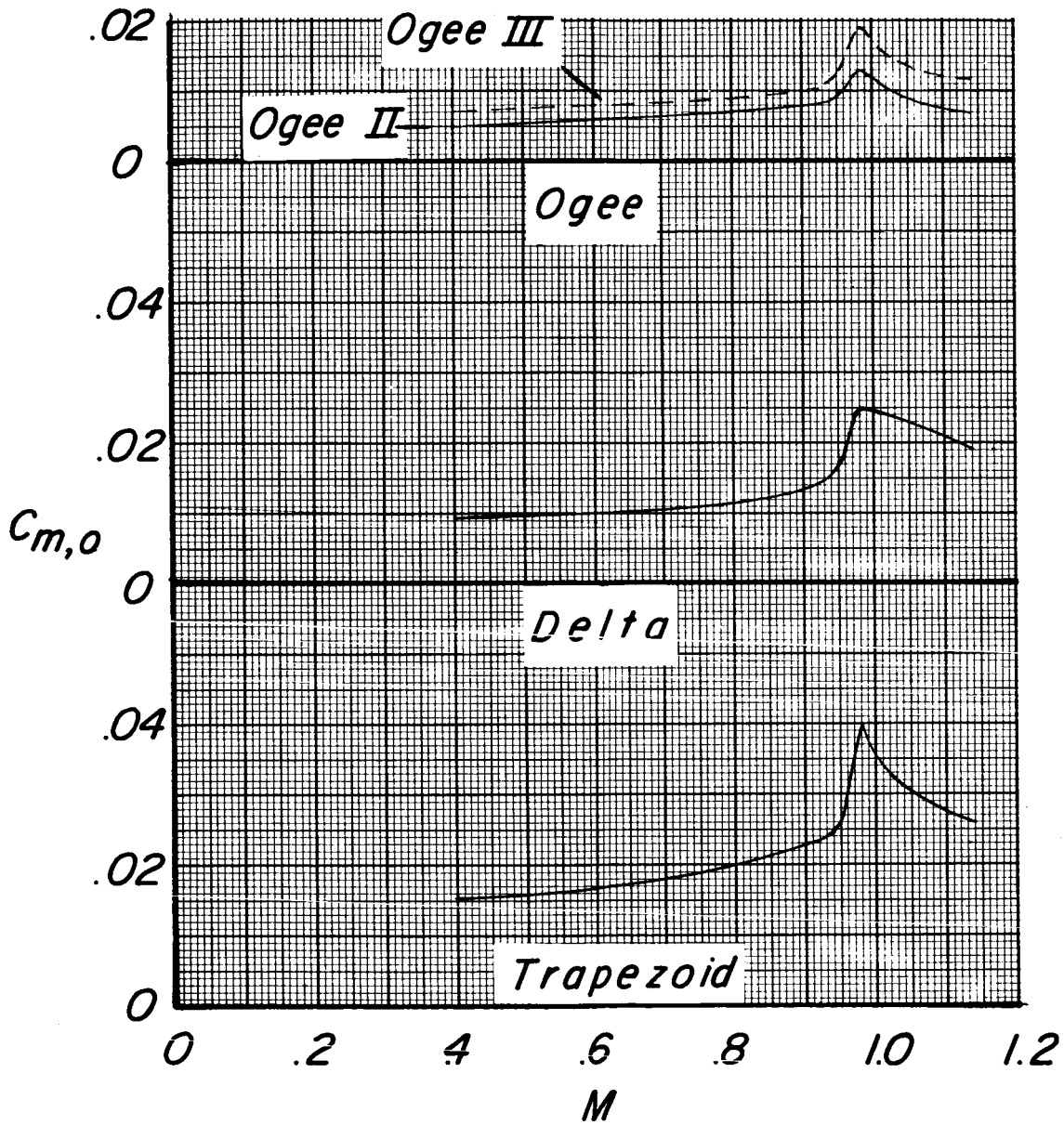

Figure 20.- Variation with Mach number of pitching-moment coefficient at zero lift $C_{m,o}$ for twisted and cambered wing configurations.

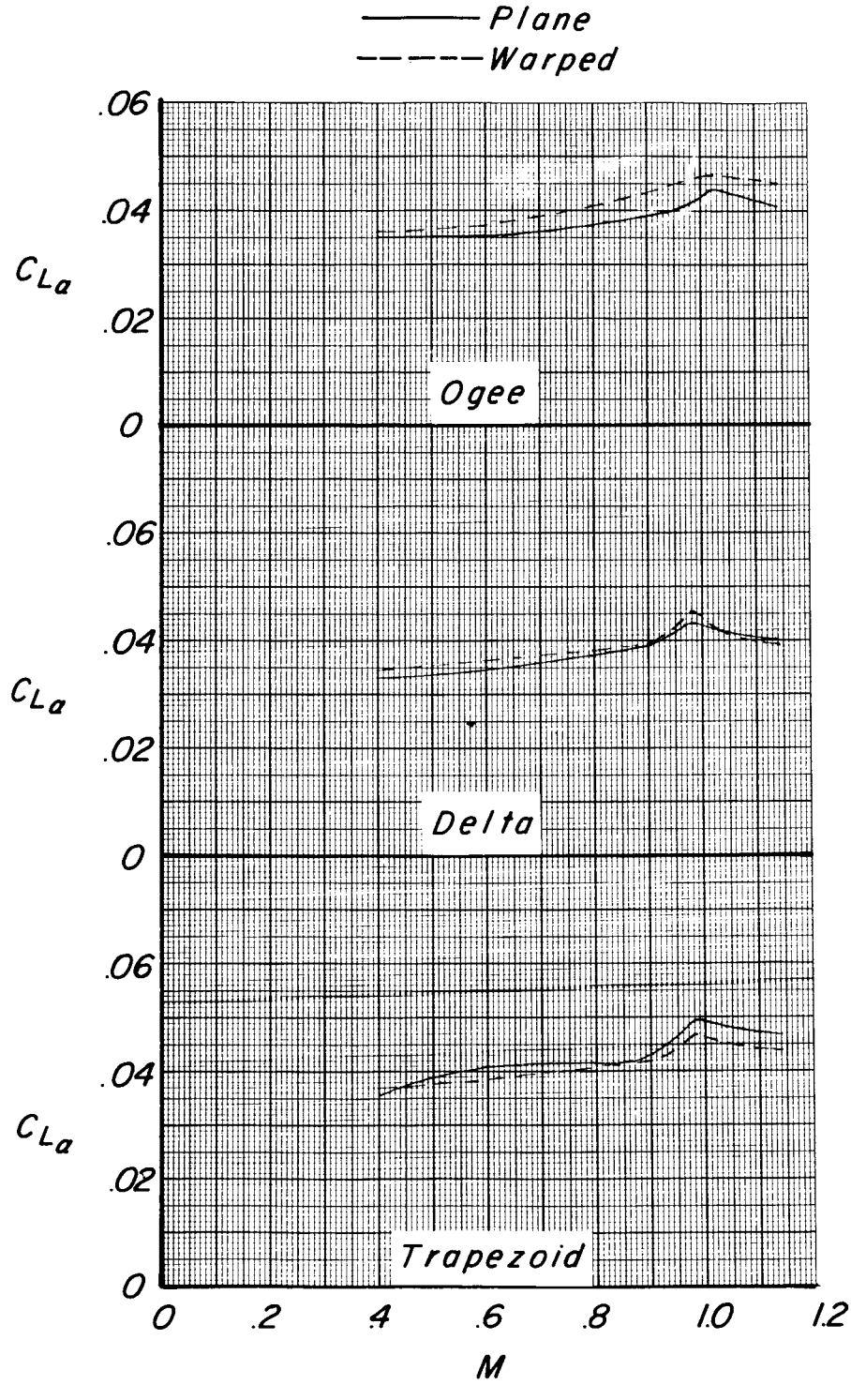

Figure 21.- Effect of twist and camber on variation with Mach number of lift-curve slope C_{L_α} for ogee, delta, and trapezoid wing configurations.

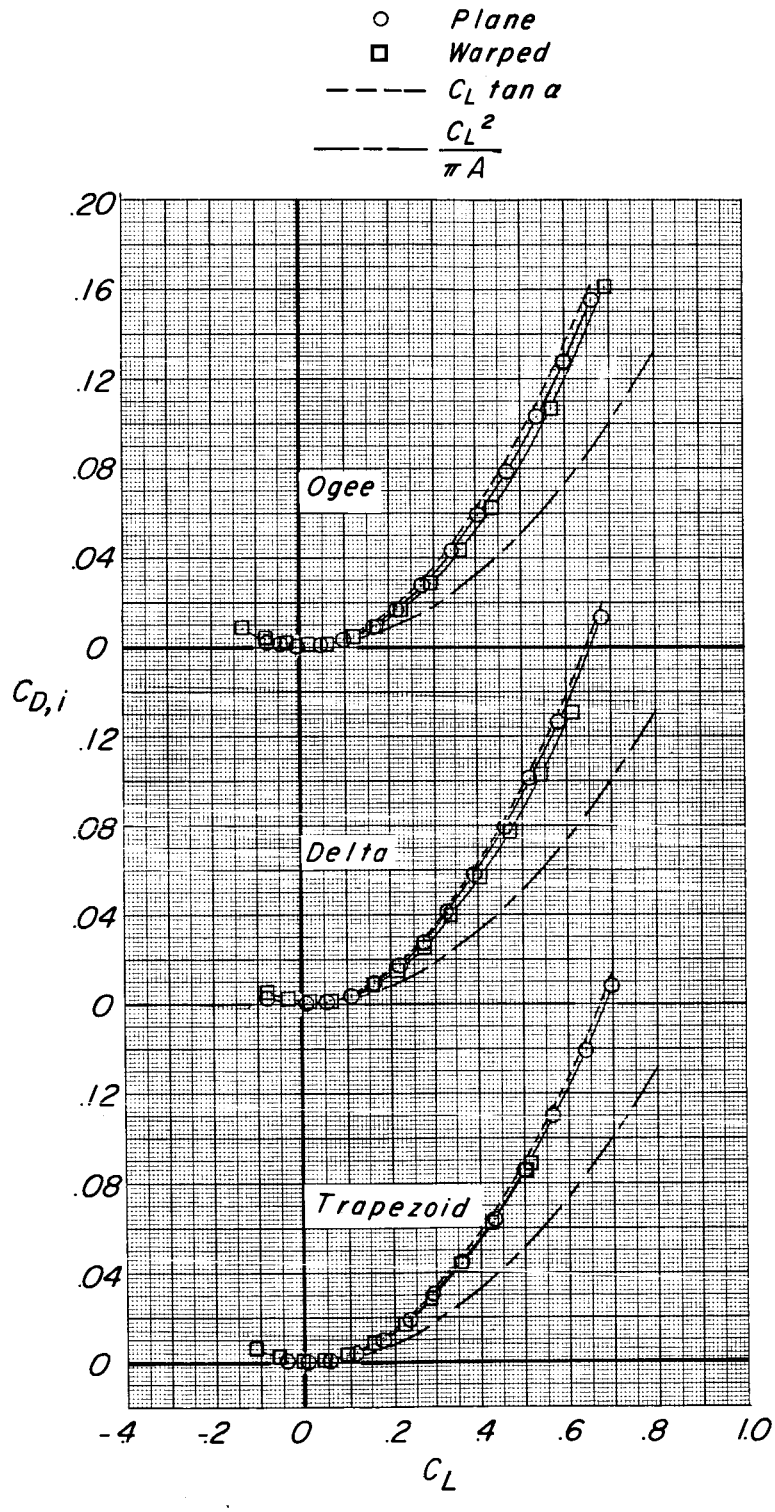

Figure 22.- Effect of twist and camber on induced drag $C_{D,i}$ of ogee, delta, and trapezoid wing configurations at M = 0.90.

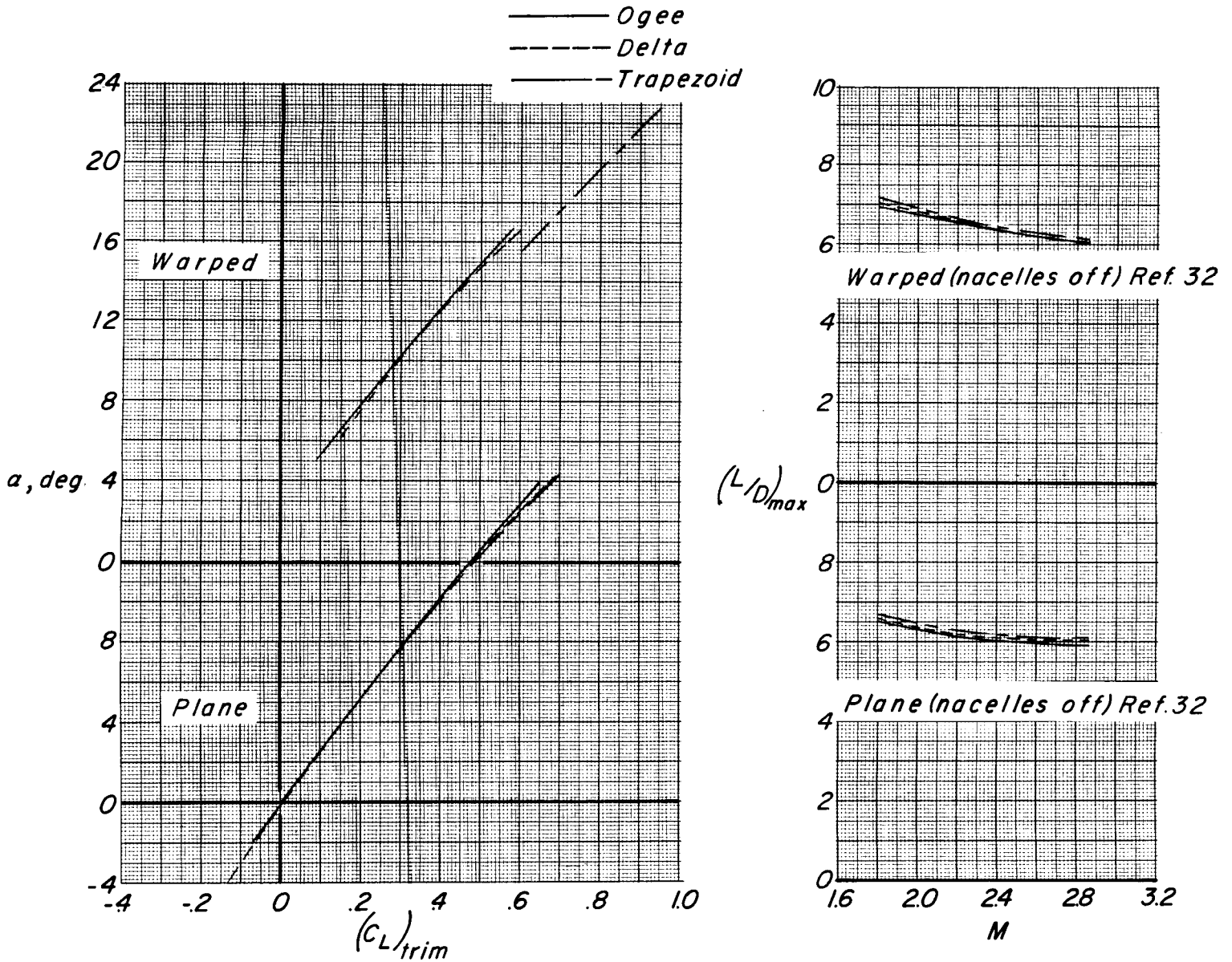

Figure 23.- Variation of angle of attack with trimmed lift coefficient $(C_L)_{trim}$ at M = 0.40 and variation of maximum lift-drag ratio $(L/D)_{max}$ with Mach number.

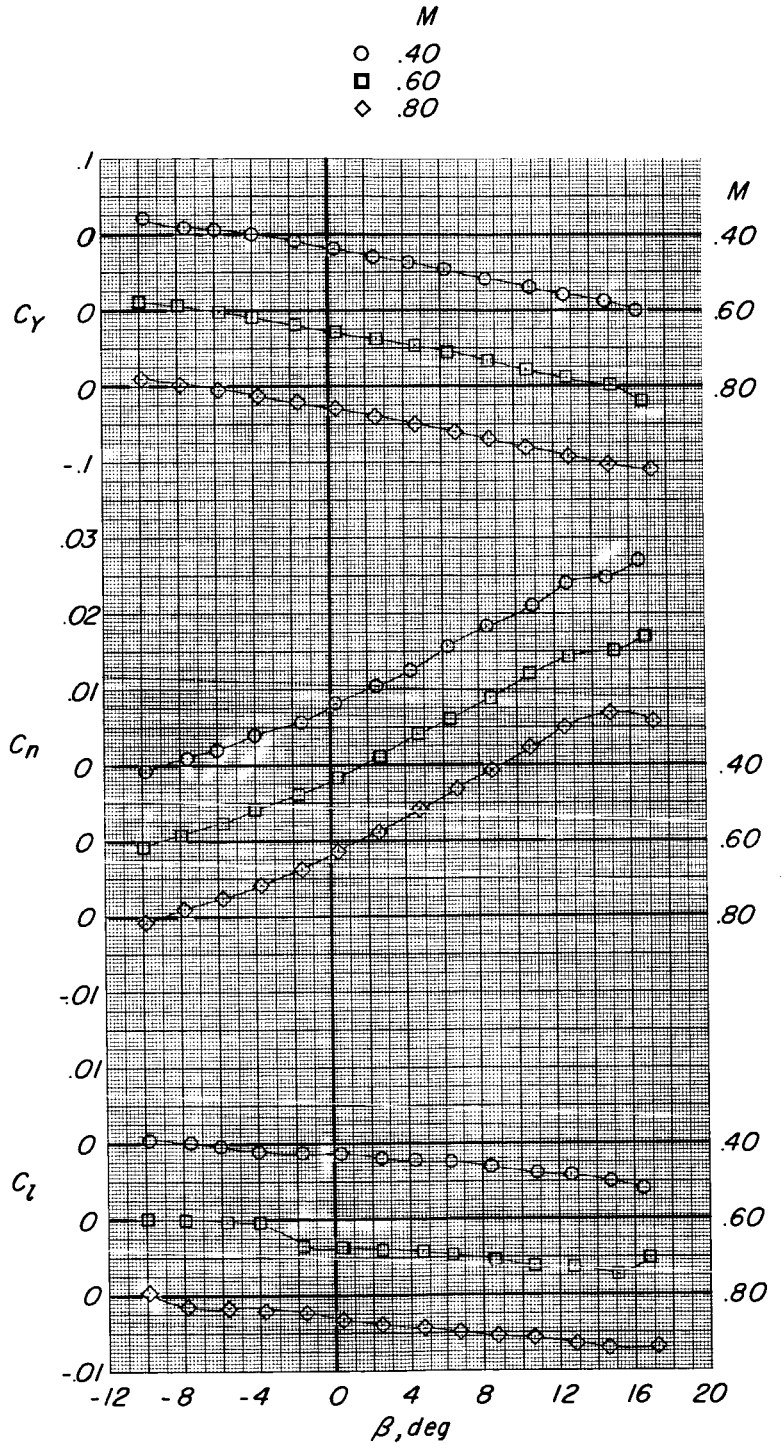

(a) M = 0.40, 0.60, and 0.80.

Figure 24.- Lateral aerodynamic characteristics of plane ogee wing configuration. $\alpha = 0^{0}$.

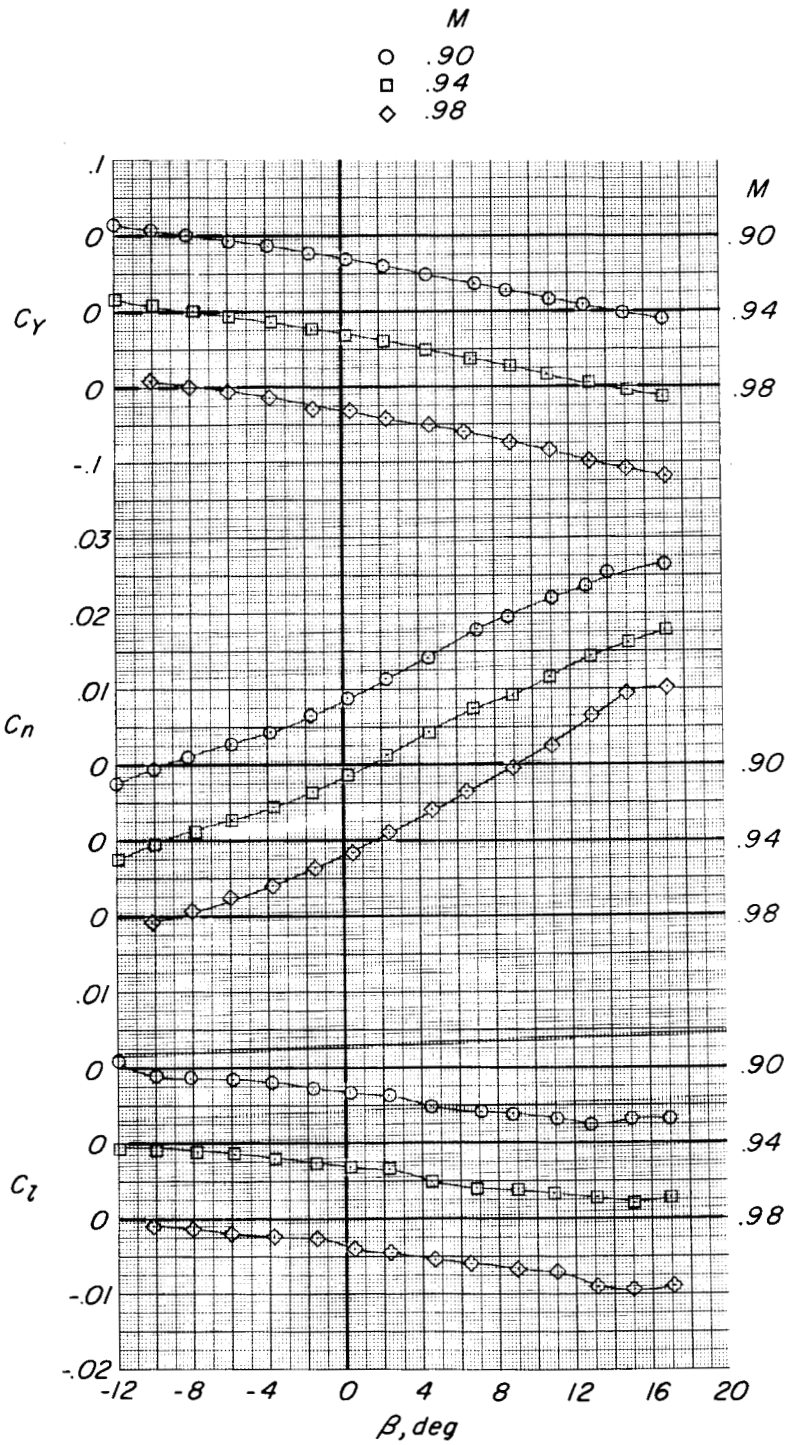

(b) M = 0.90, 0.94, and 0.98.

Figure 24.- Continued.

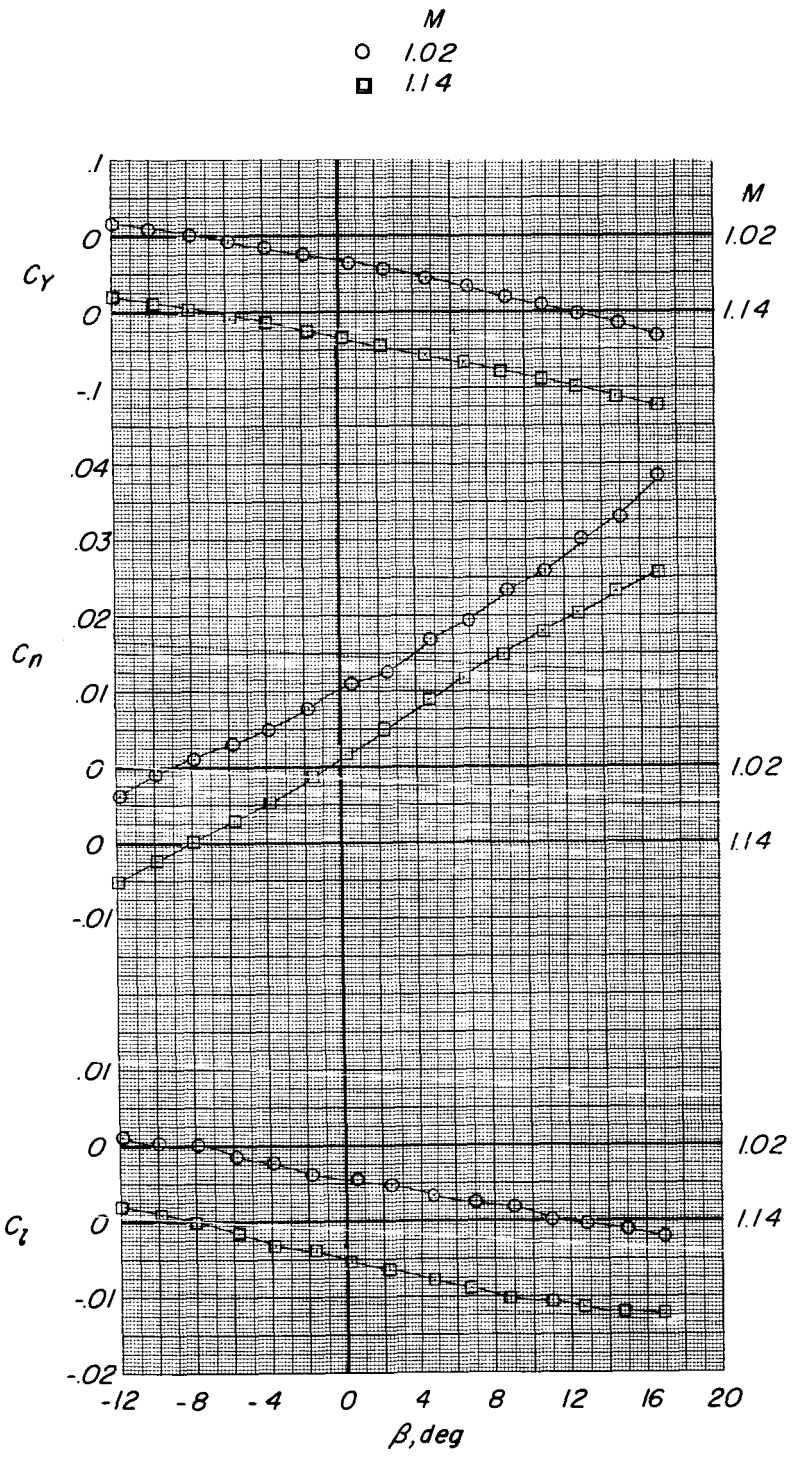

(c) M = 1.02 and 1.14.

Figure 24.- Concluded.

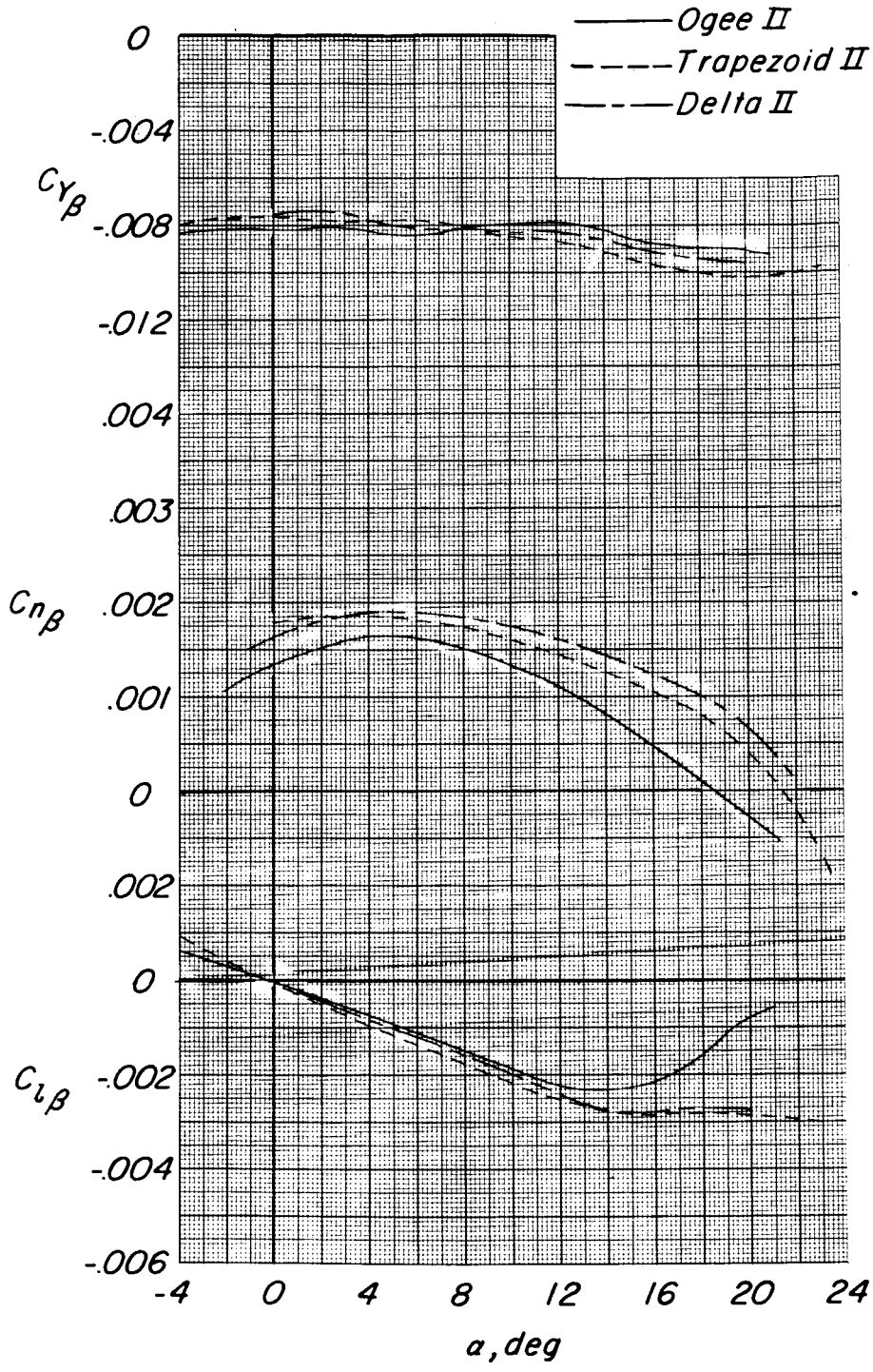

(a) M = 0.40.

Figure 25.- Comparison of lateral aerodynamic characteristics of twisted and cambered wing configurations.

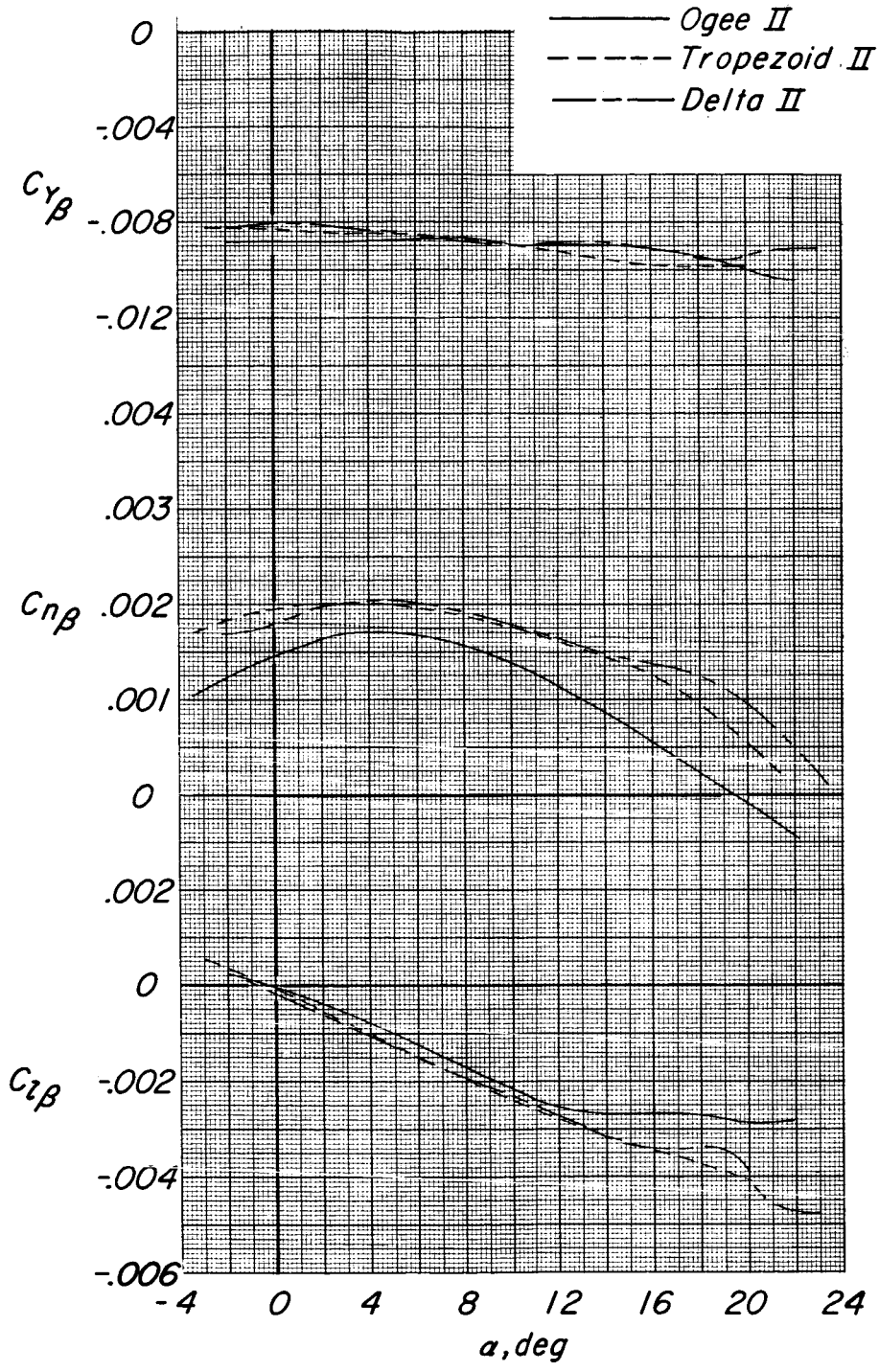

(b) M = 0.60.

Figure 25.- Continued.

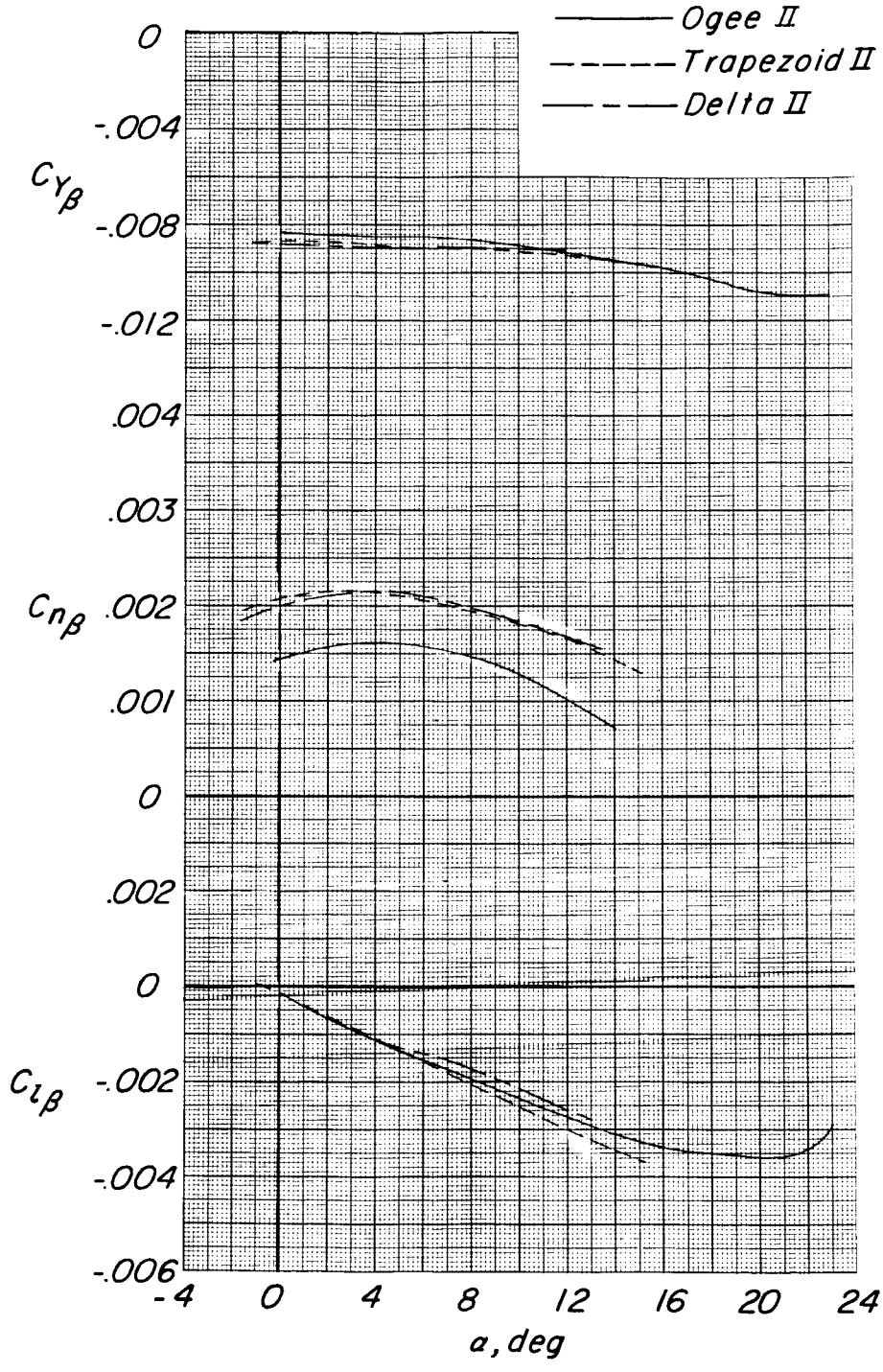

(c) M = 0.80.

Figure 25.- Continued.

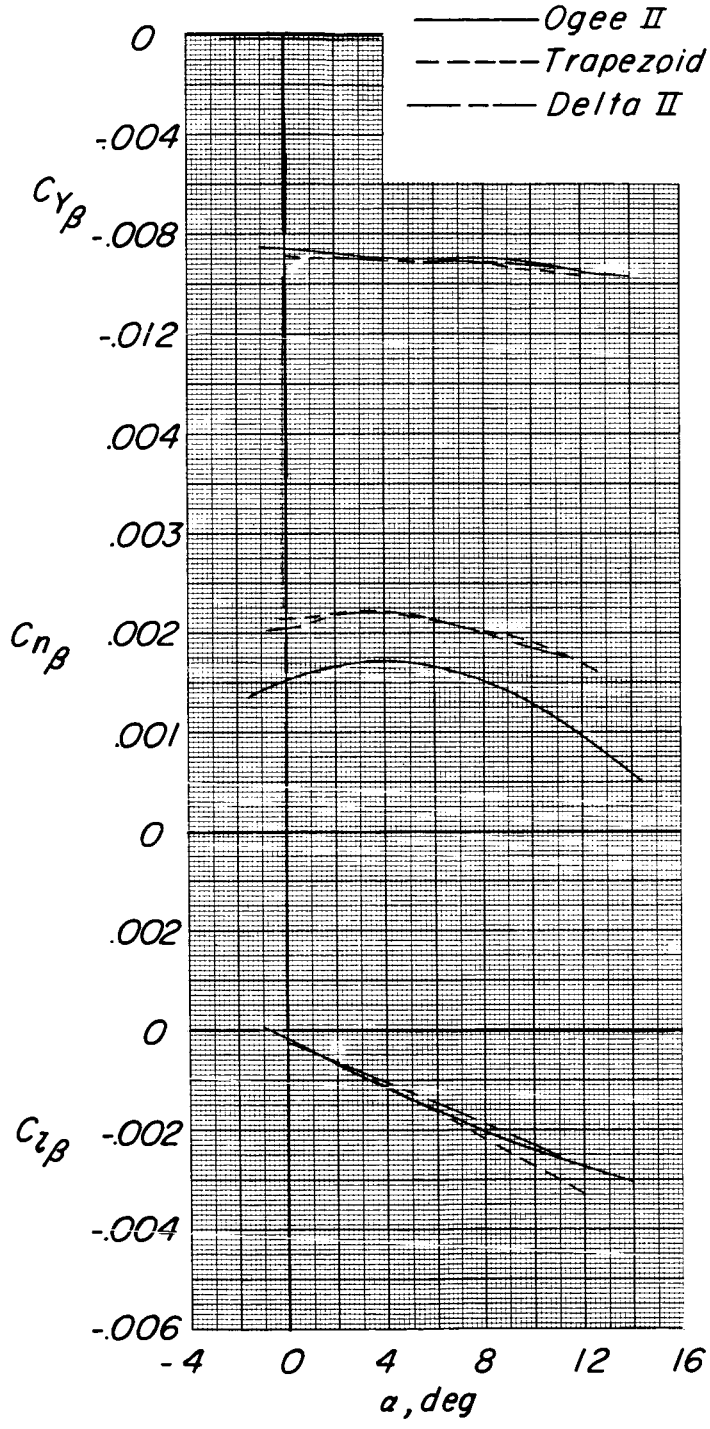

(d) M = 0.90.

Figure 25.- Continued.

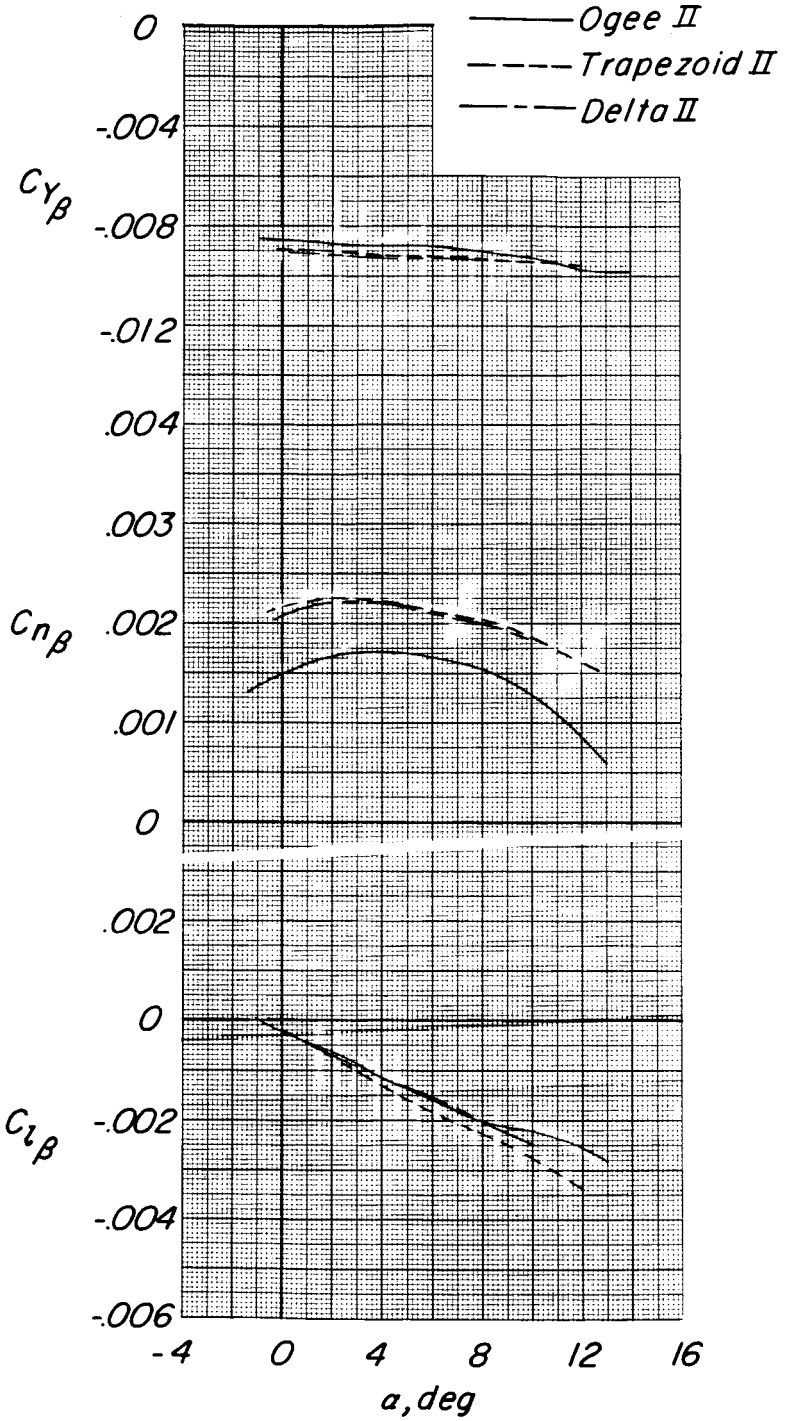

(e) M = 0.94.

Figure 25.- Continued.

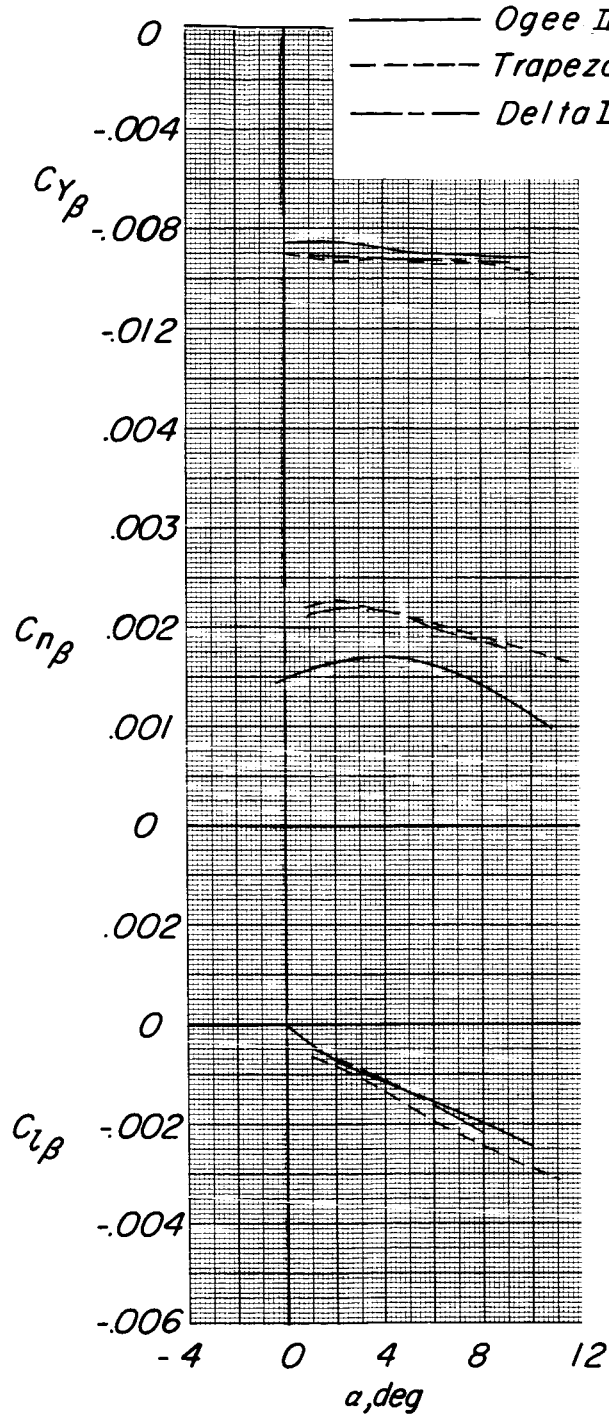

(f) M = 0.98.

Figure 25.- Continued.

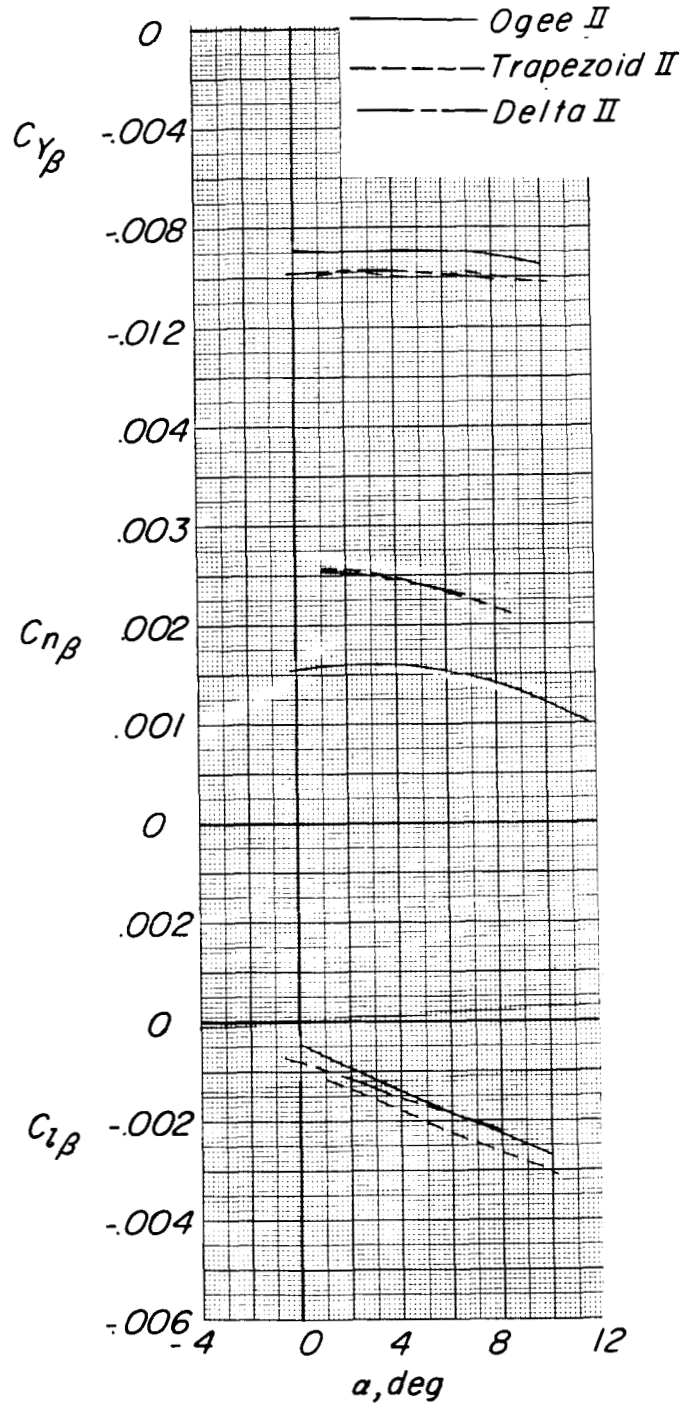

(g) M = 1.02.

Figure 25.- Continued.

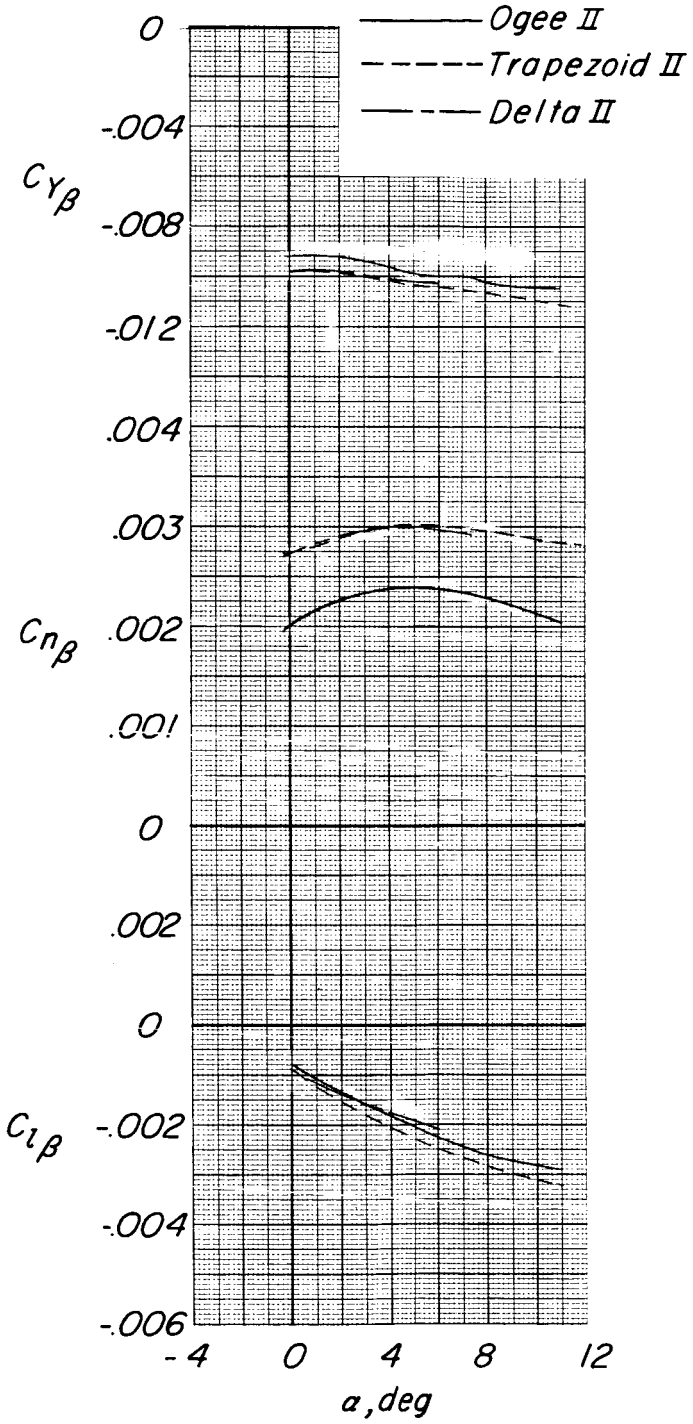

(h) M = 1.14.

Figure 25.- Concluded.